THE ROLE OF $CD8^+$ T CELLS IN WEIGHT LOSS AND WEIGHT CYCLING

By

Matthew Alexander Cottam

Dissertation

Submitted to the Faculty of the

Graduate School of Vanderbilt University

in partial fulfillment of the requirements

for the degree of

DOCTOR OF PHILOSOPHY

in

Molecular Physiology and Biophysics

June 30th, 2022

Nashville, Tennessee

Approved:

Owen McGuinness, Ph.D.

Maureen Gannon, Ph.D.

Meenakshi Madhur, M.D., Ph.D.

Jeffrey Rathmell, Ph.D.

To my family, for their endless support, encouragement, and inspiration.

ACKNOWLEDGMENTS

First and foremost, I thank my mentor Dr. Alyssa Hasty. Her guidance, support, and encouragement began before my rotation in the lab and has continued through my defense. Alyssa has always put my own goals and interests first, allowing me to explore new ideas and invest in them whole-heartedly. Beyond the lab, Alyssa has always been willing to listen to my concerns and struggles and provided advice that continues to make me a better scientist, colleague, and friend. Her mentorship was the most critical component, and most valuable gift, of my graduate training.

I would also like to express my great appreciation for my dissertation committee, Drs. Owen McGuiness, Maureen Gannon, Meenakshi Madhur, and Jeffrey Rathmell. Their knowledge, expertise, and advice were essential for the completion of experiments throughout the duration of my training. After meeting with Dr. McGuinness, I always have a deeper and more granulular understanding of my hypotheses and experiments. As I continue working towards future career goals, I hope that I can continue to channel his thoughtful and analytical outlook to improve every project I work on. Dr. Gannon was one of my rotation mentors and has since been an incredible scientific and emotional resource. I recall struggling during my qualification exams and Maureen reinvigorated my passion for science through her kind encouragement. Much of the work completed for this dissertation would not have happened without Dr. Madhur. In one of the earliest presentations that I attended as a trainee, Meena spoke about her work utilizing immunotherapy (Abatacept). I have had a personal scientific interest in immunotherapy since then, which drove many of my hypothesis in the lab. Dr. Rathmell is one of the most generous scientists I have met. He has, on multiple occasions, connected me with other scientists to collaborate and regularly shares resources and ideas. Prior to COVID, I very much looked forward to having large group dinners with Jeff and other immunology trainees at conferences. I also have always been appreciative that I was included in events for the immunology department and was able to expand my network to other departments at Vanderbilt through his invitation.

Vanderbilt uniquely encourages collaborations and many of my greatest successes during my training were through productive collaborative efforts. Alyssa always supported me by allowing me to collaborate with others and encouraged me to provide input. Early in my PhD, I was hesitant to ask questions and I truly believe that regular meetings with collaborators built my confidence as a scientist. I have been fortunate to collaborate with Vanderbilt scientists in many departments and with scientists at other institutions too. To this day, I am still honored when another scientist at any level reaches out to me for advice.

The Hasty lab is also extremely collaborative. Marnie has been a consistent voice of reason during my training. She is always there to help, chat, and support our work. I've been so lucky to watch her family grow during my time in the lab and cannot imagine my training without her. Early in my time at Vanderbilt, I made great friends in the lab. I learned many bench techniques from Reid and Arion, both who have become close friends. When Nathan and Heather joined the lab, my productivity sky rocketed. Nathan is an unbelievably curious and dedicated scientist. He always inspired me to perform more complex and interesting experiments and we have spent many hours discussing our science at happy hours. For many years, Heather and I were the only ones working on the weight cycling

project. As a result, I was very fortunate to get to work along side her on many lengthy studies and I cannot wait to see how her career continues to progress. Working alongside of Merla, Kristin, Maggie, Monica, Katie, Elysa, Jamie, and all of our incredible undergraduate and rotation students has been wonderful and I've always looked forward to our chats about science and life. I very much look forward to hearing about their success in the future and hope they will reach out if they ever need an extra hand.

Finally, I have to thank the many friends I've made in Nashville for their support and encouragement. I met Nathan, Justin, and Will early on through the IGP program and we have remained friends throughout our degrees. Having a close group of friends that were often facing similar challenges as me was essential for my early training and I'm so proud that we have shared many successes together. I also have to thank and acknowledge my closest friend and partner, Yunli "Emily" Chu, who I met during my PhD. Our relationship has flourished throughout the past few years and her support has helped me stay on track. With her, my family has grown significantly and now our household has three cats (Tiger, Tux, and Nemo) and a puppy (Lily). Her parents and sister have taken me into their family as one of their own when it seemed like the world was in unending conflict and for that I cannot thank them enough. Emily always puts me first and provides the support I've needed to make difficult decisions. I already know that she is a brilliant scientist and will be a compassionate physician, and I cannot wait to continue growing alongside her.

TABLE OF CONTENTS

LIST OF TABLES

LIST OF FIGURES

LIST OF ABBREVIATIONS

[^{14}C]2DG [^{14}C]2-Deoxyglucose

Ldha Lactate Dehydrogenase gene

Pdgfc Platelet-derived Growth Factor C

ADP Adenosine Triphosphate

AMPK Adenosine Monophosphate Activated Protein Kinase

ANOVA Analysis of Variance

APC Antigen Presenting Cell

AT Adipose Tissue

ATAC-seq assays for transposase-accessible chromatin

ATMs Adipose Tissue Macrophages

ATP Adenosine Diphosphate

AUC Area Under the Curve

BAT Brown Adipose Tissue

BCR B Cell Receptor

BMI Body Mass Index

CCR2 C-C Chemokine motif Receptor 2

CCR7 C-C motif Chemokine Receptor 7

CD Cluster of Differentiation

cDCs Conventional Dendritic Cells

CDR3 Complimentarity Determining Region 3

CITE-Seq Cellular Indexing of Transcriptomes and Epitopes by Sequencing

CLS Crown-like Structure

CNS Central Nervous System

CR Caloric Restriction

CTLA-4 Cytotoxic T-lymphocyte-associated protein 4

CTLs Cytotoxic T Lymphocytes

DAPI 4,6-diamidino-2-phenylindole

Db/Db Leptin receptor deficient mouse model

DCs Dendritic Cells

DIO Diet-induced Obesity

eAT Epididymal Adipose Tissue

ELISA Enzyme-linked Immunosorbent Assay

$EndoR_a$ Endogenous glucose Rate of Appearance

FMO Fluorescence-minus One

FOV Field of View

FoxP3 Forkhead Box P3

GIR Glucose Infusion Rate

GLP-1R Glucagon-like Peptide Receptor

GRB2 Growth-factor Receptor Bound protein 2

GSIS Glucose Stimulated Insulin Secretion

GT Ground Truth

GZMB Granzyme B

GZMK Granzyme K

Hba1c Gylcated Hemoglobin A1c

HFD High Fat Diet

HFD High-fat Diet

HIV Human Immunodeficiency Virus

IFN-γ Interferon-γ

IKK Inhibitor of $\kappa\beta$ kinases

IL Interleukin

ILCs Innate Lymphoid Cells

iNKT Invariant Natural Killer T Cell

ip Intraperitoneal

ipGTT Intraperitoneal Glucose Tolerance Test

IRS1 Insulin Receptor Substrate 1

ITAM Immunoreceptor Tyrosine-based Activation Motifs

JAK Janus Tyrosine Kinase

LAMs Lipid-Associated Macrophages

LAT Linker for Activation of T cells

LCK Lymphocyte-specific protein Kinase

LFD Low Fat Diet

LFD Low-fat Diet

mAb Monoclonal Antibody

MAIseq Murine Adipose Immune sequencing

MCP-1 Monocyte Chemoattractive Protein 1; also known as CCL2

MDI Macrophage Differentiation Index

MHC Major Histocompatibility Complex

MMe Metabolically activated Macrophages

MMPC Mouse Metabolic Phenotyping Center

moDCs Monocyte derived Dendritic Cells

MPI Macrophage Polarization Index

NEFA Non-esterified Fatty Acid

NFAT Nuclear Factor of Activated T Cells

NK Natural Killer Cell

NKT Natural Killer T Cells

Ob/Ob Leptin deficient mouse model

PCA Principle Component Analysis

PD-1 Programmed cell Death protein 1

PD-L1/L2 Programmed cell Death Ligand 1/2

pDCs Plasmacytoid Dendritic Cells

pgAT Perigonadal Adipose Tissue

PI3k Phosphatidylinositol 3-kinase

PLC-γ phospholipase C-γ

PLIN-1 Perilipin 1

PMA Phorbol Myristate Acetate

PPAR-α peroxisome proliferator-activated receptor α

PPAR-γ peroxisome proliferator-activated receptor γ

PRRs Pathogen Recognition Receptors

R_d Rate of glucose Disappearance

R_g Glucose Metabolic Index

RT Room Temperature

scRNA-seq Single Cell RNA Sequencing

SEM Standard Error of the Mean

SGLTI Sodium-glucose Transport Inhibitors

SNPs Single Nucleotide Polymorphisms

SOCS Suppressors of Cytokine Signaling

STAT Signal Tranducer and Activator of Transcription

SVF Stromal Vascular Fraction

T1D Type 1 Diabetes

T2D Type 2 Diabetes

T_{aa} Age-associated T Cell

T_{CM} Central Memory T Cell

T_{eff} Effector $CD8^+$ T Cells

T_{EM} Effector Memory T Cell

$T_{naïve}$ Naïve $CD8^+$ T Cells

T_{reg} Regulatory T Cell

TCR T Cell Receptor

Th Cells Helper T Cells

TLRs Toll-like Receptors

TNFα Tumor Necrosis Factor α

TREM2 Triggering Receptor on Expressed Myloid cells 2

TRMs Tissue Resident Macrophages

UMAP Uniform Manifold Approximation and Projection

VANTAGE VANderbilt Technologies for Advanced GEnomics

VAT Visceral Adipose Tissue

WAT White Adipose Tissue

WC Weight Cycling

WC-PF Weight Cycling - Pair Fed

WHO World Health Organization

WL Weight Loss

ZAP-70 Zeta-chain-associated Protein Kinase-70

CHAPTER 1

Introduction

1.1 The obesity crisis

In 2013, the World Health Organization (WHO) reported that 63% of global deaths can be attributed to noncommunicable diseases [1]. As of April 2021, the WHO has increased this estimate to 71%. Obesity, a complex disease defined as the accumulation of excess fat mass, increases risk of disease progression and death for all known noncommunicable diseases. Over the past 50 years, obesity prevalence, determined by frequency of elevated body mass index (BMI) per capita, has increased in every region of the world, reaching pandemic levels [2]. Worldwide, nearly 40% of adults are overweight ($BMI \geq 25 kg/m^2$) and 11-15% of adults are obese ($BMI \geq 30 kg/m^2$) [3]. In the U.S., approximately 70% of adults are overweight and 33-40% are obese [4]. As a result, nearly 10% of medical spending in the U.S. was estimated to be used for obesity-related care in 2009 [5]. Therefore, continued efforts to identify both systemic and tissue-specific mechanisms driving obesity-associated metabolic disease remain critical.

1.2 Weight cycling: The yo-yo diet effect

Currently, the most effective strategy for management and prevention of obesity-associated disease progression is weight loss (WL) [6]. The most common approach to WL is lifestyle therapy, but additional pharmacotherapy and surgical options have also been shown to promote WL [7–10]. However, it has been known for decades that failure to maintane lost weight is common [11, 12]. Recent studies report that >60% of individuals regain weight within two years [13–16].

Due to the difficulty of achieving and maintaining WL, individuals often experience a phenomenon called weight cycling (WC). WC is characterized by periodic cycles of WL and weight regain, sometimes referred to as yo-yo dieting. A dominating theory suggests

that biological mechanisms, such as hormone-driven changes in appetite and suppression of energy expenditure, are engaged during WL, thereby contributing to weight regain [17–19]. However, it should be noted that these mechanisms can be overcome by strict behavioral modifications and long-term (1-2 years) adherence to diet is a predictor of future weight maintenance [15, 20–22].

1.3 Consequences of weight cycling

Over the past three decade, a shift from small prospective studies to large, longitudinal studies has occurred, bringing to light potential consequences of WC on metabolic health. In 1991, a post-hoc analysis of the Framingham Heart Study identified increased risk of coronary artery disease and mortality in participants with high body-weight variability (measured at 9 timepoints) over 35 years [23]. Later, multiple smaller prospective cohort studies identified correlations between disease progression and body weight variability. A study on middle-aged men followed for 15 years identified increased risk of all-cause mortality in participants classified as weight fluctuators [24]. Additionally, a 16-year prospective study on participants in the Korean Genome and Epidemiology Study also found that body weight variability was associated with elevated blood pressure, gylcated hemoglobin A1c (HbA1c), and mortality [25]. Data from the Diabetes Prevention Program lifestyle intervention arm identified an increased risk of cardiometabolic disease and development of type 2 diabetes (T2D) in prediabetic patients identified as weight cyclers [26]. Furthermore, a post-hoc analysis of the Treating to New Targets trial, which included patients with coronary artery disease, identified strong correlation between increasing frequency and degree of body weight variability with risk of cardiovascular disease, stroke, and death [27]. More recently, a study utilizing the Korean National Health Insurance Service electronic medical records containing data on $\geq$ 250,000 individuals reported associations between body-weight variability and increased mortality, even in participants within the normal bodymass range [28]. Overall, these data support the notion that the WC phenemenon increases risk

of numerous comorbidities with most studies having identified risk of diabetes and cardiometabolic disease progression.

1.4 Diabetes: types 1 and 2

Diabetes is one of the many noncommunicable diseases promoted by obesity. The definition of diabetes is inability to regulate glucose due to either loss of the pancreatic hormone insulin or loss of the ability of insulin to signal. Diabetes is diagnosed clinically through measurements of glucose in the blood. The inability to regulate blood glucose through tissue-mediated uptake, driven primarily by insulin, results in elevated levels of glucose in the blood during both fasted and post-parandial states. Chronic elevated blood glucose damages numerous tissues, including the heart, kidneys, eyes, nerves, and vasculature. As a consequence, uncontrolled diabetes can lead to increased risk of myocardial infarction, loss of sensivity in the limbs, blindness, and infection. There are multiple forms of diabetes, including those that manifest due to genetic mutations, autoimmunity, and systemic metabolic disease [29]. Two of the most common forms of diabetes, types 1 and 2, have been investigated in regards to WC.

1.4.1 Type 1 Diabetes Mellitus

Type 1 diabetes (T1D), previously referred to as juvenile diabetes, is an autoimmune disease characterized by loss of insulin secreting β cells in the pancreas. In T1D, cells of the immune system recognize fragments of proteins produced by β cells and fail to receive signals that prevent autoimmune attack. As a result, activated immune cells destroy β cells in the pancreas and impair the ability of the pancreas to produce insulin. The exact trigger for autoimmunity in T1D remains unknown. However, exposure to certain environmental triggers has been linked to incidence of T1D [30]. For example, viral infection is believed to trigger T1D in some individuals and multiple viral pathogens have been correlated to incidence of T1D [31, 32]. Management of T1D is patient-centric with a focus on regular blood glucose monitoring and self-administration of recombinant insulin to maintain stable

blood glucose levels.

1.4.2 Type 2 Diabetes Mellitus

T2D is the most common form of diabetes and is characterized by progressive loss of adequate insulin production and secretion and decrease sensitivity to insulin in the periphery. Typically, screening for T2D occurs in a clinical setting for patients based on risk criteria and is conducted by measurements of fasting plasma glucose, impaired glucose tolerance, and/or HbA1c. Abnormal carbohydrate metabolism is often detected at prediabetic stages whereby HbA1c is elevated, but does not meet diagnostic criteria for T2D as defined by the American Diabetes Association [33].

T2D is a progressive disease that is most frequently linked to other components of metabolic syndrome, such as obesity and increased blood pressure. Like other noncommunicable diseases, risk of T2D increases with age [34]. However, genetic predispositions to T2D have been reported and there is clear evidence that race is also an independent risk factor for T2D development [35–39]. Impairments in the action and delivery of insulin to various tissues responsible for glucose uptake require a compensatory increase in insulin output from the pancreas. One prevailing hypothesis suggests that variability in β cell mass, largely derived early in life, may explain why some individuals are more likely to develop diabetes than others [40, 41]. β cell mass is not static and expansion of β cells in the pancreas occurs to meet systemic insulin demands and may even occur prior to overt tissue insulin resistance [42–44]. Therefore, the occurance of T2D is defined by a failure to compensate for systemic insulin demands. In some settings, insufficient insulin production is temporary. For example, insulin demand increases during pregnancy and inability to meet the demand results in gestational diabetes [45, 46]. In the case of gestational diabetes, insulin demand often decreases postpartum, but past diagnosis of gestational diabetes remains predictive of T2D risk should insulin demand again increase [33]. WL can also reduce systemic insulin demand in previously overweight or obese individuals, improving

maintenance of blood glucose [10, 47–49]. WC correlates with progression in T2D, but the mechanism remains largely unknown. In Chapter V, we explore the effects of WC on pancreatic β cells to further understand WC-associated metabolic disease.

1.5 Systemic regulation of blood glucose

Glucose is the most essential metabolite for the central nervous system (CNS). The brain is the primary consumer of glucose during settings of low nutrient intake, such as fasting. At the same time, other tissues, such as skeletal muscle and liver, shift towards uptake and utilization of fatty acids to preserve glucose for the CNS. In contrast, when glucose is readily available, such as after a meal, endogenous glucose production is reduced and peripheral tissues promote mechanisms of glucose uptake, storage, and utilization. Each component of this multi-system concert is critical for homeostatic control of blood glucose (Fig. 1.1). In the following subsections, peripheral regulation of blood glucose is explained in more detail with a focus on mechanisms that occur during hyperglycemia (i.e. elevated blood glucose).

1.5.1 Insulin production and secretion

The pancreas is composed primarily of exocrine tissue that synthesizes and secretes digestive enzymes [50]. However, approximately 1-3% of pancreatic tissue consists of mini-organs called islets of Langerhans. β cells, α cells, and δ cells are found within these endocrine islets. In mice, α cells, which secrete glucagon in response to low blood glucose, and somatostatin secreting δ cells are found in the periphery of the islet while β make up the core of islets [51]. The most abundant cell type found in islets of mice and humans, β cells, produce and secrete insulin in response to elevated blood glucose. In humans, α cells are also found in the core of islets and are more abundant (˜30% in humans versus ˜10-15% in mice; Fig. 1.2) [52–54]. The δ cells are more common in humans and regulate both α and β cell hormone secretion through production of an additional hormone called somatostatin [54].

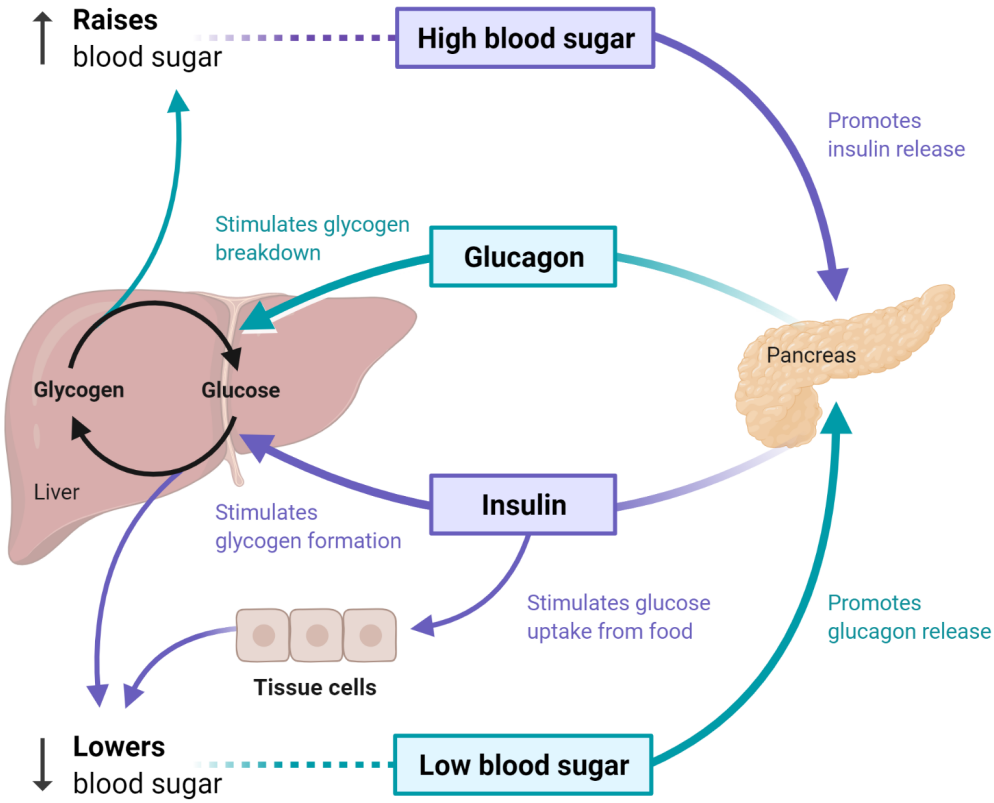

Figure 1.1: Systemic regulation of blood glucose. In settings of high blood glucose, insulin is secreted from the pancreas, driving glucose uptake by the liver and other tissues. Insulin also promotes glycogen synthesis for storage of glucose and blunts endogenous glucose production in the liver. In settings of low blood glucose, glucagon is secreted from the pancreas and stimulates gluconeogenesis by the liver to break down stored glycogen and release glucose. Schematic adapted from "Regulation of Blood Glucose", by BioRender.com (2020).

Islet β cells sense glucose levels through a rapid multi-step process [55]. First, glucose enters the cell through plasma membrane GLUT2 transporters. Glucose is metabolized within the cell at the mitochondria, generating adenosine triphosphate (ATP). ATP-dependent potassium channels close in response to increasing ratio of ATP to adenosine diphosphate (ADP), causing the cell membrane to depolarize. Changes in membrane voltage induce opening of voltage-dependent calcium channels and subsequent Ca^{2+} influx into the cell. Ca^{2+} influx then stimulates additional Ca^{2+} release from the endoplasmic reticulum, insulin synthesis, and mobilization of secretory granules to release insulin into the

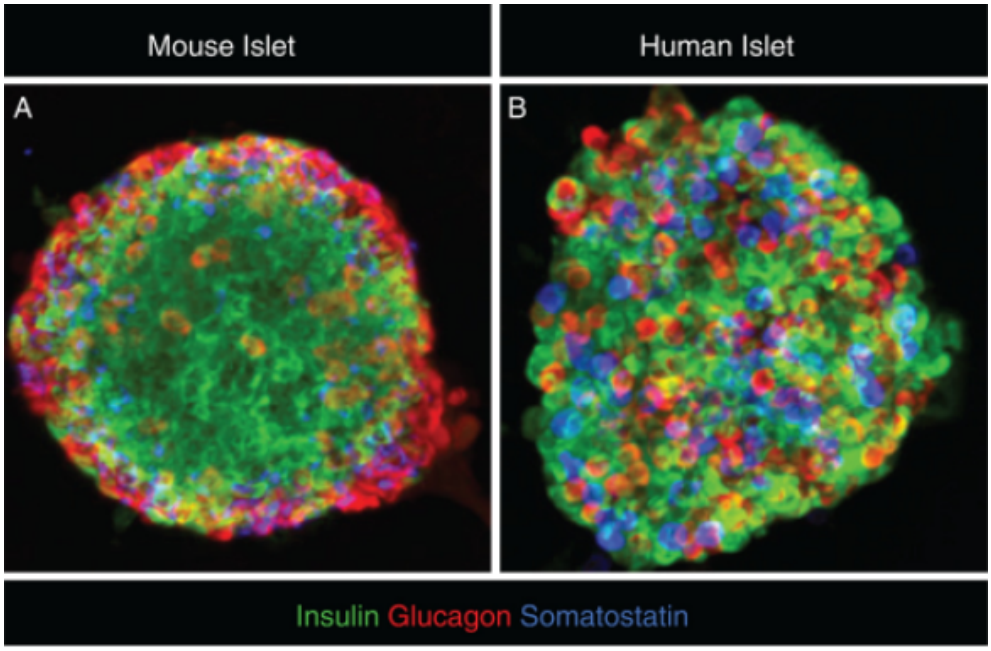

Figure 1.2: Species differences in islet architecture. Immunofluorescence imaging of insulin (green), glucagon (red), and somatostatin (blue) in mouse (**A**; left) and human (**B**; right) islets. Reproduced with permission from Aamodt *et al.*, Figure 1, 2017.

blood stream.

Importantly, changes in systemic factors can impair successful synthesis and secretion of insulin by β cells. For example, the inflammatory cytokines interleukin-6 (IL-6), interleukin-1β (IL-1β), and tumor necrosis factor α (TNFα) can induce endoplasmic reticulum stress that reduces insulin synthesis [56–58]. In addition, chronic hyperglycemia can invoke β cell stress and lead to dedifferentiation and/or apoptosis of islet β cells [59].

1.5.2 Insulin delivery

Even though islets only comprise ˜3% of the pancreas, they receive approximately 15% of pancreatic blood flow [60]. Once insulin is successfully exocytosed from β cells, it enters the veinous portal circulation [61]. Through the portal circulation, insulin proceeds to the liver where $\geq$50% of insulin is extracted (termed first-pass insulin extraction) [62, 63]. Remaining insulin passes through the hepatic vein to the heart before ultimately entering arterial circulation to reach skeletal muscle, adipose tissue (AT), kidneys, and again

returns to the liver. At peripheral tissues, insulin delivery occurs through diffusion out of microvasculature. Therefore, alterations in blood flowrate through capillaries, capillary permeability, and capillary structure can all disrupt insulin delivery to the site of insulin action [64–66]. For example, endothelial cells that line the microvasculature are sensitive to inflammation and glucotoxicity during chronic hyperglycemia, which can disrupt the integrity and perfusion of capillaries within peripheral tissues [67]. Importantly, alterations in insulin delivery are challenging to measure and therefore are rarely quantified during assessments of insulin resistance.

1.5.3 Insulin action

Insulin binds with highest affinity to the insulin receptor [68]. The insulin receptor is found on most mammalian cells, including immune cells, but has two isoforms generated via alternative splicing of insulin receptor transcripts. Insulin receptor isoform B is more prevalent in the plasma membrane of cells classically associated with glucose uptake (e.g. myocytes, hepatocytes, and adipocytes) [69]. The insulin receptor is a receptor tyrosine kinase, which tranduces signals through phosphorylation of insulin receptor substrates (IRS) [70]. Once phosphorylated, IRS binds phosphatidylinositol 3-kinase (PI3K). PI3K phosphorylates lipid signaling molecules that ultimately engage pathways involved in cell growth, translocation and stability of the insulin-dependent glucose transporters for glucose uptake, and induction of glycogen synthesis for glucose storage [71].

Disruptions in the ability of insulin to signal (i.e. insulin action) are termed insulin resistance. Insulin resistance can occur due to loss of expression of the insulin receptor or loss of signaling downstream of the receptor. Inflammatory cytokines, such as TNFα, can impair IRS phosphorylation by the insulin receptor through phosphorylation at serine residues via alternative kinases (e.g. inhibitor of $\kappa\beta$ kinases; IKK) [72, 73]. In addition, suppressors of cytokine signaling (SOCS) proteins induced by interferon-γ (IFN-γ), IL-1β, and IL-6 repress autophosphorylation of the insulin receptor upon engagement with

circulating insulin and also induce ubiquitin-mediated degredation of IRS proteins [74, 75]. Chronic hyperinsulinemia, as a result of compensatory increases in insulin secretion and decreases in insulin extraction, can also increase insulin receptor endocytosis, thereby reducing surface insulin receptors and exacerbating insulin resistance [76].

1.6 Adipose tissue homeostasis

AT is a highly specialized form of connective tissue found in multiple depots throughout the body [77]. AT is most commonly associated with storage of energy in the form of lipids, which typically form large lipid droplets within adipocytes. In addition to roles in metabolite storage, AT plays essential roles as an endocrine organ through the production of various hormones that regulate long-term energy homeostasis.

Importantly, not all AT depots are alike and vary greatly in their function and morphology. AT depots can be generalized as belonging to either white AT (WAT) or brown AT (BAT) designations [78, 79]. Adipocytes found in WAT have one large (unilocular) lipid droplet that fills the majority of the cell cytoplasm (Fig. 1.3). Unlike WAT, BAT adipocytes contain multiple smaller (multilocular) lipid droplets, have many mitochondria, and play roles in thermoregulation through uncoupling of mitochondrial metabolism to produce heat. In addition, AT can adapt to organismal needs through ”beiging” of WAT in settings of cold-exposure and of BAT in settings of excess nutrient storage [80]. In general, AT depots located under the skin (i.e subcutaneous AT; sAT) are considered to be more beige than peritoneal depots and have smaller adipocytes [81, 82].

AT depots can be further classified by their anatomical location. sAT is found beneath the skin throughout the body, while peritoneal AT is found surrounding internal organs. Numerous further classifications of peritoneal AT, such as visceral AT (VAT), mesenteric AT surrounding the intestines, perirenal AT surrounding the kidneys, and perigonadal (pgAT) surrounding reproductive organs are also recognized (Fig. 1.4) [83]. VAT historically refers to AT which directly releases free-fatty acids to the portal circulation and has been highly

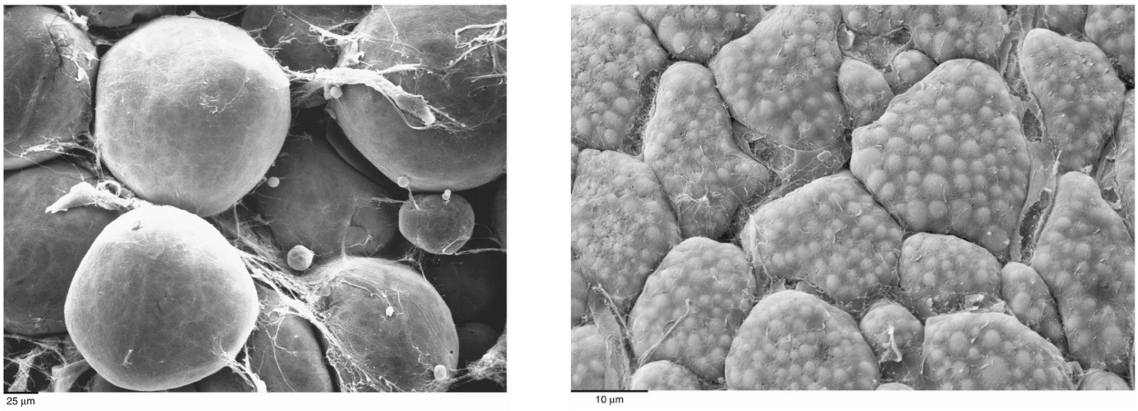

Figure 1.3: Electron microscopy of white and brown adipocytes. Unilocular white adipocytes (left) and multilocular brown adipocytes (right) imaged by scanning electron microscopy. Scale is shown in the lower left of each image. Figure panels reproduced with permission from Frontini *et. al*, Figure 1, 2010.

correlated with insulin resistance. However, this definition has been expanded to include the retroperitoneal AT, which has a weaker association with incidence of diabetes in humans [84]. VAT is also frequently used interchangably with other peritoneal AT depots, such as the pgAT, in primary scientific literature despite differences in anatomical position. Overall, peritoneal AT depots are more highly correlated with insulin resistance in both humans and rodents than sAT [85–87]. Therefore, the majority of basic research has focused on understanding the mechanisms by which the WAT peritoneal depots are altered in settings of obesity and insulin resistance. Due to size and ease of isolation, the pgAT depots are most frequently investigated in rodent models and, when isolated from male mice, is often referred to as epididymal AT (eAT).

As previously mentioned, AT is essential for nutrient storage. In settings of increased caloric load driven by increases in intake and/or decreases in expenditure, adipocytes can rapidly expand to store metabolites as lipids [88]. Adipocytes express the insulin receptor and translocate GLUT4 to the surface to take up glucose in response to insulin signaling [89]. Adipocytes are the primary source of the hormone leptin, which regulates long-term energy homeostasis by reducing food intake when acting on various regions of the brain [90]. For example, afferent projections from leptin receptor expressing cells reach the par-

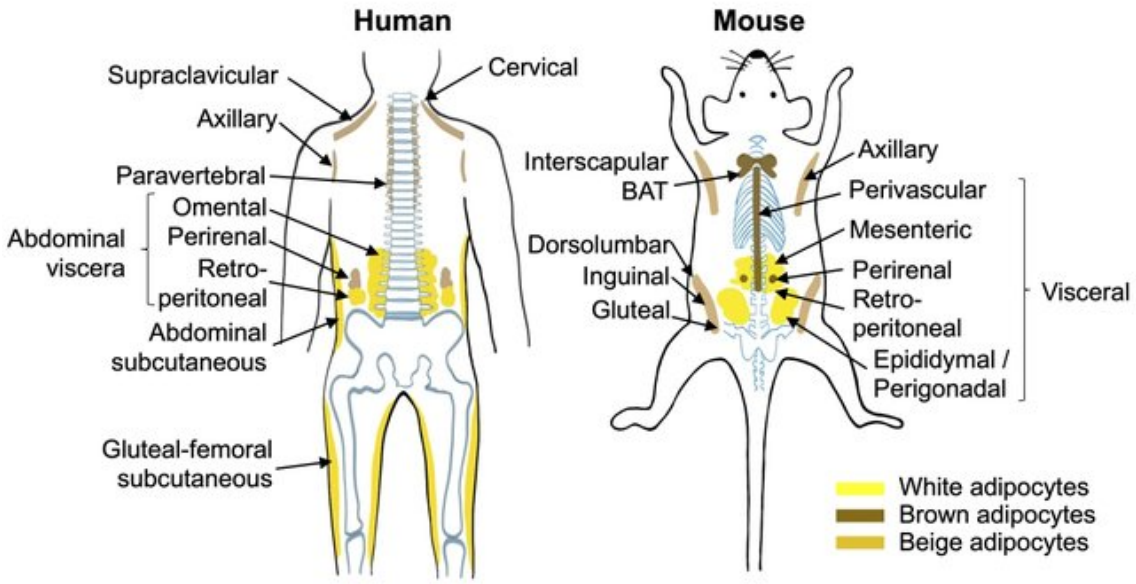

Figure 1.4: Adipose tissue depots in humans and mice. Adipose tissue depots are labeled in human (left) and mouse (right) and colored by cell subtype. Reproduced from Cheong *et al.*, 2021.

aventricular nucleus of the hypothalamus, which regulates feeding behavior, and neurons downstream of leptin-responsive projections are activated during leptin infusion [91]. During obesity, systemic leptin levels are elevated (i.e. hyperleptinemia) and leptin-resistance (i.e impaired response to leptin) is observed. In rodent models of diet-induced obesity, neurons in the arcuate nucleus of the hypothalamus, important for regulation of feeding behavior, have reduced projections [92]. As a result, response to leptin signalins that are transduced through afferent cell projections are reduced, partially explaining diminished response to leptin. Leptin and its receptor are also important tools for obesity research. Discovered at Jackson Labs through selective breeding, leptin deficient mice (referred to as Ob/Ob mice) and leptin receptor deficient mice (referred to as Db/Db) are hyperphagic due to loss of systemic leptin signaling resulting in early-onset obesity (Fig. 1.5) [93]. Mutations resulting in leptin deficiency are rare in humans and only monogenic mutations have been reported, but result in extreme cases of hyperphagia and early-onset obesity [94]. Fortunately, recombinant leptin administration is therapeutically efficacious in settings of

genetic leptic deficiency as long as signaling through the receptor remains intact [95, 96].

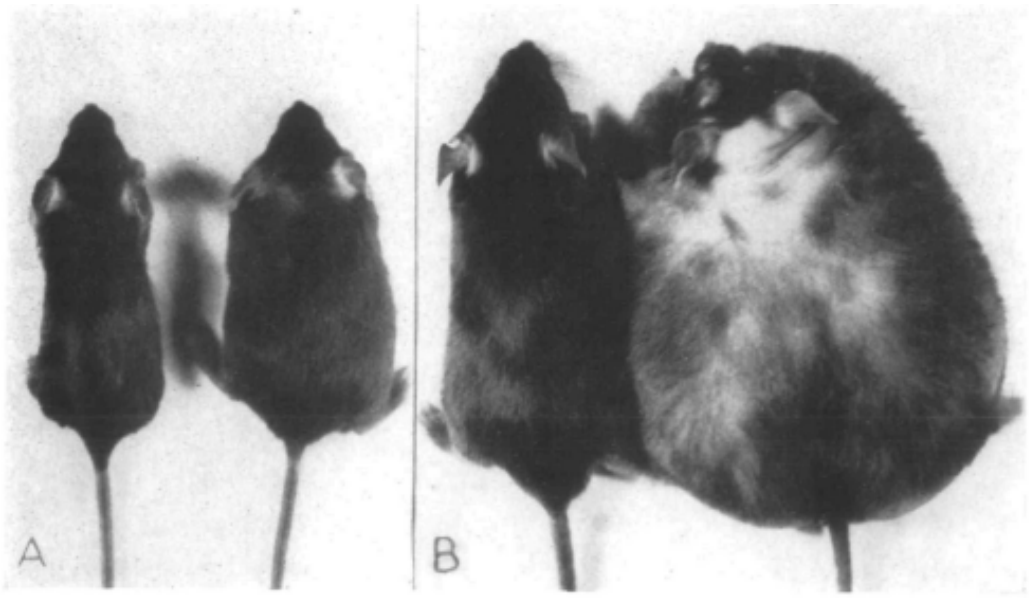

Figure 1.5: The fat mouse grows up. *A* - shows normal control and an obese mouse at 21 days of age. The former weighed 12 grams; the latter 16. *B* shows a normal and obese mouse at ten months of age, when the obsese mouse weighed 90 grams and the normal mouse 29 grams. Figure reproduced with permission and caption reproduced verbatim from Ingalls *et al.*, Figure 4, 1950.

Adipocytes also express the hormone adiponectin. Unlike leptin, adiponectin levels are reduced in settings of obesity [97]. Adiponectin plays roles in insulin sensitivity through activation of factors like adenosine monophosphate activated protein kinase (AMPK) and peroxisome proliferator-activated receptor α (PPAR-α) [98]. Adiponectin expression is at least partially driven by expression of peroxisome proliferator-activated receptor γ (PPAR-γ) [98, 99]. Thiazoledinediones, a class of PPAR-γ agonists, have shown therapeutic efficacy by improving insulin sensitivity in obese individuals. However, PPAR-γ agonist usage has decreased over the past decade due to side-effects of weight gain, liver damage, and cardiovascular events [100, 101].

In addition, AT contains many immune cell subtypes that help maintain adipocyte function through complex physical and paracrine signaling. For example, large phagocytes are known to surround and clear dying adipocytes through the formation of crown-like struc-

tures (CLS) that prevent local lipotoxicity from uncontrolled fatty-acid release (Fig. 1.6) [102]. During settings of cell stress, adipocytes release chemoattractive molecules, such as monocyte chemoattractive protein 1 (MCP-1; also known as CCL2) to recruit immune cells from circulation [103]. Adipocytes can also release inflammatory cytokines like TNFα and IL-1β [104]. Furthermore, many AT immune cells express the leptin receptor and leptin signals through similar pathways as the inflammatory cytokine IL-1β [90].

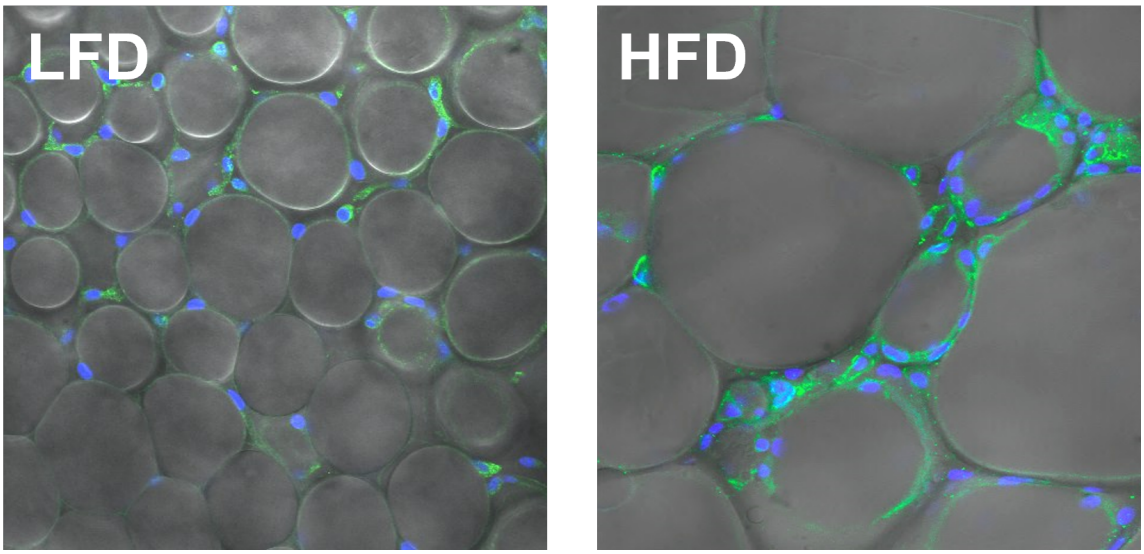

Figure 1.6: Crown-like structure. Immunofluorescence of adipose tissue from a low-fat diet (LFD; left) and high-fat diet (HFD; right) fed mouse for the myeloid marker F4/80 (green) and nuclear label DAPI (blue) overlayed onto differential interference contrast image to show adipocytes (grey). Images reproduced from Hill *et al.*, 2015.

1.7 Innate immune cells

Immune cells can be largely separated into two types: innate and adaptive immune cells. Innate immune cells are non-selective in their response to stimuli and primarily respond to signals through TLRs and pathogen recognition receptors (PRRs). In addition, innate immune cells express Fc (short for fragment crystallizable) receptors that recognize the constant region of antibodies produced by adaptive immune cells.

Macrophages are the most abundant innate immune cells found in both lean and obese AT and were also the first immune cells described within AT [105, 106]. AT macrophages

(ATMs) can be either tissue resident or differentiate from recruited monocytes. In lean AT, the majority of macrophages are yolk-sac derived and these tissue resident macrophages (TRMs) are thought to self-sustain through proliferation within AT [107]. These TRMs express platelet-dervied growth factor C (*Pdgfc*), which has been shown to be essential in fruit flies and mice [108]. With aging and obesity, circulating C-C motif chemokine receptor 2 (CCR2) expressing monocytes infiltrate into AT where they differentiate into macrophages [109–111]. Although ATMs were historically classified as either M1-like (pro-inflammatory) or M2-like (anti-inflammatory), these designations have been phased out in favor of more functional descriptions. For example, subsets of macrophages expressing high levels of iron transport proteins and enriched for iron, called MFehi macrophages, are thought to regulate local iron availability within the AT microenvironment [112, 113]. Recent studies have identified patterns of protein expression related to trafficking and metabolism of lipids, highlighting the unique state of obese ATMs that does not match in vitro models of M1-polarized macrophages [114]. This phenotype has been described as a metabolically activated macrophages (MMe) [115]. Recent advances in single cell sequencing approaches have offered more insight into specific changes in ATMs and a population of lipid-associated macrophages (LAMs) expressing the fatty acid transporter CD36 and a lipid scavenging receptor, triggering receptor expressed on myeloid cells 2 (TREM2), have been identified [116].

Dendritic cells (DCs) can also be derived from monocytes and are found in high abundance in WAT [117]. DCs express high levels of major histocompatibility complex (MHC) proteins and engage in presentation of peptides. Therefore, DCs are a critical component of innate and adaptive immune cell cross-talk. There are multiple DC subtypes, including type 1 and 2 conventional DCs (cDCs) and plasmacytoid DCs (pDCs) [118]. Type 2 cDCs are more abundant in lean AT, while Type 1 cDCs numbers increase in obese AT. Both cDCs subsets found in AT are typically found in a relatively immature state, expressing low levels of CD80 and CD86 [119]. When activated, cDCs are thought to mature and mi-

grate to draining lymph nodes where they interact with adaptive immune cells by displaying antigenic peptides obtained in AT on their surface [120]. The much more rare pDCs are enriched in obese AT, specifically surrounding clusters of adaptive immune cells, and have increased markers of trafficking and type 1 inflammatory cytokine expression [121].

Eosinophils and mast cells are most frequently associated with response to allergies or parasites. In lean AT, eosinophils are abundant (˜20% of immune cells) and are important producers of the allergy-associated cytokine IL-33. In obese AT, eosinophil numbers are greatly reduced, but can be restored with WL [122]. Importantly, induction of AT eosinophilia does not resolve obesity-associated insulin resistance or improve suppressed energy expenditure in mice [123]. Eosinophils are notoriously challenging to measure using transcription-based approaches because they highly express RNase enzymes and readily degranulate [124]. Mast cells are found in low numbers in both lean and obese WAT. Early studies suggest that AT may act as a reservoire for mast cell progenitors [125]. In humans, AT mast cells have been implicated in cold-induced beiging of sAT by degranulation and histamine release [126].

Neutrophils are the most rapidly recruited immune cells to AT during early diet-induced obesity [127]. Neutrophils in both lean and obese AT also express IL-1β at very high levels and may be early drivers of adipocyte inflammation that results in secretion of chemoattractive proteins like MCP-1 [128].

In addition to the cells of the myeloid and granulocyte developmental trajectories, a small population of innate lymphoid cells (ILCs) can be found in AT. ILCs respond rapidly like innate cells and without the specificity of other lymphocytes, yet produce many of the same inflammatory mediators as T cells [129]. IL-13 expressing type 2 ILCs (ILC2s) are recruited to AT following recognition of IL-33. ILC2s also produce interleukin-5 (IL-5), a critical cytokine for maintenance of AT eosinophils [130]. During obesity, AT ILC2s become outnumbered by type 1 ILCs (ILC1s) that proliferate in response to interluekin-12 (IL-12) and produce IFNγ [131]. Type 3 ILCs (ILC3s) have been described in human single

cell transcriptome analyses of WAT [132]. It is speculated that they play a role in adipocyte metabolic function through production of interleukins 17 and 22 (IL-17 and IL-22), but the mechanism of their recruitment, proliferation, and activation remain unknown. Natural killer (NK) cells, unlike the other ILCs, are common in AT. NK cells produce similar cytokines as ILC1s and also increase in number in AT during obesity, but are unique in their ability to also produce cytolytic proteins [133, 134]. However, circulating NK cells are reduced in abundance in obese patients and have impaired cytolytic activity, limiting their role in anti-tumor immunity [135].

1.8 Adaptive immune cells

Adaptive immune cells respond to specific cues through selective receptors. The diversity of these selective receptors is generated through somatic recombination whereby multiple gene fragments are spliced and joined to form a productive transcript in a process called V(D)J recombination [136]. Most adaptive immune cells require additional costimulatory signals and must bypass checkpoint mechanisms for complete signal transduction. T cells recognize antigens bound to cell surface MHC molecules on antigen-presenting cells (APCs) through surface T cell receptors (TCRs). T cells are generated from hematopoietic stem cells in the bone marrow and subsequently mature in the thymus where the TCR, generated through V(D)J recombination (Fig. 1.7), can be challenged by APCs. In a process of negative and positive selection, T cells with too weak (non-reactive) or too strong (autoreactive) interactions with APCs are destroyed during maturation in the thymus [137]. B cells recognize cell-free antigens through the plasma-membrane bound B cell receptor (BCR). Through V(D)J recombination, each naïve B cell contains a unique BCR [138]. After activition by an antigen, B cells undergo a process of somatic hypermutation whereby antibodies are tuned to improve specificity (i.e affinity maturation) [136].

T cells can be classified into multiple subtypes based on the presence or absence of protein features. The two major classes of T cells are those expressing TCRs made up of

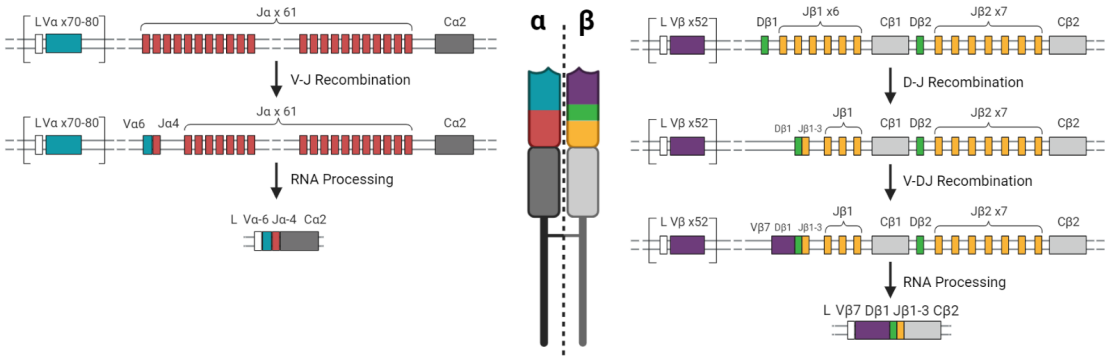

Figure 1.7: V(D)J recombination. Simplified schematic of TCR-α chain (left) and TCR-β chain (right) recombination to produce a productive T cell receptor. Figure generated using BioRender.

either TCR-α and TCR-β chains (α/β T cells) or TCR-γ and TCR-δ chains (γ/δ T cells). α/β T cells are far more abundant and have greater repertoire diversity than γ/δ T cells [139]. The α/β T cells can be further split into two major subtypes based on their ability to recognize different MHC molecules presented on other cells. $CD4^+$ T cells recognize MHC class II (MHC-II) and $CD8^+$ T cells recognize MHC class I (MHC-I) [140].

$CD4^+$ T cells are frequently referred to as helper T (Th) cells due to their important role in regulating the function of other cells. In lean AT, the most common T cell subtype is the $CD4^+$ regulatory T cell (T_{reg}). T_{regs} are an immunosuppressive T cell subset that restrain $CD8^+$ cytotoxic T cells through production of anti-inflammatory cytokines [141]. Many of the T_{reg} functional programs are driven by the transcription factor forkhead box P3 (FoxP3) [142]. AT T_{regs} also highly express PPAR-γ, the same transcription factor that supports adipocyte function. As a result, thiazoledinediones (i.e. PPAR-γ agonists) also stimulate T_{reg} proliferation and immunosuppressive capability within AT [143, 144]. Current evidence suggests that AT is seeded with T_{regs} early in development and that these cells are maintained through proliferation [145]. Indeed, AT T_{regs} often share similar or identitical TCRs, suggesting they are self-proliferative clones [145]. Naïve cells with induced expression of a T_{reg}-specific TCR migrate to AT and reduce the effects of an obesogenic diet in mice, suggesting that clonal T_{regs} are essential for maintance of AT [146]. However,

AT T_{regs} are greatly reduced in number following obesity and the remaining cells have reduced TCR clonality [147, 148]. In Chapter IV, we also show that T_{reg} clonality is not restored with WL.

In addition to T_{regs}, lean AT contains a small population of type 2 $CD4^+$ helper T cells (Th2). IL-33 responsive $CD4^+$ Th2 T cell function is regulated by the transcription factor GATA3 [149]. When activated, Th2 T cells produce IL-4 and IL-13 to promote M2-like macrophage polarization in AT. Like T_{regs}, Th2 T cells are reduced in number with the onset of obesity [150]. Type I $CD4^+$ T cells, which produce inflammatory cytokines such as TNFα and IFN-γ, are rare in lean AT, but increase greatly in abundance early in obesity [150, 151]. Th1 T cells express the transcription factor T-bet encoded by the gene *Tbx21* [152]. $CD4^+$ and $CD8^+$ mice are protected from AT inflammation, and adoptive transfer of Th1 T cells impairs insulin sensitivity, highlighting Th1-driven inflammation as an important contributor to AT dysfunction [153].

$CD8^+$ T cells are present in lean AT, but are much more abundant in AT during weight gain. During diet-induced obesity, $CD8^+$ T cells infiltrate AT from the periphery early on, possibly preceeding macrophages, and playing a role in inflammatory macrophage recruitment [154]. Typically, $CD8^+$ T cells are associated with cytolytic activity and are frequently referred to as cytotoxic T lymphocytes (CTLs). CTLs function by secreting their cytolytic granules into the synapse formed by the TCR/MHC-I complex in a complex process that can take approximately 30 hours for complete signal transduction [155]. For a $CD8^+$ T cell to become fully activated, recognition of an antigen and cognate MHC must occur, followed by generation of costimulatory interactions and absense of coinhibitory signaling. Currently, no specific antigen responsible for activation of AT $CD8^+$ T cells has been identified. Since every nucleated cell expresses MHC-I, it also remains unknown what cells, if any, are specifically targeted by $CD8^+$ T cells in AT.

γ/δ T cells have much more restricted TCR diversity and do not always require MHC or antigen peptide recognition to carry out functions, often classifying them as innate-like

T cells [139]. γ/δ T cells are most commonly found in the skin and gut mucosa. However, a population of γ/δ T cells are found in AT of both lean and obese mice. In murine AT, γ/δ T cells are the primary producers of interleukin-17A (IL-17A) and are thought to enhance $CD4^+$ T_{reg} proliferation and survival [156].

A subset of NK cells also express a TCR and are therefore referred to as NKT cells. NKT cells express α/β TCRs, but recognize MHC molecules that display lipid antigens (e.g CD1d) [157]. Importantly, reports of NKT cells in AT are largely limited to cells with expression of invariant TCRs (iNKT cells). Reports of iNKT cells in AT are controversial, with some correlating iNKT cells with protection against obesity and others reporting iNKT-associated inflammation in mice [158–160]. These findings are further complicated by lack of clear data supporting which cells express CD1d and can successfully present antigen to NKT cells. One group has suggested that adipocytes express CD1d and present lipid antigens to iNKT cells [161–163]. However, adipocyte targeted adeno-associated viral overexpression of CD1d in a $CD1d^{-/-}$ mouse failed to rescue iNKT cells and instead induced $CD8^+$ T cell proliferation [164]. Recently, a report identified differences in iNKT-driven AT inflammation depending on whether macrophages or DCs present antigen on CD1d [165].

1.9 Adipose tissue immune cells

Interactions between between adipocytes and immune cells have been studied for decades. Interestingly, adipose tissue surrounding lymph nodes is found even in very lean or starving animals, a trait that is largely preserved across all mammals [166, 167]. Immune cells in lean WAT are characterized as belonging to a type 2 immunity classification, associated with wound repair, extracellular matrix remodeling, and reductions in inflammatory signals. However, during progression towards obesity, a dramatic shift occurs in which infiltration of type 1 pro-inflammatory immune cells into AT occurs (Fig. 1.8) [168].

In lean AT, anti-inflammatory cytokines, such as interleukins 4, 10, 13, and 33 (IL-4,

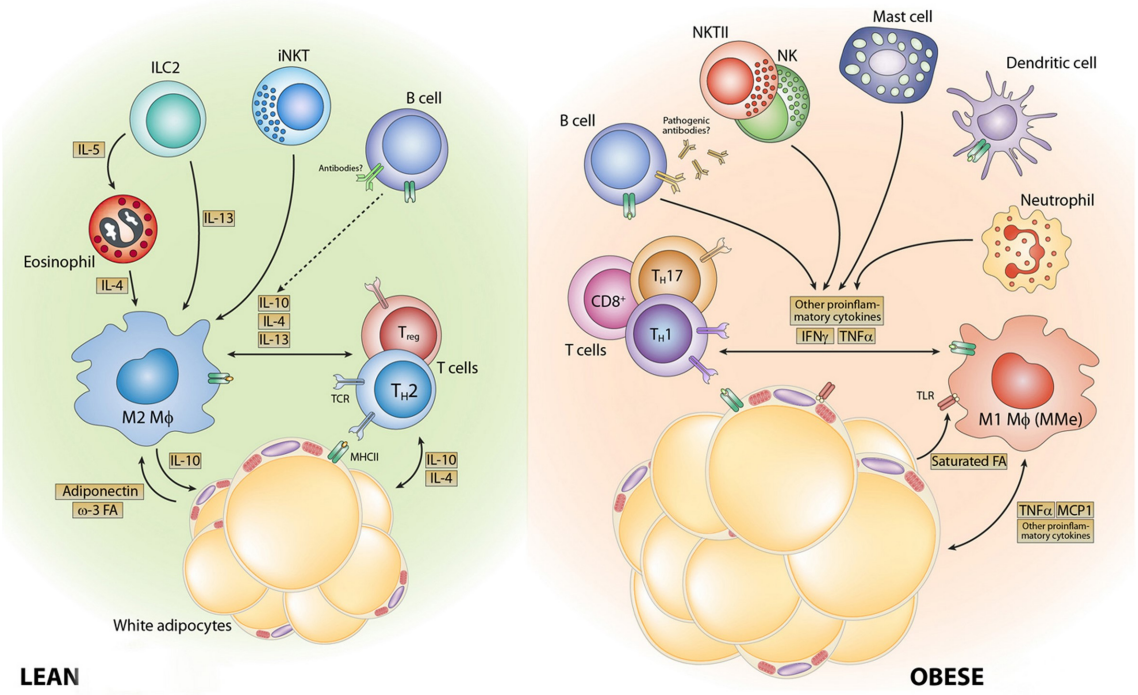

Figure 1.8: Immune cells in lean and obese adipose tissue. Lean AT (left) is primarily characterized by the presence of tissue-resident immune cells, such as M2-like macrophages and regulatory T cells. Obesity (right) induces recruitment of proinflammatory immune cells, such as M1-like macrophages, CD8+ T cells, and mast cells. Reproduced with permission from Villarroya *et al.*, 2018.

IL-10, IL-13, and IL-33, respectively), maintain WAT function and engage transcriptional patterns of activation for wound repair genes and suppression of genes encoding inflammatory cytokines. IL-4 stimulates lipolysis in adipocytes by upregulating expression of hormone sensitive lipase [169, 170]. IL-4 and IL-13 signaling through janus tyrosine kinase (JAK) and signal tranducer and activator of transcription (STAT) 3 also promotes M2-like polarization of macrophages [171]. In response, M2-like macrophages produce IL-10. IL-10 suppresses adipocyte thermogenic genes through chromatin remodeling, supporting the role of adipocyte energy storage machinery [172, 173]. Paradoxically, IL-10 has also been correlated with insulin resistance due to suppression of adipocyte energy expenditure [174]. IL-13, stimulated by IL-33, also supports M2-like macrophage polarization and regulatory T cell survival. In obesity, IL-33 producing cells, such as eosinophils, are reduced

in abundance, but can be recovered with WL [122, 123, 175]. Additionally, an IL-13 decoy receptor, IL13Rα2, can impede IL-13 mediated signaling and has elevated expression in obese adipose tissue [176].

In addition to overall reductions in anti-inflammatory cytokine signaling, obese AT is characterized by increases in inflammatory cytokines. TNFα, IL-1β, and MCP1, produced by adipocytes, T cells, and M1-like macrophages in obese AT, recruit additional monocytes that differentiate within the tissue and polarize towards an M1-like phenotype [177]. Adipocytes are directly affected by inflammatory cytokines and increases in endoplasmic reticulum stress, induction of lipolysis, and upregulation of pro-apoptotic pathways in response to cytokine exposure have been reported [178, 179]. As previously discussed, inflammatory cytokines also impair insulin sensitivity (e.g. through induction of SOCS3) in many insulin-responsive cells, including adipocytes [74, 75]. Stressed adipocytes also release saturated fatty acids, such as palmitate, into the tissue microenvironment. Palmitate and other saturated fatty acids interact with many surface receptors, including toll-like receptors (TLRs) found in innate immune cells (e.g. TLR-4), inducing activation and cytokine production in a feed-forward loop [180, 181]. Taken together, obesity induces an overall inflammatory mileu within AT, largely driven by recruitment of pro-inflammatory immune cells, that impair maintenance of the AT homeostatic niche.

1.10 CD8$^+$ T cells in systemic immunity

CD8$^+$ T cells play a well-defined role in immunity. All nucleated cells express MHC-I, which captures antigens for presentation on the surface. The majority of antigens presented on MHC-I are self-antigens that, under normal conditions, fail to elicit an immune response. However, self-reactive CD8$^+$ T cells occasionally evade these tolerogenic mechanisms, resulting in autoimmune responses [182]. T1D is a well-documented case of CD8$^+$ T cell-mediated autoimmunity and multiple specific antigens have been identified [183]. In humans, mismatch between human leukocyte antigen (HLA) isoforms, which encode

the MHC, and transplanted cells induces an autoimmune response known as transplant rejection [184]. Self-antigens on MHC-I can be replaced by peptide fragments from mis-processed proteins or viral/bacterial peptide fragments and can elicit an effective $CD8^+$ response [185–187].

1.10.1 TCR-dependent signal transduction in $CD8^+$ T cells

$CD8^+$ signal transduction is TCR-dependent, but the TCR itself does very little signaling. In the endoplasmic reticulum, the TCR is complexed with CD3 before being translocated to the surface [188, 189]. CD3 iself is a multi-subunit complex, with most of the membrane-bound protein residing in the cell cytoplasm [189]. The CD8 receptor itself is composed of two parts, an α and a β subunit. Simultanous antigen recognition by the TCR and MHC-I recognition by CD8 result in recruitment of a receptor tyrosine kinase, lymphocyte-specific protein kinase (LCK), to the cytoplasmic tail of CD8. LCK phosphorylates specific sites on the CD3ζ chain, designated as immunoreceptor tyrosine-based activation motifs (ITAMs) [190]. Additional kinases, such as Zeta-chain-associated protein kinase-70 (ZAP-70), recognize phosphorylated ITAMs and in turn phosphorylate adaptor proteins, such as linker for activation of T cells (LAT). T cell adaptor proteins act as scaffolds for recruitment and phosphorylation of downstream effector molecules like phospholipase C-γ (PLC-γ) and growth-factor receptor bound protein 2 (GRB2). Through this signal transduction network, multiple downstream transcription factors that promote growth, proliferation, survival, and cytokine production are engaged (Fig. 1.9).

Signals transduced through TCR and CD8 alone are usually insufficient to generate a productive effector response. Costimulatory signals derived from additional surface proteins on both the T cell and APC enhance TCR-dependent signal transduction [191]. CD28, a receptor found on the surface of T cells, binds the B-7 ligands CD80 and CD86 found on APCs. CD28 is essential for induction of effector activity in naïve T cells and $CD28^{-/-}$ mice fail to illicit TCR-mediated immune responses [192]. However, conflicting evidence

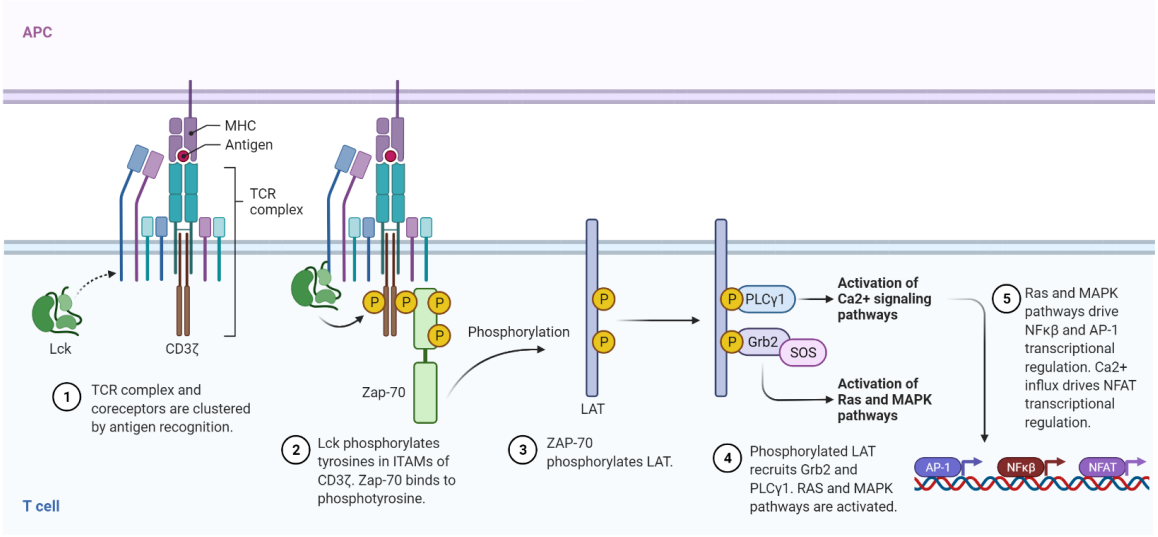

Figure 1.9: TCR signal transduction in CD8$^+$ T cells. The TCR found on the T cell plasma membrane recognizes a complimentary antigen. The CD8 receptor also recognizes MHC-I and recruits LCK. LCK phosphorylates ITAM sites on CD3, generating docking sites for ZAP-70. ZAP-70 phosphorylates LAT that in turn phosphorylates the adaptor proteins PLC-γ and GRB2, engaging the Ras and MAPK pathways. Downstream signaling from the active pathways induces expression and translocation of transcription factors that promote CD8$^+$ T cell proliferation, survival, and cytokine production. Figure modified from a BioRender template.

suggests that antigen-experienced memory CD8$^+$ T cells do not always require CD28 costimulation [193, 194]. CD$^+$ T cells also express the surface receptor CD27 that binds CD70 on the surface of APCs. Unlike CD28, CD27 is not necessary for induction of effector activity [195]. However, CD27 is critical for proliferation and survival of CD8$^+$ T cells after activation and CD27$^{-/-}$ mice fail to generate long-lived memory T cells [195]. In knockout mouse models, CD70 was not required for memory T cell survival in a viral infection model, suggesting that alternative CD27 ligands exist [196]. Importantly, induction of the costimulatory ligands on APCs can be driven by CD4$^+$ T cell help, indirectly linking CD4$^+$ and CD8$^+$ function in immunity. Mechanisms that interfere with costimulation are numerous and include both cell-extrinsic and cell-intrinsic factors. For example, recombinant antibodies that block the CD28/CD86 interaction are therapeutically efficacious in reducing autoimmunity observed in rheumatoid arthritis [197]. Likewise, CD8$^+$ T cells can

express cytotoxic T-lymphocyte-associated protein 4 (CTLA-4), which has higher affinity for CD80/CD86 than CD28 and therefore intereferes with CD28-mediated costimulation [198].

1.10.2 Clonal expansion

Proliferation of $CD8^+$ T cells is one of the earliest outcomes of successful TCR and costimulatory signaling. Nuclear factor of activated T cells (NFAT) is a transcription factor that translocates to the nucleus following PLC-γ induced calcium influx in a calcineurin-dependent manner [199]. NFAT has long been known to bind with the AP-1 transcription factor to form a DNA-binding complex that promotes expression of cytokines like interluekins 2 and 15 (IL-2 and IL-15) [200]. IL-2 and IL-15 can act in an autocrine fashion, inducing proliferation of $CD8^+$ T cells through STAT-5 [201, 202]. Additionally, APCs produce interleukin-12 (IL-12) during TCR-mediated T cell activation, which acts upon T cells to induce prosurvival and proliferation pathways [203, 204].

Expansion of effector $CD8^+$ T cells, marked by secretion of inflammatory cytokines and cytotoxic capacity, occurs in cells that have already undergone events of V(D)J recombination to produce productive TCRs. Therefore, daughter cells from antigen-stimulated $CD8^+$ T cells express the same TCR and are termed clonal T cells. V(D)J recombination provides great potential for diversity and most T cells in circulation are not clonal. In settings of antigen-mediated proliferation of T cells, such as during infection or vaccination, systemic clonal diversity decreases due to enrichment for a single clonotype (one epitope, such as for monoclonal vaccines) or multiple clones (i.e, polyclonal; >1 epitope) [205, 206]. Importantly, after resolution of the antigenic stimulus, a portion of the remaining expanded clonal T cells remains persistent and these cells have improved sensitivity to activation against the same antigen [207]. These T cells are termed memory T cells and can persist for decades in humans, providing an immunologic surveillance system with high specificity against known biological threats.

1.10.3 Long-lived memory T cells

How memory T cells are formed from the expanded pool of clonal T cells has been a question of much interest over the past three decades. Current evidence most strongly supports two models of memory T cell differentiation [208]. The first model suggests that memory cells differentiate from remaining effector cells in the absence of continued antigen stimulation. The second model suggests that early exit from the effector differentiation pathway promotes memory formation, while fully differentiated cells become terminal effectors that undergo apoptosis in the absence of continued stimulation (Fig. 1.10). Most likely, a combination of these models is accurate and dependent on strength of TCR stimulation, costimulatory molecule signaling, and presence of coinhibitory receptors [200].

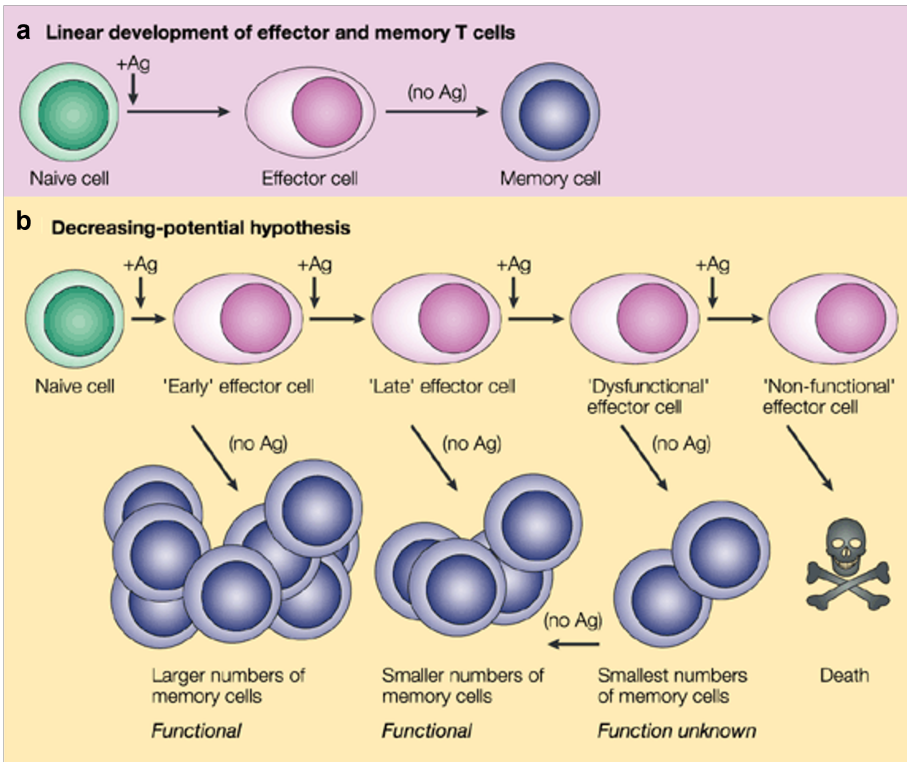

Figure 1.10: Models of memory T cell differentiation. The linear development model (**A**) suggests that memory T cells differentiate from remaining effector T cells in the absense of further antigen stimulation. The differentiation-potential model (**B**) suggests that memory T cells are formed from cells that exit the effector differentation pathway early. In this model, the terminal effector cells are unable to later differentiate into memory T cells. Figure modified with permission from Kaech *et. al*, Figure 5, 2002.

Memory T cells express unique surface markers that are used for their identification and characterization. In humans, memory T cells express the CD45 isoform CD45RO while naïve T cells express the CD45RA isoform. Expression of the C-C motif chemokine receptor 7 (CCR7) is also used to differentiate between circulating memory T cells (T_{CM}) and effector memory T cells (T_{EM}), where CCR7 is present on T_{CM} and absent on T_{EM} [209]. Mice do not express the CD45 isoforms and surface markers that correlate with memory T cells are used instead. CD44, a surface receptor with binding affinity for extracellular matrix proteins and osteopontin, is upregulated on activated T cells and maintained on memory T cells [210]. Memory T cells are also marked by low expression of CD62L, a lymphoid-homing surface protein that is shed upon TCR-induced activation [211]. Therefore, T_{CM} are considered to be $CD44^{+}CD62L^{+}$ while T_{EM} are considered to be $CD44^{+}CD62L^{low}$ [212].

1.10.4 Age-associated T cells

In humans, age is strongly associated with overall reductions in clonal diversity of $CD8^{+}$ T cells [213]. This observation is likely due to multiple contributing factors, including the life-time enrichment and homeostatic proliferation of antigen experienced cells (i.e memory T cells) and concomittant age-associated thymic involution that reduces production of naïve T cells [214]. In addition, aging is associated with increased systemic inflammation with elevated levels of circulating cytokines and chemokines (i.e inflammaging) [215]. In both humans and mice, aging is associated with the enrichment of a clonal $CD8^{+}$ T cell population in both lymphoid and non-lymphoid tissues that express coinhibitory receptors [216]. This population notably lacks expression of the cytolytic enzyme granzyme B (GZMB) and instead express the non-cytotolytic granzyme K (GZMK) [216, 217]. The mechanisms driving this unique age-associated T cell (T_{aa}) phenotype remains unclear, but GZMK produced by T_{aa} is able to induce inflammatory cytokine secretion in nearby senescent cells [216]. Taken together, $CD8^{+}$ T cells likely contribute to obesity-associated

inflammation in cellular aging, termed inflammaging [218, 219].

1.10.5 T cell exhaustion

Early during T cell activation, a cohort of proteins can be expressed and act as immune check points. Programmed cell death protein 1 (PD-1) is upregulated in the first 24 hour of TCR activation in $CD8^+$ T cells [220]. PD-1 plays a critical role in modulating T cell activity and suppresses effector T cell function in the presence of cognate programmed cell death ligands (PD-L1 and PD-L2). PD-1 deficient mouse models develop immunopathology due to either impaired T cell response against pathogens or unregulated effector T cell autoimmune activity [221, 222]. At the same time, loss of PD-1 on effector T cells reduces survival and many T cells become terminally exhausted, a term associated with inability of T cells to respond to antigenic stimuli through effector functions [220, 223].

PD-1, PD-L1, CTLA-4, and other coinhibitory proteins/receptors are of great interest therapeutically. Antibody immunotherapies that block or inhibit signaling through coinhibitory or costimulatory receptors can improve T cell response in settings of exhaustion and dysfunction (e.g cancer) or blunt T cell response in settings of excessive activity (e.g rheumatoid arthritis). Recent reports have identified a population of PD-1 expressing $CD8^+$ T cells in obese AT [224]. Interestingly, while obese individuals with cancer have more rapid tumor progression and associated immune dysfunction, in some cases checkpoint blockade (e.g PD-1 immunotherapy) has improved efficacy and overall survival during treatment is higher [225]. These findings suggest that AT resident T cells may be responsive to immunotherapy and also that AT can contribute effector T cells in response to systemic demands.

1.11 Adipose tissue as a T cell reservoire

In addition to potential roles in anti-tumor immunity, AT T cells may play important roles in other diseases. For example, human immunodeficiency virus (HIV) infects T cells, resulting in impaired systemic immune function, and HIV infected T cells are found in AT [226].

Currently anti-retroviral therapies are efficacious and patients with controlled HIV have similar life expectancy to HIV-negative patients [227]. However, HIV-positive patients are at increased risk of metabolic syndrome and cardiovascular disease [228]. Interestingly, AT from HIV$^+$ patients is enriched for T_{EM}, suggesting a link between metabolic risk and long-lived memory T cell populations in AT [229, 230]. While this finding requires further experimentation, it begs an interesting question: Can AT act as a reservoire for T cells that contribute to disease pathology, in part explaining increased risk of disease progression in many obesity-associated comorbidities?

1.12 Summary

Chapter I reviews our current knowledge of physiology, inflammation, and immunity as it pertains to AT during obesity and WL. However, many unknowns remain that limit our understanding of the interplay between immune cells in AT and how these cells respond to WL. Since immune-mediated inflammation in AT is a critical component of obesity-associated pathology and so few therapeutics have been successful at reducing weight regain, better understanding of immune cell function during obesity, WL, and weight regain is essential. Fortunately, improvements in the availability and utility of tools that assess a large number of cells at single-cell resolution can offer insights into these important biological questions. In Chapter III, I describe the use of cellular indexing of transcriptomes and epitopes (CITE-seq) to accurately annotate immune cell populations and report changes in abundance and transcriptional profile in AT during settings of obesity, WL, and WC. In Chapter IV, I expand upon this work by focusing on CD8$^+$ T cells, identifying clonal enrichment for dysfunctional T cells that may be responsive to diabetes-associated antigens. In Chapter V, I describe a thorough assess systemic glucose regulation and identify a defect in insulin secretion that contributes to WC-associated impaired glucose disposal. Finally, in Chapter VI, I summarise the work that has been completed and highlight additional questions that remain unanswered.

CHAPTER 2

Materials and Methods

2.1 Animal models

All animal procedures were approved by Vanderbilt's Institutional Animal Care and Usage Committee. The animal facility housing room was maintained at a controlled temperature (23°C) and humidity (30%) and 12 h light-dark cycles. Mice were provided free access to water and were housed on paper bedding. Body composition analysis was performed in Vanderbilt's Mouse Metabolic Phenotyping Center (MMPC) using a Bruker Minispec (Woodlands, TX). Euthenasia was performed by isoflurane overdose, immediately followed by cervical disslocation. Animals were perfused through the left ventricle of the heart with 20 mL of 1X PBS to remove circulating blood. Tissues were isolated, weighed, and either fixed in 1% paraformaldehyde (AT, Liver), 4% paraformaldehyde (pancreas, spleen), or further processed to isolate immune cells.

2.1.1 Diet-induced obesity

For Chapters III and IV, 7-8 week old male C57BL/6J mice were purchased from Jackson Laboratory and maintained in the Vanderbilt animal facility. Animals were acclimated to the facility for one week and then cages were randomized to receive study diets *ad libitum* unless otherwise stated. Lean mice were provided diet containing 10% kcal from fat (low fat diet; LFD; Research Diets #D12450B) for 27 weeks. Obese mice received LFD for the first 9 weeks, followed by 18 weeks of diet containing 60% kcal from fat(high fat diet; HFD; Research Diets #D12492). WL mice were provided HFD for the first 18 weeks, followed by 9 weeks of LFD. WC mice received HFD for the 9 weeks, followed by 9 weeks of LFD and then an additional 9 weeks of HFD. For shorter-term diet studies ($\leq$18 weeks) shown in Chaper III, Lean mice were provided LFD for 3, 9, or 18 weeks. Obese mice received HFD for 3 or 9 weeks, or were given LFD for 9 weeks and then switched to

HFD for 9 weeks. WL mice received HFD for 9 weeks, and then were switched to LFD for 9 weeks.

For Chapter V, lean, obese, and WC groups were provided diet as in Chapters III and IV. An additional caloric restriction (CR) group was included, which received HFD for the entire 27 weeks. Between weeks 9-18, CR mice were provided with only enough food to match the estimated caloric intake of WC mice receiving LFD during the same period each day, thereby limiting their food intake.

For all studies, animals and remaining food from each cage were weighed weekly. Food provided was also weighed before being added to each cage.

2.1.2 Antibody treatment

For the anti-CD8 antibody depletion pilot study, C57BL/6J male mice were placed on HFD for a total of 12 weeks. Between weeks 7 and 8, mice were treated every other day (3 times) with 100 μg monoclonal anti-CD8 antibody (BioLegend Cat#114120) or IgG-matched control antibody (BioLegend Cat#400566) via intraperitoneal delivery. For the WC anti-CD8 antibody depletion study, obese or WC C57BL/6J male mice were treated every other day (3 times) with 100 μg monoclonal anti-CD8 antibody or IgG-matched control antibody via intraperitoneal delivery between weeks 17 and 18.

For the anti-PD-1 neutralizing antibody studies, C57BL/6J male mice were placed on HFD for a total of 12 weeks. Between weeks 8 and 12, mice were treated every other day (3 times) with 200 μg monoclonal anti-PD-1 antibody (BioXCell Cat#BE0146) or IgG matched control (BioXCell Cat#BE0089) antibody via intraperitoneal delivery.

2.2 Immune cell isolation and flow cytometry

Tissue isolated for flow cytometry was weighed, minced in 1X PBS without Ca^{2+} or Mg^{2+} and with 1% fetal bovine serum using fine scissors, and placed on ice until tissues from all animals were collected.

2.2.1 Tissue dissociation

For AT, tissue was enzymatically digested in 6 mL of 2 mg/mL collagenase type IV (Worthington #LS004189) for 20 minutes at 37 °C on an orbital shaker. Tissue was briefly vortexed after 10 minutes of digestion. After 20 minutes, enzymatic digestion was neutralized by the addition of 10 mL cold PBS with 1% FBS solution. Digested tissue was passed through a 100 μL filter and centrifuged at 400 xg for 5 minutes at 4°C. The top layer containing adipocytes was removed and the remaining supernatant was poured off to leave a pellet containing the stromal vascular fraction (SVF). Erythrocytes were lysed using 3 mL of ACK lysing buffer (Gibco #A1049201) for 3 minutes on ice, then diluted with 10 mL cold PBS with 1% FBS solution and centrifuged at 400 xg for 5 minutes at 4°C. Remaining cells were resuspended in 400 μL cold PBS with 1% FBS solution and passed through a 35 μm filter for downstream processing steps.

For spleen, tissue was passed through a 100 μL filter using the blunt end of a rubber syringe plunger and centrifuged at 400 xg for 5 minutes at 4°C. The supernatant was then poured off and erythrocytes in the remaining pellet were lysed using 3 mL of ACK lysing buffer for 3 minutes at room temperature (RT). ACK lysing buffer was diluted with 10 mL cold PBS with 1% FBS solution and cell suspension was centrifuged at 400 xg for 5 minutes at 4°C. Remaining cells were resuspended in 1 mL cold PBS with 1% FBS solution and passed through a 35 μm filter for downstream processing steps.

For blood, samples were diluted with 10 mL of ACK lysing buffer centrifuged at 400 xg for 3 minutes at 4°C. Supernatant was removed using a vacuum flask attached to a sterile pipette and ACK lysing buffer was repeated once. The supernatant was again removed and remaining cells were resuspended in 400 μL cold PBS with 1% FBS solution before being passed through a 35 μm filter for downstream processing steps.

2.2.2 Flow cytometry

Estimated number of cells and viability of isolated cells was determined by taking an aliquot of sample cell suspension. Cells were labeled with 0.25 μg/mL 4,6-diamidino-2-phenylindole (DAPI) prior to measurement on a Miltenyi MacsQuant 10 flow cytometer. For staining, approximately 1 million viable cells were immunolabeled in 100 μL with antibodies at a pre-determined concentration for 20 minutes on ice covered with foil. Samples were washed twice with 1-2 mL of cold PBS with 1% FBS solution and centrifuged at 400 xg for 5 minutes at 4°C. Samples were resuspended in 200 μL PBS with 1% FBS for measurement on a Miltenyi MacsQuant 10 flow cytometer. The flow cytometry panel used for measurement of AT $CD8^+$ T_{EM} is described in Table 2.1.

Target	Fluorophore	Purpose	Clone	Concentration
DNA	DAPI	(-) Cell Viability		0.25 μg/mL
CD45	BV510	(+) Pan-Leukocyte	30-F11	1 μg/mL
CD8α	FITC	(+) $CD8^+$	53-6.7	2.5 μg/mL
CD62L	PE	(low) $CD8^+$ T_{EM}	MEL-14	1 μg/mL
PD-1	PerCP-Cy5.5	(+) Early Activation/Exhaustion	RMP1-30	1 μg/m
CD44	PE-Cy7	(+) $CD8^+$ T_{EM}	IM7	1 μg/mL
CD4	AF-700	(+) $CD4^+$	RM4-5	2.5 μg/mL
TCR-β	APC-Cy7	(+) T Cells	H57-597	1 μg/mL

Table 2.1: $CD8^+$ T_{EM} Flow Cytometry Panel

For intracellular immunolabeling, cell surface markers were first immunolabeled as before. Then, cell suspensions were fixed and permeabolized using the Cyto-Fast Fix-Perm Buffer Set (Biolegend #426803). Samples were washed and immunolabeled in permeabilization buffer at RT with pre-determined concentrations of intracellular antibodies.

2.2.3 Cell sorting

Fluorescence-activated cell sorting was performed on a BD FACSAria III at Vanderbilt's Flow Cytometry core facility. Samples were prepared and immunolabled as discussed in the Flow Cytometry section. After sorting, sample cell suspensions were centrifuged at 400 xg for 5 minutes at 4°C for subsequent experiments.

For magnetic cell sorting, samples were prepared and one surface marker was immunolabeled with a magnetic bead-conjugated antibody. Samples were washed and sorting was performed on a Miltenyi AutoMACs magnetic sorter. After sorting, sample cell suspensions were centrifuged at 400 xg for 5 minutes at 4°C for subsequent experiments.

2.3 Ex vivo cell stimulation

Cells were isolated as described in the Tissue Dissociation section and split into two tubes for each sample (one unstimulated and one stimulated). Both of the unstimulated and stimulated pairs were treated with 5 μg/mL Brefeldin A (Biolegend #420601) for 6 hours. Additionally, stimulated samples received phorbol 12-myristate-13-acetate (PMA) and ionomycin (Biolegend #423302) for the entire 6 hour treatment duration. Samples were then washed and immunolabeled for flow cytometry as described in the Flow Cytometry section.

2.4 RNA isolation

RNA isolation was performed at RT according to manufacturer instructions using the RNeasy Plus Mini kit (Qiagen #74134). Specifically, isolated cells or tissue were lysed and homogenized in 350 μL RLT buffer containing 10 μL of 14.3 M β-mercaptoethanol. Cell lysate was transfered to a genomic DNA column and centrifuged for 1 minute at 8,000 xg. The column was discarded and 350 μL of 70% EtOH was added. Sample was then transfered to a new spin column, centrifuged, and washed twice, discarding the flow-through after each centrifugation step. Sample was eluted from the membrane in 30 μL of RNase-free water by centrifuging at 21,000 xg for 1 minute. The column was discarded and flow-through was used for further sample preparation.

2.5 RNA sequencing

Sample processing and sequencing were completed by the VANderbilt Technologies for Advanced GEnomics core (VANTAGE).

2.5.1 Bulk RNA-seq

Isolated RNA was submitted directly to VANTAGE for subsequent processing. Poly-A selection for enrichment of mRNA was performed using poly-A magnetic beads (New England Biolabs #E7490L) and cDNA library preparation was performed using the NEBNext Ultra kit (New England Biolabs #7760L). Paired-end sequencing (150 bp) was performed on an Illumina NovaSeq 6000 targeting 50 million reads per sample. Demultiplexed FastQ files were processing using fastp version 0.23.1 [231] to trim adapters and remove poor quality sequences. Quantification of sequences was performed using Salmon version 1.5.2 [232] by aligning to the C57BL/6J GRCm39 reference assembly. Data was analyzed using EdgeR version 3.36.0 [233] in R version 4.1. Differential expression between group comparisons was assessed via the Exact Test function (EdgeR) and results were confirmed using DESeq2 version 3.15 [234] in R.

2.5.2 Single cell RNA-seq and CITE-seq

All samples were submitted to VANTAGE and processed for sequencing on the same day to minimize batch effects. Sample preparation was conducted using the 5' assay for the 10X Chromium platform (10X Genomics) targeting 20,000 cells per diet group (5,000 cells per biological replicate). 50,000 reads per cell were targeted for PE-150 sequencing on an Illumina NovaSeq6000. FastQ files obtained from sequencing were processed using CellRanger V3 (10X Genomics) with feature barcoding. Outputs from CellRanger were further processed using Velocyto V0.17 [235] for downstream RNA velocity analysis. The R package SoupX V1.5.2 [236] was used to remove ambient contaminating RNA. The Seurat V4 [237] R package was used for quality control, data set integration, clustering, cell type annotation, differential expression, and visualization. The Python package scVelo V0.2.3 [238] was used for modeling and visualizing RNA velocity through R using Reticulate V1.22. Strict quality control parameters were utilized post sequencing to ensure that only viable cells, which could be traced back to each individual mousem, were used for fur-

ther analysis. For quality control of sequenced cells, only cells that had at least 200 gene features, at least 500 total measured RNA sequences, and less than 5% mitochondrial RNA content, were retained. Furthermore, only cells designated as singlets after hashtag demultiplexing (i.e. cells containing at least one hashtag, but not more than one) were used for visualization and analysis. DoubletFinder V3 [239] was used to detect heterotypic doublets and further confirm singlets. Recipricol PCA-based integrated was used to integrate the four sequencing datasets. For more detailed pre-processing information, the minimal necessary data and three vignettes containing code for preprocessing, data integration, and cell type annotation at: https://github.com/HastyLab/Multiomics-WeightCycling-Vignettes.

Cluster annotation was performed following dimensional reduction using the integrated data assay. First, broad clusters were identified using low resolution (0.4) and annotated by common cell type markers. Each identified broad cluster, referred to as "Cell Types", were further subclustered and subclusters were annotated by comparing differentially expressed markers to published literature. Cluster annotations were further supported using SingleR V1.6.1 [240] with the Immgen and MouseRNAseq databases from the Celldex package V1.2.0 [240].

All downstream analyses comparing cells across diet groups, individual biological replicates, or clusters were performed using the normalized RNA assay. Differential expression was performed using the Wilcoxon Ranked-Sums test in Seurat V4 for single cells. For pseudobulk analysis on the web-based tool, the likelihood ratio test in DESeq2 V1.32.0 was used. Differential abundance testing was conducted using the MiloR package V1.0.0 [241] in R. Metaclusters identified by MiloR were further tested with permutation testing using the scProportionTest R package V0.0.9000 (https://github.com/rpolicastro/scProportionTest). For exploring macrophage phenotype, the R application MacSpectrum V1.0.1 [114] was used with provided index information. RNA velocity was estimated using Veloctyo and visualized using scVelo.

Raw sequencing files, processed data matrices, dimensional reduction embeddings,

cell metadata, and a fully integrated Seurat v4 R data object associated with Chapter III are available via the NCBI GEO with the primary accession code GSE182233. Example code to reproduce our processed and integrated Seurat v4 object used in Chapter III is available at: https://github.com/HastyLab/Multiomics-WeightCycling-Vignettes. This GitHub repository contains information for 1) Preprocessing and Quality Control, 2) Data Integration, and 3) Cell Type Annotation. All code necessary to reproduce the figures for Chapter III are available at via GitHub at: https://github.com/HastyLab/Multiomics-WeightCycling-Figures.

2.5.3 Single cell V(D)J sequencing

Raw V(D)J sequencing files were processed using CellRanger V3 (10X Genomics). Filtered contig output files were associated with annotated scRNA-seq data using custom-built scripts. Briefly, cell barcodes were aligned between transcript and V(D)J datasets. Associated nucleotide and translated amino acid sequence for each gene (V, D, J, and C) of each α/β chain was preserved. The resulting complimentarity determining region 3 (CDR3) nucleotide and protein sequences were also retained for each α/β chain.

For generating α/β TCR constructs, the identified gene usage and associated CDR3 amino acid sequence for each chain was used to generate the full α and β TCR chain sequences via StitchR v1.0.0 [242]. Nucleotides encoding a BglII restriction site were added to the beginning of the α chain sequence and nucleotides encoding a T2A linker region were incorportated aat the end of the α chain. Nucleotides encoding a BamH1 restriction site were added to the end of the β chain along with a termination sequence. The resulting approximately 1,800 bp nucleotide sequences can be cloned into a pMIG-II plasmid (Addgene Cat#52107).

2.6 Immunoblotting

Immunoblotting was performed on inguinal adipose tissue (iWAT) and gastrocnemius muscle. Triton X-100 tissue lysates were prepared 1:1 in Laemmli buffer. Prepared pro-

tein samples (5-15μg/lane) were separated via Criterion Tris-glycine eXtended-PAGE precast gels (Bio-Rad). The same amount of protein was loaded within each respective tissue across gels. Proteins were transferred onto polyvinylidene difluoride membranes and blocked overnight at 4with 5% non-fat dry milk (Tris buffered saline 0.05% Tween 20, TBS-T). Membranes were washed with TBS-T and probed with primary antibodies overnight at 4. After primary antibody incubation, membranes were washed and probed with species appropriate HRP-conjugated secondary antibodies in 5% nonfat dry milk for 2 hours at RT. Individual bands were detected via chemiluminescence. Intensity of individual protein bands were quantified using Image Lab (version 6.0.0, BioRad Laboratories, Inc.), and expressed as a ratio to β-actin. For phosphorylated protein quantification, band intensities were expressed as a ratio to the parent protein (e.g. pAKT relative to total AKT). Values are expressed as fold-difference normalized to the lean control group.

2.7 Tissue imaging

All imaging was performed on a Leica DMI8 widefield microscope and captured with a Leica DFC9000GT camera.

2.7.1 Tissue preparation

AT tissue was fixed in 1% paraformaldehyde for 1 hour and stored in 70% EtOH overnight before paraffin embedding by the Vanderbilt Tissue Pathology Shared Resource core. Tissues were sectioned at 5 μm and allowed to dry overnight.

For liver and pancreas, tissues were fixed in 4% paraformaldehyde for 2 hours and stored in 70% EtOH overnight before paraffin embedding by the Vanderbilt Tissue Pathology Shared Resource core. Tissues were sectioned at 5 μm and allowed to dry overnight.

2.7.2 Histology

Slides were deparaffinized in xylene and dehydrated throuugh an EtOH gradient. Then, slides were washed in deionized water and stained with Mayer's hematoxylin (Sigma

Cat.#MHS1) for 8 minutes. Slides were rinsed in running tap water for 5 minuutes. Slides were further rinsed in 95% EtOH by dipping 10 times, then counterstained in Eosin-Y (Sigma Cat.#318906) for 30-60 seconds. Slides were dehydrated through 95% and 100% EtOH, and cleared in xylene washes before being mounted with Permount (FisherScientific Cat.#SP15-100).

2.7.3 Immunofluorescence imaging

For AT, slides were deparaffinized in xylene and dehydrated through an EtOH gradient, then immunolabeled with Rabbit anti-Perilipin-1 (Abcam #9349T; Clone D1D8) at 1:200 overnight at 4°C. After washing, Goat anti-Rabbit IgG conjugated to AF647 (Abcam #ab150079) was applied for two h at RT prior to washing and coverslipping with Prolong Gold (Invitrogen #P36931) containing DAPI. Image tiles were taken across the entirety of each section and stitched using the LAS X software suite. Merged images were processed in ImageJ and adipocytes were counted using an in-house macro. Briefly, the AF647 channel was processed by enhancing contrast and applying a gaussian blur with a sigma = 5. Background subtraction was performed with a rolling basis of 30. Auto thresholding using the "Triangle dark" setting was used to preserve adipocyte borders. The images were then skeletonized and then Image J's analyze particles function was used with a size threshold range of 300-315000, circularity of 0.4-1. Only cells with a measured diameter greater than 10 microns were included in our analysis. Data was plotted in R V4.1.

For pancreas, slides were deparaffinized in xylene and dehydrated through an EtOH gradient. Antigen retrieval was performed by microwaving slides for 14 minutes in sodium citrate buffer containing 10 mM trisodium citrate in 1 L of water. Immunolabeling with primary antibody was performed overnight at 4°C and with secondary at RT for 2 hours. Primary antibodies used in Chapter V are reported in Table 2.2. Slides were coverslipped with Prolong Gold containing DAPI and dried for at least 24 hours. Image tiles were taken across the entirety of each section and stitched using the Leica LAS X software

suite. Images shown were taken at 40X magnification (332.79 x 332.79 μM x 332.79 μM; 6.1539 pixels/μM). For islet area quantification, every 10th slide was used (3 slides/mouse) to ensure no islet was measured twice (minimum distance between sections of 150 μM). ImageJ was used to threshold for DAPI and insulin and the area of each threshold was outlined manually for total pancreas area and islet area, respectively. Islets containing fewer than five total nuclei were excluded. For quantification of α/β cell ratio, QuPath was used to identify islets and select intra-islet cells based on DAPI$^+$ nuclei. Cells were designated as α, β, or other based on cytoplasmic pixel intensity of glucagon or insulin. Further annotation of Ki-67$^+$ cells was performed using QuPath based on positive nuclear staining.

Antibody	Manufacturer	Identifier	Dilution
Rabbit anti-insulin	Cell Signaling Technology	Cat. #3014	1:1000
Guinea Pig anti-insulin	Dako	Cat. #IR00261-2	
Mouse anti-glucagon	MilliporeSigma	Cat. #G2654	1:500
Rabbit anti-glucagon	Cell Signaling Technology	Cat. #2760	1:500
Rabbit anti-Ki-67	Cell Signaling Technology	Cat. #9129	1:500
Rabbit anti-NKX6.1	Novus Biologicals	Cat. #49672	1:400
Rabbit anti-MAFA	Cell Signaling Technology	Cat. #79737	1:1000
Goat anti-Rabbit IgG H&L (AlexaFluor 488)	Abcam	Cat. #ab150077	1:1000
Goat anti-Rabbit IgG H&L (AlexaFluor 555)	Abcam	Cat. #ab150078	1:1000
Goat anti-Rabbit IgG H&L (AlexaFluor 647)	Abcam	Cat. #ab150070	1:1000
Goat anti-Mouse IgG H&L (AlexaFluor 555)	Abcam	Cat. #ab150114	1:1000
Goat anti-GuineaPig IgG H&L (AlexaFluor 488)	Abcam	Cat. #ab150185	1:1000

Table 2.2: Primary and secondary antibodies used for immunofluoresence imaging for Chapter V.

2.7.4 Electron Microscopy

For Chapter V, tissue preparation was performed by Vanderbilt's Cellular Imaging Shared Resource core and image analysis was performed with extensive support from Drs. Rafael Arrojo e Drigo, Nathan C. Winn, and Monica Bhanot. Mice were euthanized via lethal dose of isoflurane for tissue harvest and pancreata were fixed in 2% glutaraldehyde/2% PFA/0.1 M sodium cacodylate/2 mM $CaCl_2$ for 1 hour at RT, followed by 24 hours at 4°C. Tissue was immersed in 1% tannic acid, followed by 1% uranyl acetate, and en bloc stained with

1% uranyl acetate. The samples were dehydrated in a graded ethanol series and infiltrated with Epon-812 using propylene oxide as the transition solvent; the resin was polymerized at 60°C for 48 hours. Samples were sectioned on a Leica UC7 at a nominal thickness of 70 nm, collected onto 300 mesh nickel grids, and post-stained with 2% uranyl acetate and lead citrate. Imaging was performed on a Tecnai T12 operating at 100 keV using an AMT CMOS camera. Single images were acquired using the AMT software. Images for tiling were acquired and stitched using SerialEM and IMOD/eTomo respectively. Segmentation of individual insulin granules was performed using semi-supervised machine learning segmentation tools and thresholding. Briefly, mature insulin granules in random quadrants (between 256 and 512 pixels in XY) of large islet EM micrographs were manually segmented using Labkit to create binary masks to serve as ground-truth (GT) images. At least 5x random GT-EM image pairs per animal were used to train a 2D-Unet model using Aivia software (Leica Microsystems). The trained model was applied to the large EM micrographs to generate probability maps that were thresholded to create a binary 8-bit mask with the top 10 highest probability pixels. Each resulting 8-bit object was detected using the "analyze particles" function using a threshold of $>2500\text{pixel}^2$. Individual granules were approximated by applying a binary watershed and the "measurement" function was applied to determine insulin granule area. The area of the nuclei, vessels, and non-beta-cells were subtracted from the total tissue area to determine the beta cell cytoplasmic area in each image. To determine the relative density of empty secretory granules, six unique regions within β cells of each EM image per mouse were randomly selected, and the number of mature insulin granules and empty vesicles were manually quantified. All the above analyses were performed while blinded to image and treatment group identity.

2.8 Glucose tolerance test

After a 5 h fast basal blood glucose levels were measured (average of -60 and -10 min recording) via tail cut followed by intraperitoneal (ip) injection of 2.0 g dextrose/kg fat free

mass. Post injection blood glucose was sampled at 15, 30, 45, 60, 90, 120, and 150 minutes using a hand-held glucometer (Bayer Contour Next EZ meter). Glucose area under curve from baseline was calculated using the trapezoidal rule.

2.9 Mixed-meal tolerance test

After a 5 h fast, blood was collected from a carotid artery indwelling catheter before oral gavage administration of a liquid meal (Ensure, 15 kcal/kg fat free mass or 2.5% of total daily energy intake). The percentage of daily energy intake measurement was based on average daily energy intake over 3 weeks preceding the meal challenge. Arterial blood was collected at 15, 30, 45, and 60 minutes post gavage.

2.10 Plasma Biochemistry

Plasma non-esterified fatty acids (NEFA) (Wako HR series NEFA-HR) were determined via colorimetric assay according to manufacturer's instruction. Plasma insulin and c-peptide were determined by radioimmunoassay (Millipore #PI-13K) at Vanderbilt's Hormone Assay & Analytical Services core. The assay utilizes ^{125}I-labled insulin and a double antibody technique to determine serum, plasma, or tissue culture media insulin levels. The assay was modified by the Vanderbilt Hormone and Analytical Services Core to improve the sensitivity to 0.01 ng/ml for the sensitive mouse assay and 0.1 ng/ml for the regular mouse assay. The crossreactivity between human and mouse insulin is 100% in the radioimmunoassay used. Exogenous insulin was determined using a human-specific insulin antibody (Alpco #80-INSHU-E01.1).

2.11 Islet perifusion

Islet collection and perifusion studies were conducted by the Vanderbilt University Medical Center's Islet Procurement & Analysis Core. Mouse islets were isolated as described previously [243] and cultured in RPMI 1640 containing 10% FBS and 5 mmol/L glucose at 37°C overnight. Glucose stimulated insulin secretion (GSIS) was assessed by perifu-

sion using size-matched islets and normalized to islet equivalents. Three secretagogues, glucose (16.7 mmol/L), 3-isobutyl-1-methylxanthine (IBMX; 100 μmol/L), and potassium chloride (KCl; 20 mmol/L) were used during perifusion. Insulin in the culture medium was determined by enzyme linked immunosorbent assay (ELISA). Islet size was assessed with MetaMorph version 7.7 (Universal Imaging).

2.12 Hyperinsulinemic euglycemic clamp

Hyperinsulinemic euglycemic clamp experiments performed for Chapter V were carried out by Vanderbilt's MMPC. [3-^{3}H]glucose was primed and continuously infused from t=-90 min to t=0 min (0.04 μCi/min). The insulin clamp was initiated at t=0 min with a continuous insulin infusion (4 mU/kg/min) and variable glucose infusion rate (GIR), both maintained until t=155 min. The glucose infusate contained [3-^{3}H]glucose (0.06 μCi/μL) to minimize changes in plasma [3-^{3}H]glucose specific activity. Arterial glucose was monitored every 10 min to provide feedback to adjust the GIR so as to maintain euglycemia. Erythrocytes were infused to compensate for blood withdrawal. [3-^{3}H]glucose kinetics were determined at -15 min and -5 min for the basal period, and every 10 min between 80-120 min for the clamp period to assess whole-body glucose appearance (R_a), glucose disappearance (R_d), and endogenous glucose production (endoR_a). A 13 μCi intravenous bolus of 2-[^{14}C]-deoxyglucose ([^{14}C]2DG) was administered at 120 min to determine the glucose metabolic index (R_g), an index of tissue-specific glucose uptake. Blood samples were collected at 122, 125, 130, 135 and 145 min to measure [^{14}C]2DG disappearance from plasma. At 145 min, mice were anesthetized, euthanized, and tissues immediately harvested and freeze-clamped.

2.13 Hyperglycemic clamp

Hyperglycemic clamp experiments performed for Chapter V were carried out by Vanderbilt's MMPC. Catheters were surgically placed in the carotid artery and jugular vein for sampling and infusions, respectively, one week before clamps were performed. Mice were

fasted for 5h before clamp procedures. Mice were neither restrained nor handled during clamp experiments. Arterial glucose was clamped at 250 mg/dL using a variable GIR. GIR is an index of glucose tolerance during the hyperglycemic clamp. Plasma insulin, C-peptide, and NEFA were determined during clamps. Full step-by-step descriptions of the surgery, isotope clamp method, and calculations are available from Vanderbilt's MMPC website (www.vmmpc.org).

2.14 Statistics

Student's t-tests were run for between group comparisons. In experiments that contained more than two groups, one-way analysis of variance (ANOVA) or two-way ANOVA models were conducted with pairwise comparisons corrected for multiple comparisons using Tukey, Sidak, or Bonferroni corrections. Brown-Forsythe correction was applied to groups with unequal variance. In Chapter III, Wilcoxon-Ranked Sum test was used for differential expression between scRNA-seq clusters. Data are presented as mean ± standard error of the mean (SEM). An adjusted p value of <0.05 was used to determine significance.

CHAPTER 3

Multiomics reveals persistence of obesity-associated immune cell phenotypes in adipose tissue during weight loss and weight regain in mice

Adapted from Cottam, M.A., et. al. *Nature Communications*, 2022. May 26, 2022. doi: 10.1038/s41467-022-30646-4

3.1 Introduction

Obesity affects more than 650 million adults worldwide and is associated with nearly every leading cause of death, including cardiovascular disease, diabetes, and several types of cancer [244, 245]. In lean AT, regulatory type 2 immune cells contribute to tissue homeostasis [246–249]. In contrast, weight gain promotes the infiltration of circulating immune cells, and tissue resident cells polarize towards a type 1 pro-inflammatory phenotype. These inflammatory changes contribute to metabolic dysfunction – promoting lipolysis, fibrosis and insulin resistance.

WL is known to improve metabolic outcomes associated with obesity. However, low success rates and failure to maintain lost weight are common, with recent studies reporting that most individuals (>60%) regain weight within a few years [11, 14–16]. Importantly, WC further increases risk for developing diabetes and cardiometabolic diseases in humans [24, 26, 27]. We generated a mouse model of WC using an alternating HFD and LFD feeding paradigm [250]. These mice display worsened glucose tolerance compared with obese mice, despite similar body weight, fat mass, and total time on the HFD. As assessed by flow cytometry, metabolic dysfunction was associated with increases in AT T cell populations, but not macrophages, consistent with other models of WC [251].

With obesity, cells can upregulate type 1 and type 2 transcriptional profiles and metabolic pathways simultaneously [114, 115]. Moreover, recent single-cell RNA-sequencing (scRNA-seq) studies have revealed multiple distinct AT immune cell populations and subsets, such

as LAMs, which are unique from traditional macrophage polarization states [114, 116, 252]. scRNA-seq allows for the interpretation of changes to immune populations and unbiased gene expression across the entire immune landscape simultaneously. Further developments, such as CITE-seq and cell hashing, offer opportunities to interrogate surface protein repertoire and include biological replicates during scRNA-seq experiments [253, 254].

To date, no studies have thoroughly characterized AT immune populations following WC by a comprehensive technique like scRNA-seq, and many published scRNA-seq datasets are difficult to explore further without bioinformatics expertise. Moreover, most reports are limited to single cell types and fail to capture the dynamic changes across multiple immune cell types. Due to the associated costs, personnel time, and necessary bioinformatics training, there remains a critical need to improve accessibility of high-resolution data provided within scRNA-seq datasets. Therefore, the aims of this study were two-fold: 1) To comprehensively map the changes in adipose immune populations with obesity, WL, and WC and identify key links between WC and metabolic disease and 2) To provide a freely accessible resource for hypothesis generation and testing for the scientific community in a novel dataset that spans four distinct physiological states of AT. We report that obesity-associated inflammatory changes such as T cell exhaustion, antigen presentation, lipid handing, and inflammation persist following WL and worsened with weight regain in male mice, suggesting a memory-like immunological imprinting that may contribute to WC-accelerated metabolic disease.

3.2 Results

3.2.1 Diet induced WC exacerbates glucose intolerance in male mice

We used 9-week bouts of HFD and LFD feeding to generate models of obesity, WL, and WC in male mice (Fig. 3.1a) [250]. This model is robust, as shown across 6 cohorts (totaling 252 mice). Changes in weekly body mass and energy intake were tightly linked to prescribed diets (Fig. 3.1b & 3.1c). Cumulative energy intake was not different between

obese, WL, and WC groups (Fig. 3.1d). After 26-weeks on diet, obese and WC mice had identical lean and fat mass, which was elevated compared to lean and WL mice (Fig. 3.1e). WL animals had greater lean mass but no differences in fat mass compared to lean controls. Obese mice had impaired glucose tolerance by intraperitoneal glucose tolerance tests (ipGTT) compared to lean mice, which was further worsened by WC (Fig. 3.1f). Fasting insulin concentrations were not different between obese and WC animals (Obese, 5.2 $\pm$ 0.8 ng/ml and WC, 5.1 $\pm$ 0.9 ng/ml, p=0.9, n=8/group). A small improvement in glucose tolerance was observed in WL mice compared to lean control mice. Fat free tissue comprises the bulk of insulin-stimulated glucose disposal and is positively associated with postprandial glucose clearance [255, 256]. Given that lean mass was greater in WL versus lean mice and WL animals had greater glucose clearance than the lean group, lean tissue mass was covaried against GTT area under the curve (AUC). The decrease in glucose clearance in WL compared to lean animals manifested after statistically accounting for differences in lean mass (estimated marginal means: Lean AUC, 19,865 $\pm$ 915; WL AUC, 16,750 $\pm$ 1,125, $p<0.05$).

We also assessed the effects of our diet paradigm at different time intervals during the diet intervention on body composition and glucose tolerance (Fig. 3.2). At 3, 9, and 18 weeks of HFD, total body mass, lean mass, and fat mass are increased and glucose tolerance is impaired compared to lean control mice. A diet switch at 9 weeks to induce WL (9wk HFD $\rightarrow$ 9wk LFD) reduced total body mass, lean mass, and fat mass, as well as improved glucose tolerance compared to obese mice (9wk LFD $\rightarrow$ 9wk HFD).

Liver and sAT weights were similar between lean vs. WL and obese vs. WC mice. However, WL mice had reduced eAT mass compared to lean mice, and WC mice had increased eAT mass compared to obese mice (Fig. 3.3a). While sAT and liver mass as a proportion of total body mass were similar between lean vs. WL mice and obese vs. WC mice, the percentage of eAT mass was significantly higher in WC vs. obese mice, albeit very modest (Fig 3.3b). Immuno-fluorescence staining for perilipin-1 (Plin1), a lipid

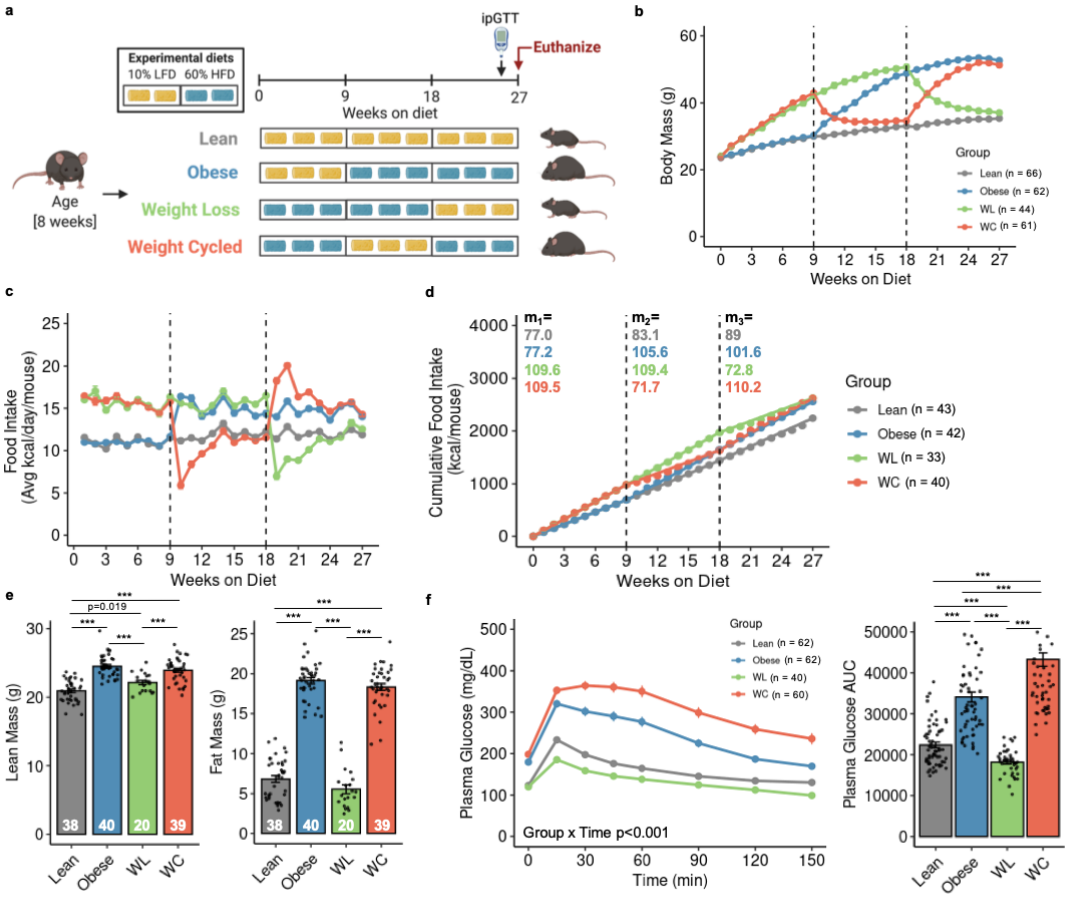

Figure 3.1: Mouse models of lean, obese, weight loss (WL) and weight cycling (WC). **a** Schematic of dietary approaches to generate WL and WC mice using 10% low fat diet (LFD) and 60% high fat diet (HFD). **b** Body mass over time measured weekly with diet switch indicated by dashed lines. **c** Food intake over time measured weekly. **d** Cumulative food intake measured throughout the duration of the studies with slope (m) for each 9-week segment indicated. **e** Lean and fat mass measured by nuclear magnetic resonance. **f** Blood glucose during an intraperitoneal glucose tolerance test (ipGTT) dosed at 1.5 g dextrose/kg lean mass one week prior to the end of the study and area under the curve (AUC) for ipGTT. For diet groups, grey = lean, blue = obese, green = WL, orange = WC. Pairwise two-tailed Student's t-tests with Bonferroni correction for multiple comparisons were used to compare groups for body composition and ipGTT AUC. Two-way ANOVA was used to compare groups for ipGTT. Significant p values shown or ***pad$<$0.001. Data is plotted as mean $\pm$ SEM. Sample size (mouse per group; n) is indicated in corresponding figure legends. Figure 3.1a was generated using Biorender.

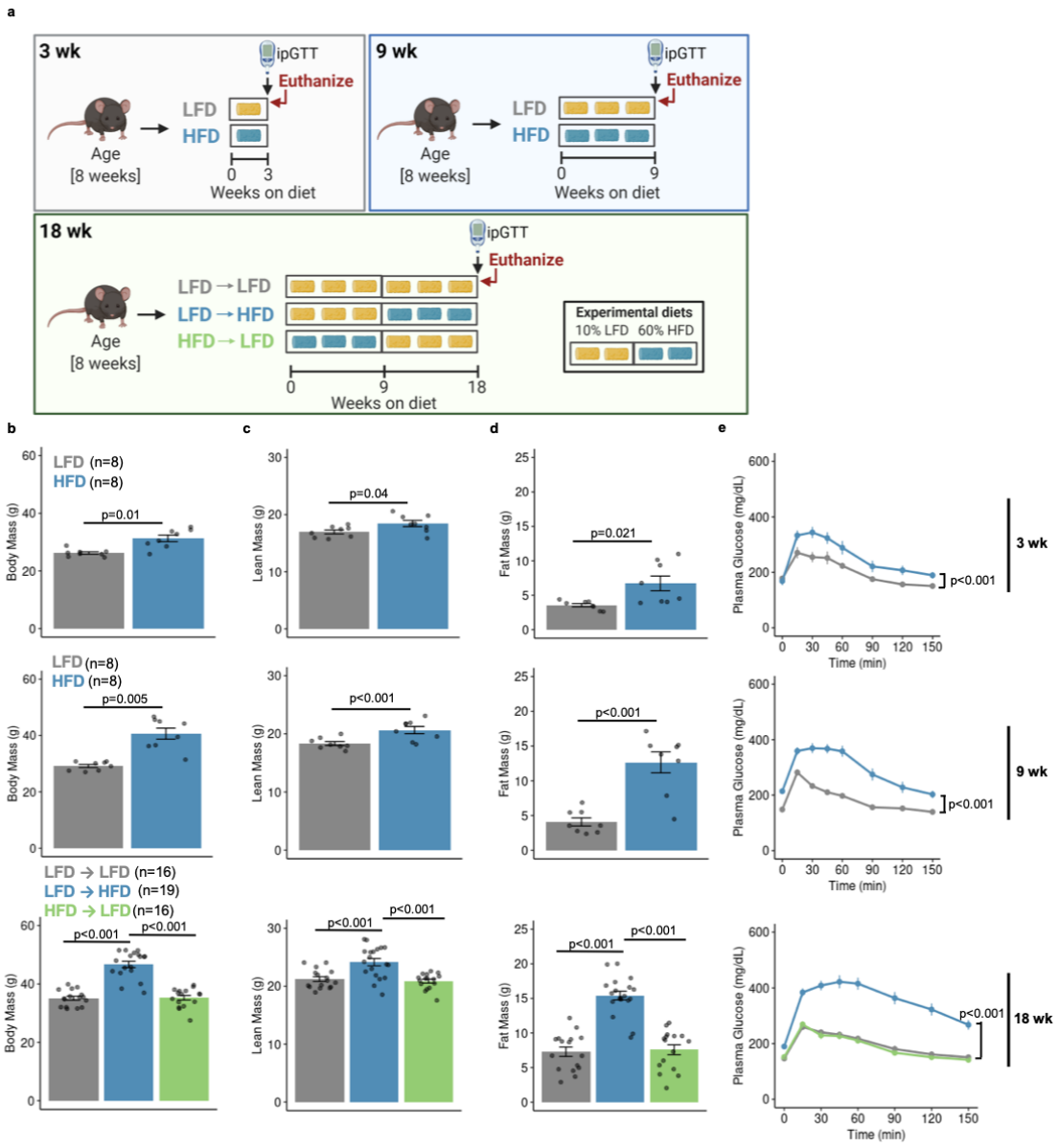

Figure 3.2: Interim body mass and ipGTT for male mice. a Schematic of interim study timepoints using 10% low fat diet (LFD) and 60% high fat diet (HFD).**b** Body mass, **c** lean mass, **d** fat mass, and **e** intraperitoneal glucose tolerance test (ipGTT) at weeks 3, 9, and 18 for male mice (mean ± SEM). For diet groups, grey = lean, blue = obese, green = WL. Pairwise two-tailed t-tests (3 and 9-week timepoints) with Bonferroni correction for multiple comparisons (18-week timepoint only) were used to compare groups for body mass, body composition, and ipGTT area under the curve. Significant p values are shown. Data are not paired, mice at each timepoint represent independent cohorts that were sacrificed at the indicated time. Figure 3.2a was generated using BioRender.

droplet membrane protein, revealed a slight reduction in lipid droplet diameter in eAT of WL compared to lean mice, while no difference was observed between obese and WC mice (Fig. 3.3c & d).

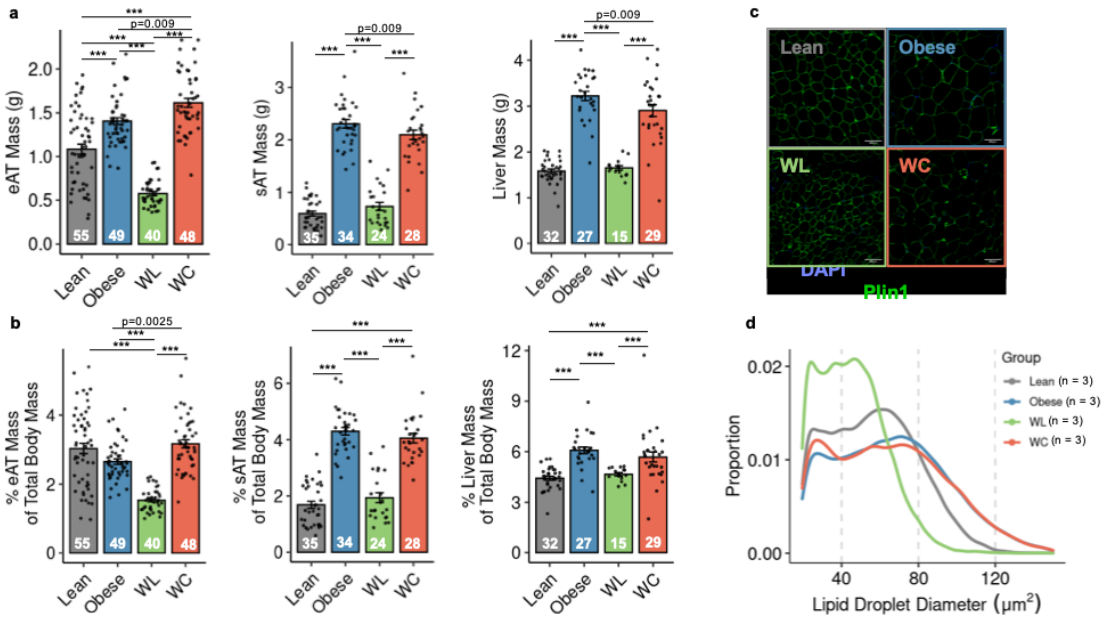

Figure 3.3: Tissue mass and adipocyte size for male mice. **a** Tissue mass for epididymal adipose tissue (eAT), subcutaneous adipose tissue (sAT), and liver and **b** tissue mass as percentage of body mass at sacrifice.**c** Representative imaging of perilipin-1 (Plin1) and 4,6-diamidino-2-phenylindole (DAPI) immunofluorescence for lipid droplet size. **d** Distribution of lipid droplet size. For diet groups, grey = lean, blue = obese, green = WL, orange = WC. Pairwise two-tailed Student's t-tests with Bonferroni correction for multiple comparisons were used to compare groups for tissue mass; significant p values shown or *** = pad$<$0.001. Data is plotted as mean $\pm$ SEM. Sample size (mouse per group; n) is indicated in corresponding figure legends or by white text at the bottom of each histogram.

We also determined whether WC worsened metabolic control in female mice. At the end of the 27-week study, body weight, lean mass, and fat mass were greater in both obese and WC females than lean controls, whereas no differences were detected between obese vs. WC groups (Fig. 3.4a & 3.4b). In contrast to male mice, WC did not significantly exacerbate glucose intolerance in female animals (i.e., glucose AUC); however, there was a modest delay in glucose clearance during the glucose excursion between WC and obese

females (Fig. 3.4c).

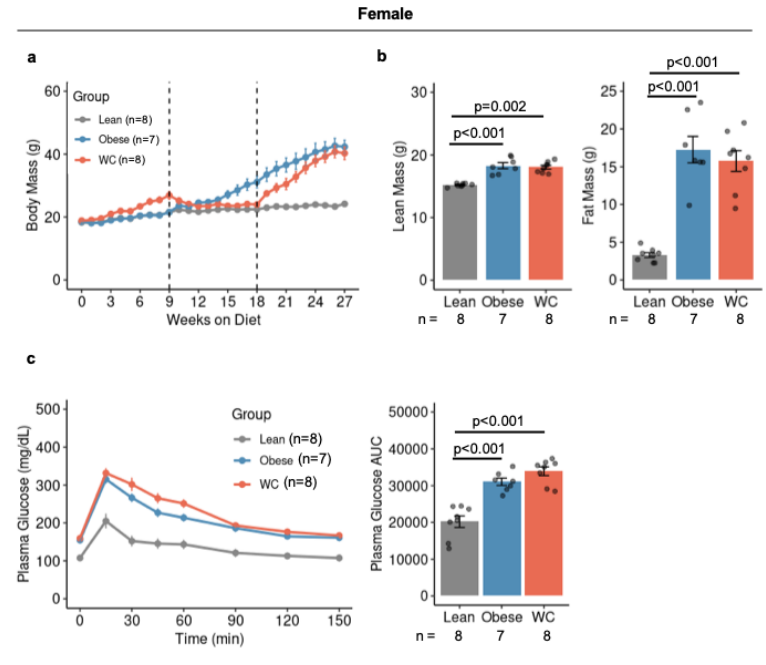

Figure 3.4: Weight cycling in female C57BL/6J mice. **a** Body mass over time, **b** body composition after 27-weeks of diet, and **c** intraperitoneal glucose tolerance test and corresponding area under the curve (AUC) after 27-weeks of diet for female lean, obese, and weight cycled (WC) mice (number of mice indicated for each panel; n). For diet groups, grey = lean, blue = obese, orange = WC. Pairwise two-tailed t-tests with Bonferroni correction for multiple comparisons were used to compare groups for body composition and ipGTT area under the curve; significant p values shown.

Together, these data demonstrate that our mouse model provides a robust representation of WC-accelerated metabolic disease in male mice, which were used for all subsequent experiments.

3.2.2 Multimodal single-cell sequencing highlights the diversity of adipose immune cells

To profile the immune landscape across lean, obese, WL, and WC groups, we performed droplet based scRNA-seq with CITE-seq, whereby oligo-conjugated antibodies specific for surface protein targets are simultaneously sequenced with endogenous mRNA. CITE-seq antibodies were used to confirm and improve cell annotation as follows: T cells (CD3, CD4,

CD8α, TCR γ/δ), NK cells (NK1.1), B cells (CD19), myeloid cells (CD11b), macrophages (FCγR1, MAC2/GAL3), DCs (CD11c), and neutrophils (CD39) as well as co-stimulation and activation/inhibition markers (CD279/PD- 1, TIGIT, CD44, CD80, CCR7/CD197). Cells were isolated via collagenase digestion, $CD45^+$ magnetic enrichment, and FACS for viability before preparation for sequencing using the 10X Chromium platform. We also used cell hashing via antibodies conjugated with unique oligos targeting ubiquitous surface proteins to pool and index 4 biological replicates per group. CITE-seq antibodies were validated by comparing sequenced protein expression levels to gene expression levels for matched targets (i.e. CD4 vs. *Cd4*), largely exclusive targets (i.e. CD4/*Cd4* vs. CD19/*Cd19*), and for commonly associated targets (i.e. CD4/*Cd4* vs. CD3/*Cd3*ε) (Fig 3.5).

Importantly, biological replicates are frequently ignored in scRNA-seq experiments, and we sought to address this concern using cell hashing antibodies. Cell types were well represented in all biological replicates without any major outliers driving our interpretation and cell classification (Fig. 3.6a), and all data shown are normalized to the number of cells analyzed per mouse to correct for differences in total cell numbers. Across the four sample groups (16 mice), a total of 33,322 cells that met strict quality control metrics (see Methods) were retained and integrated (Fig. 3.6b). Large cell clusters generated using low resolution nearest-neighbor clustering were first annotated using differentially expressed protein and gene signatures. Further subcluster annotation was conducted by subsetting large cell type clusters.

Differential expression between clusters was used to annotate sequenced cell types (Fig. 3.7a). Cell cluster designations were further confirmed by published gene markers (Fig. 3.7b). Antibody-based protein measurements for highly expressed surface proteins were also robust for cell type identification (Fig. 3.7c). Finally, a dendrogram was produced using the 2,000 most highly variable genes to elucidate broad relationships between cell subclusters (Fig. 3.7d).

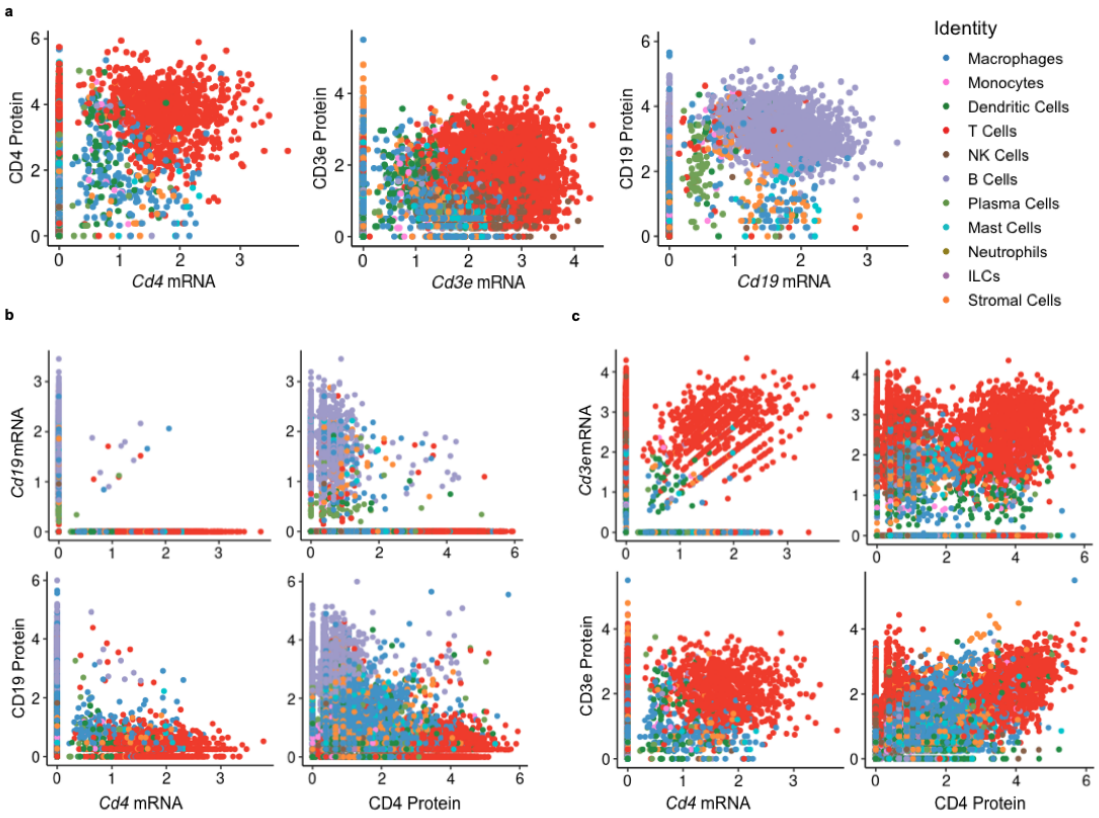

Figure 3.5: Validation of CITE-seq antibodies. **a** Comparison of genes for *Cd3e*, and *Cd19* with their corresponding surface proteins measured using CITE-seq. Individual cells are colored by annotated cell type. **b** Comparison of cell type exclusive genes *Cd4* and *Cd19* with their corresponding surface proteins. **c** Comparison of co-expressed genes *Cd4* and *Cd3e* with their corresponding surface proteins.

3.2.3 Obesity-associated immune cell phenotypes are confirmed by single cell sequencing

To validate our scRNA-seq dataset, we compared cells isolated from obese male mice to those from lean male mice, as these differences are well documented. To explore how relative frequency of immune cells changed during obesity, we grouped cells into metacells (a group of cells connected by proximity to a representative index cell in our dimensional reduction) and compared abundance by diet group (Fig. 3.8a). By linking metacells to original cell type designations, we observe subpopulations of T cells, DCs, and macrophages that are differentially abundant in lean and obese eAT (Fig. 3.8b), consistent with published

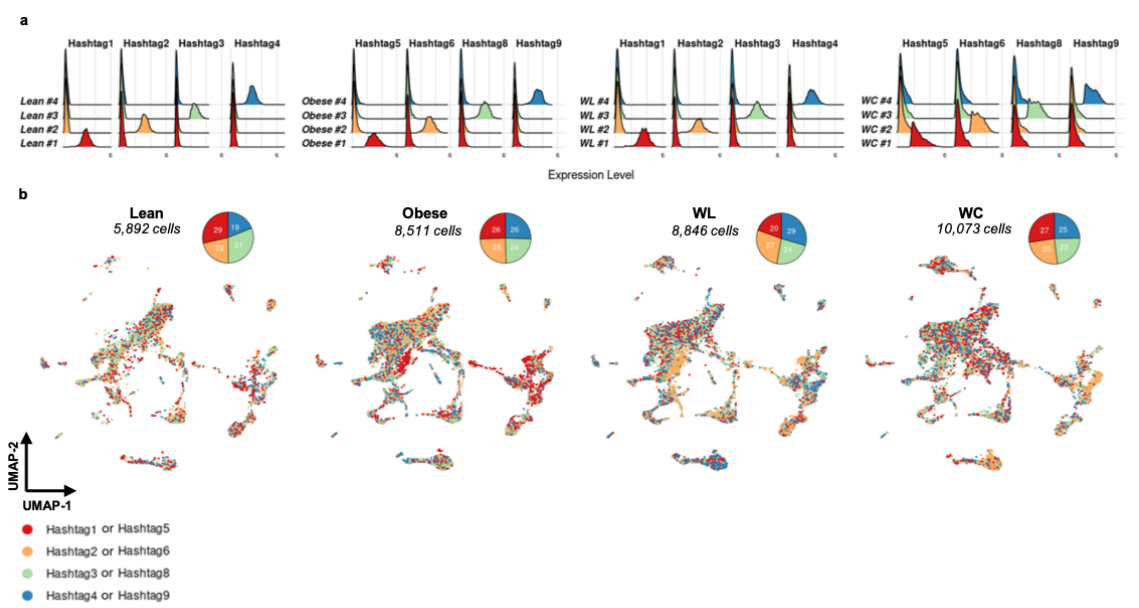

Figure 3.6: Biological replicates identified by Hashtag demultiplexing are well represented within diet groups.. **a** Hashtags demultiplexed for each individual mouse per diet group (n=4 per group; total of 16 mice sequenced). **b** Uniform manifold projection with total cell counts retained following QC for each diet group and distribution of hashtags measured within each diet group (inset).

literature [249, 257, 258]. Furthermore, metacells were reclassified by high-resolution subclusters to identify potential subpopulations of interest, such as Tregs, ILC2s, and TRMs – abundant in the lean state; and LAMs, $CD8^+$ T_{EM}, and activated DCs – abundant in the obese state (Fig. 3.8c). By tracing cells back to each individual mouse, we were also able to perform pairwise comparisons of cell number for cell subtypes classically associated with lean AT (Fig. 3.8d) and obese AT (Fig. 3.8e). These data validate our cell isolation strategy and cell type identification by confirming, with high fidelity, many of the previously established changes associated with lean and obese AT.

3.2.4 Obesity-associated T cell exhaustion persists after WL

Adaptive T-lymphocytes are important regulators and drivers of inflammation in AT. We explored AT T cells by scRNA-seq (Fig. 3.9a) and identified specific subsets of α/β-T Cells by expression of conventional T cell markers (*Cd3ε, Cd4, Cd8b1*), phenotype

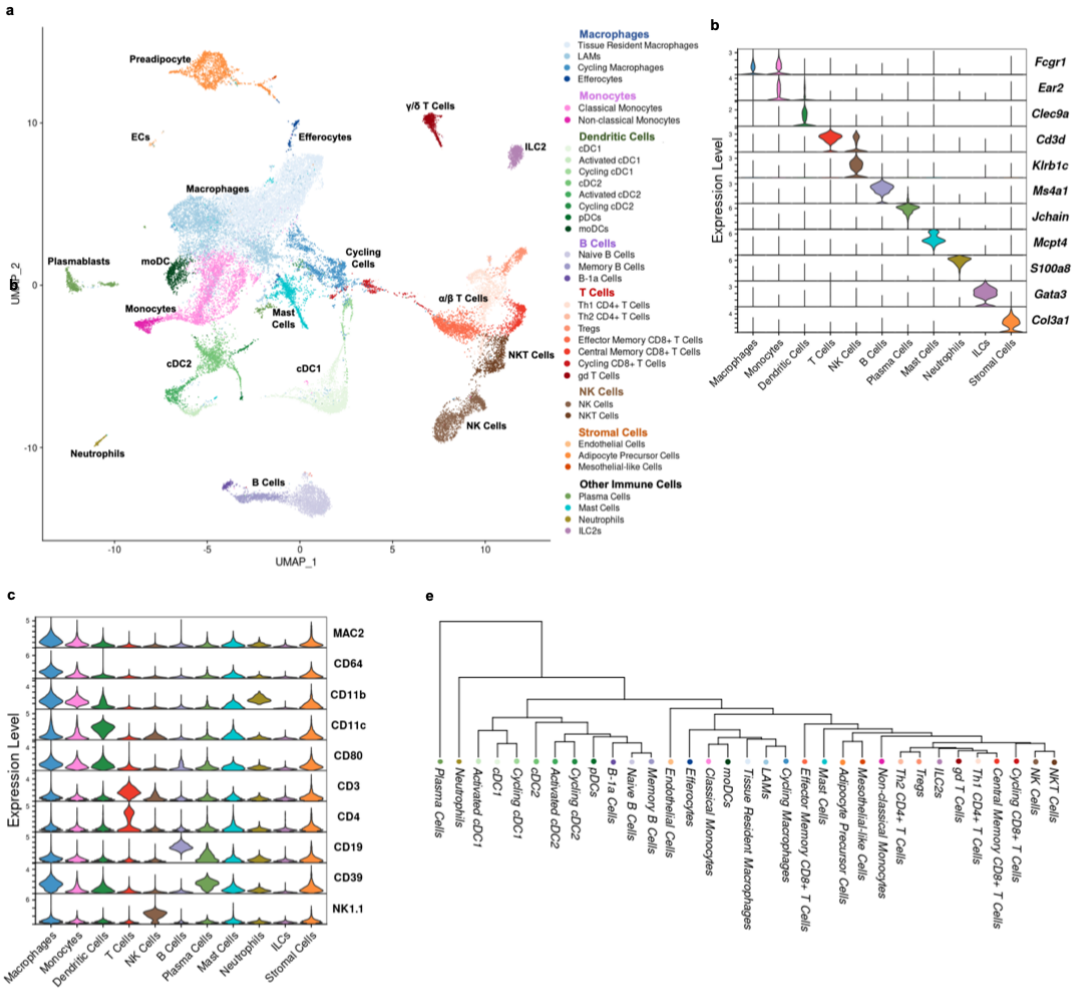

Figure 3.7: Adipose tissue immune cell populations observed by CITE-seq.a Unbiased clustering of 33,322 single cells labeled broadly by cell type category and colored by high-resolution cell type identities via Uniform Manifold Approximation and Projection (UMAP). Populations include lipid associated macrophages (LAMs), conventional dendritic cells (cDCs), plasmacytoid DCs (pDCs), monocyte-derived DCs (moDCs), T helper (Th) cells, T regulatory cells (Tregs), γ/δ (gd) T cells, natural killer (NK) cells, and type 2 innate-like lymphoid cells (ILC2s). Selected markers of specific cell subsets based on **b** gene expression and **c** surface protein. **d** Phylogenetic tree of high-resolution cell type identities. Figure 2a was generated using Biorender.com

markers (*Foxp3,Cxcr3, Ccr7, Sell*) [259, 260], and markers of cell cycling (Stmn1, Pclaf) [148, 261] (Fig. 3.9b). A population of γ/δ-T cells was identified by expression of the common T cell δ chain (*Trdc*) and both NK and NKT were identified by expression of

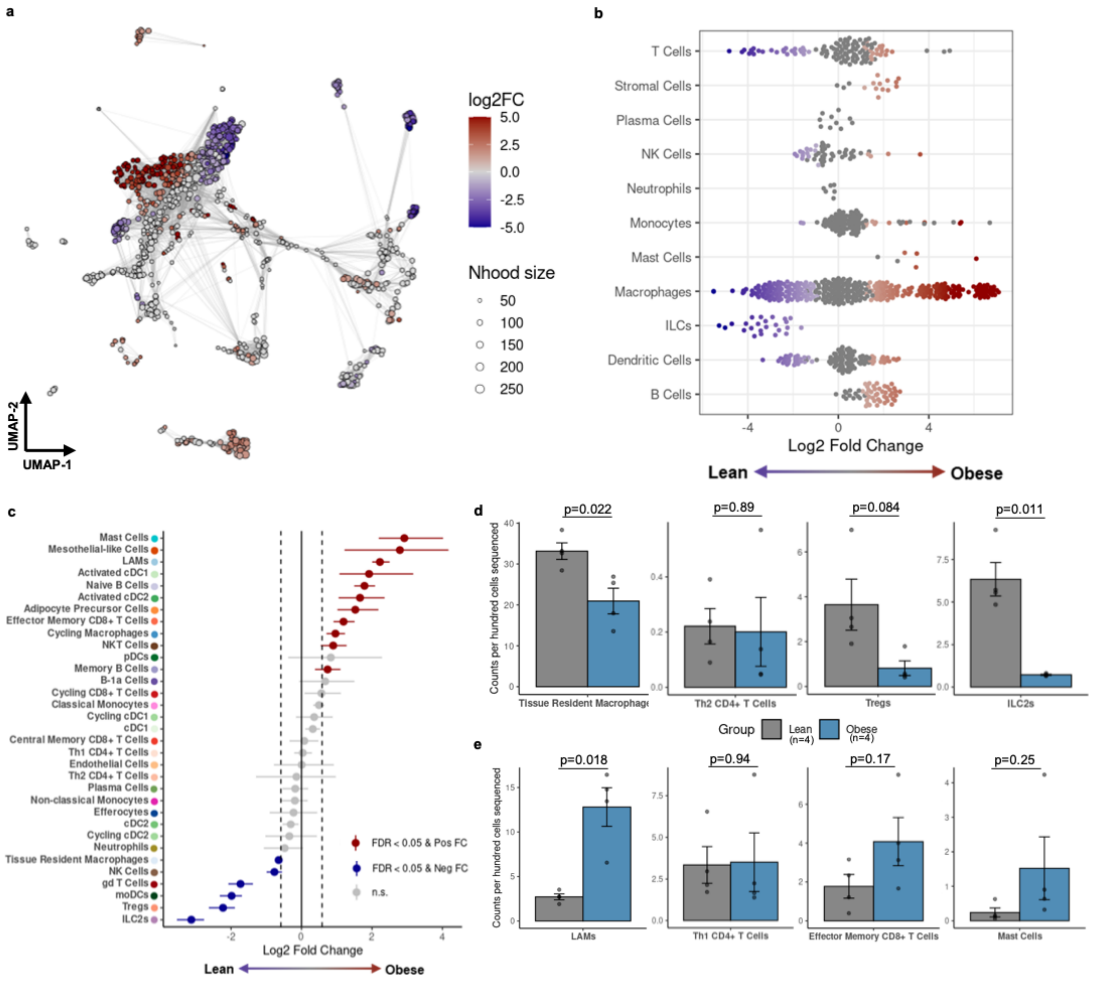

Figure 3.8: CITE-seq recapitulates obesity-associated immune cell changes in adipose tissue. **a** Differential abundance by log fold change (FC) of metacells (index cells representing a neighborhood (Nhood) of cells connected by proximity in Uniform Manifold Approximation and Projection; UMAP) comparing cells from obese mice to lean mice. **b** Differential abundance of annotated cell types comparing cells from obese mice to lean mice. **c** Permutation testing of high-resolution clusters to calculate the proportional difference comparing cells from obese mice to lean mice by false discovery rate (FDR). Populations include lipid associated macrophages (LAMs), conventional dendritic cells (cDCs), plasmacytoid DCs (pDCs), monocyte-derived DCs (moDCs), T helper (Th) cells, T regulatory cells (Tregs), γ/δ (gd) T cells, natural killer (NK) cells, and type 2 innate-like lymphoid cells (ILCs). **d, e** Counts per hundred cells sequenced for lean-associated immune cell subsets and obesity-associated immune cell subsets in lean and obese mice (mean $\pm$ SEM; n=4 mice; two-tailed t-test with indicated p values).

killer lectin receptors *Klrb1b* and *Klrb1c* with and without expression of *Cd3ε*, respectively [262]. Th1 $CD4^+$ and all three $CD8^+$ T cells subsets were not elevated in WC but $CD8^+$ effector memory T cells were increased in AT from WL mice (Fig. 3.9c). Tregs expressing *Foxp3* trended towards being reduced in proportion by obesity and remain low following WL and WC. Using differential expression, we observed that obesity not only affected Treg number but also reduced the expression of *Il1rl1*, which codes for the IL-33 receptor, ST2 (Fig. 3.9d).

Because $CD8^+$ T cells have the capacity to clonally expand in response to antigen, we were interested in exploring if cycling T cells (marked by expression of *Pclaf*, *Stmn1*, and *Mki67*) [148] are precursors for AT memory T cell populations. Therefore, we utilized RNA velocity, which estimates cell state progression by comparing the frequency of spliced and unspliced mRNA sequences between cells. RNA velocity indicates cycling $CD8^+$ T cells are likely upstream of other effector and memory populations in AT, but also that bidirectional transition between effector memory and circulating memory can occur (Fig. 3.10a). Differential expression across diet groups also identified that cycling and effector memory (T_{EM}) $CD8^+$ T cells express the activation/exhaustion signature gene *Pdcd1* (coding for PD-1). To further explore whether AT T cells contain an exhausted signature following obesity, we generated an exhaustion module containing multiple established gene expression features of T cell exhaustion: *Pdcd1, Tox, Entpd1, Tigit, and Lag3* [263, 264]. We observed that T cells from AT of obesity, WL, and WC were all enriched for our exhaustion module and that $CD8^+$ T_{EM} were most associated with an exhausted phenotype (Fig. 3.10b). This was further confirmed by a T cell exhaustion module based on protein expression of PD-1 (CD279) and TIGIT from our CITE-sequencing antibodies (Fig. 3.10c). T cell exhaustion is frequently studied in models of viral infection and in the tumor microenvironment, so we utilized ProjecTILs V1.0.0, a published scRNA-seq reference atlas [265], to further confirm our exhaustion profile. We observed that cells captured in our experiments projected accurately onto an LCMV chronic infection atlas (Fig. 3.10d). Con-

cordant with our exhaustion module, more CD8$^+$ T cells aligned with the LCMV exhausted precursor cells in obese, WL, and WC groups than in the lean control group.

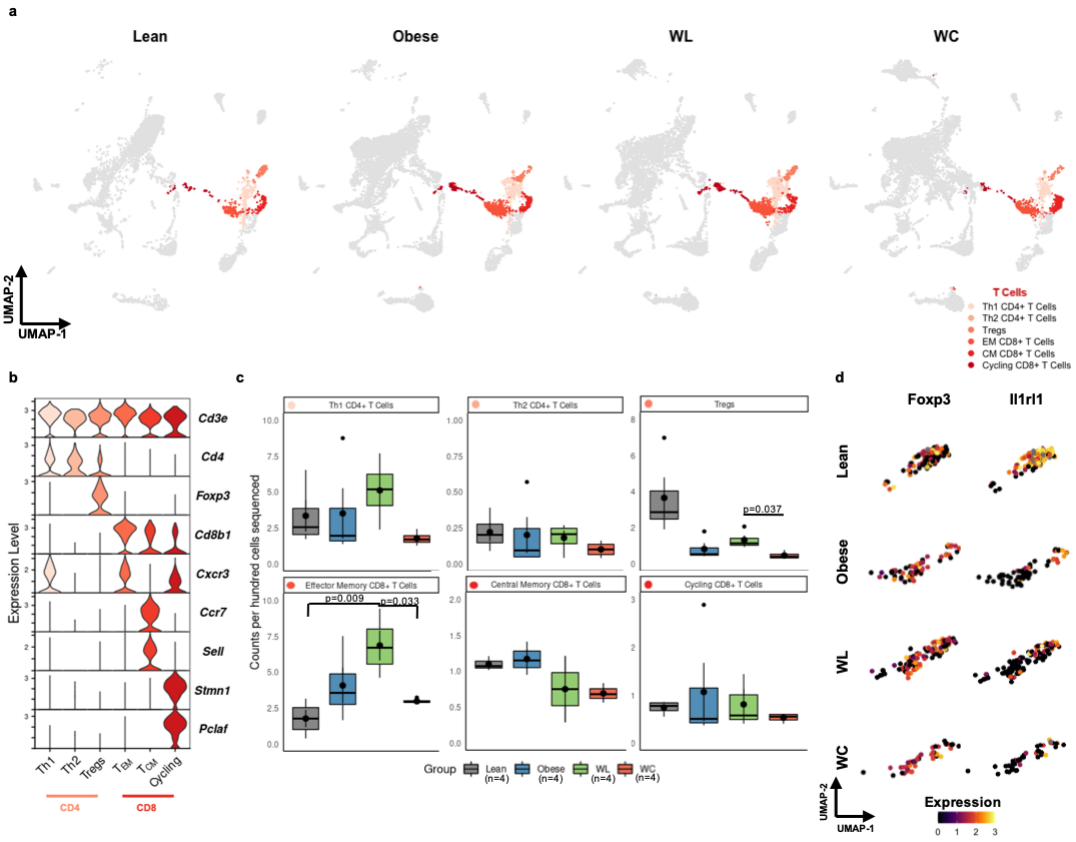

Figure 3.9: Obesity-induced changes in adipose tissue T cells are not reversed by weight loss. **a** Uniform Manifold Approximation and Projection (UMAP) of T cell subclusters by diet group for lean (grey), obese (blue), weight loss (WL; green), and weight cycled (WC; orange) mice. **b** Expression of markers enriched in T cell subclusters. **c** Counts per hundred cells sequenced for α/β T cell subclusters (mean $\pm$ SEM; n=4 mice). Box indicates interquartile range (25th-75th percentile) with 50th percentile indicated by solid line and mean indicated by large circle. Range of whiskers indicates largest and smallest values within 1.5 times the interquartile range and values outside of the range are indicated by small circles. **d** Expression of the T_{reg} markers *Foxp3* and *Il1rl1* within the T_{reg} subcluster across diet groups. Pairwise two-tailed t-tests with Bonferroni correction for multiple comparisons were used to compare groups for cell counts; significant p values shown.

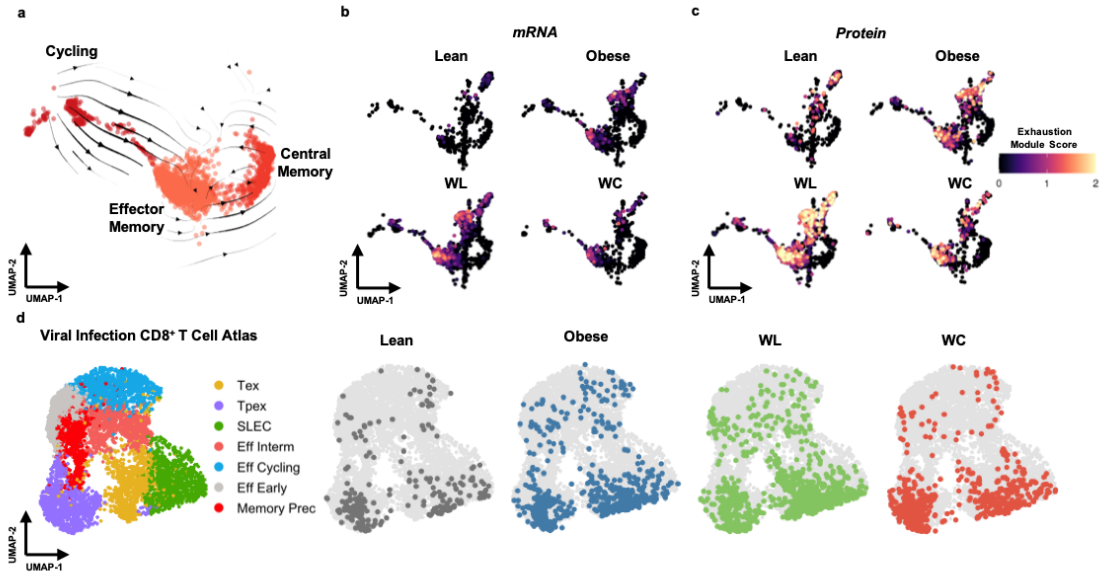

Figure 3.10: Adipose tissue T cells are retained and express markers of exhaustion in mice that have gained, lost, and regained weight. **a** Embedding of RNA velocity displayed on the uniform maniphold approximation and projection (UMAP) for $CD8^+$ T cells. **b** $CD8^+$ T cells colored by an exhaustion module containing the mRNA features *Pdcd1*, *Tox*, *Tigit*, *Lag3*, and *Entpd1*. **c** $CD8^+$ T cells colored by an exhaustion module containing the CITE-seq features PD-1 (CD279) and TIGIT. **d** $CD8^+$ T cells plotted onto a viral infection $CD8^+$ T cell reference atlas using ProjecTILs. ProjectTILs populations $CD8^+$ include terminally-exhausted (T_{ex}), $CD8^+$ precursor-exhausted (T_{pex}), short-lived effector cells (SLEC), effector interim (Eff Interm), and memory precursors (Memory Prec).

3.2.5 Monocytes are abundant in AT, but do not have an altered transcriptional profile in response to obesity, WL, or WC

The AT immune cell compartment contains a large population of both monocytes and DCs (Fig. 3.11a). Monocytes were subclustered into classical (*Ly6c2*$^+$*Ccr2*$^+$*Cx3cr1*$^+$) and non-classical (*Ly6c2*$^-$*Ccr2*$^-$*Cx3cr1*$^+$) subsets [266, 267] (Fig. 3.11b). Additionally, we observed that many classical monocytes expressed *Fcgr1* and that *Ear2* and *Ace* were highly specific for non-classical monocytes in AT. We did not observe strong correlation between diet group and number of either classical or non-classical monocytes (Fig. 3.11c). While monocyte recruitment to the adipose tissue is observed with obesity, population changes are time-dependent and often masked by large changes in the proportion of other cell types

[116, 252]. Upon further assessment of cytokine, chemokine, and other functional markers, there were few differences in non-classical monocytes, but we did observe an increase in genes associated with lipid handling (*Trem2, Cd36, Cd9*) [116], activation/adhesion (*Cd9, Cd81, and Cd63*) [268, 269], and co-stimulation (*Cd86, Cd40*) [270], which were not reversed with weight loss in the classical monocyte subset (Fig. 3.11d). While *Cd86* gene expression increased following obesity, no change in *Cd80* mRNA or protein expression was observed due to diet within the classical monocyte subcluster.

3.2.6 DCs shift towards an activated transcriptional signature with obesity and these signatures are retained with WL and WC

DCs, a class of professional APCs, make up approximately 10-15% of captured AT immune cells. We classified DCs into two cDC subsets, cDC1s (*Clec9a*$^+$*Xcr1*$^+$) and cDC2s (*Sirpa*$^+$*Cd209*$^+$) [271, 272], and further refined subclustering using markers of DC activation (*Ccr7*) [273] and cell cycle induction (*Pclaf* and *Stmn1*) [261] (Fig. 3.12a). AT DCs were largely unchanged in relative proportion by diet condition with the exception of monocyte-derived DCs (moDCs), which were enriched in lean AT (Fig. 3.12b). Activated subsets of DCs were elevated in obese AT and remained elevated upon WL and WC. Expression of *Ccr7* correlated positively with expression of *Fscn1* and *Mreg* and negatively with expression of cDC1 and cDC2 markers, indicating that activated DC subsets are mature (Fig. 3.12c). *Il15ra*, which codes for the receptor that trans-presents IL-15 to NK and T cells to support homeostatic proliferation [274, 275], was also correlated with *Ccr7*. RNA velocity was used to determine whether activated DCs were precursors or downstream of other cDC subsets and suggested that activated cDCs mature from other local cDC subsets (Fig. 3.12d). Expression of *Ccr7* also negatively correlated with lactate dehydrogenase expression (*Ldha*), suggesting the potential for a shift in metabolite usage upon activation. Activated cDC1s, but not cDC2s, also expressed high levels of *Il12b* and may be primed to induce a local Th1 response within AT. The activated DC subset also expressed very

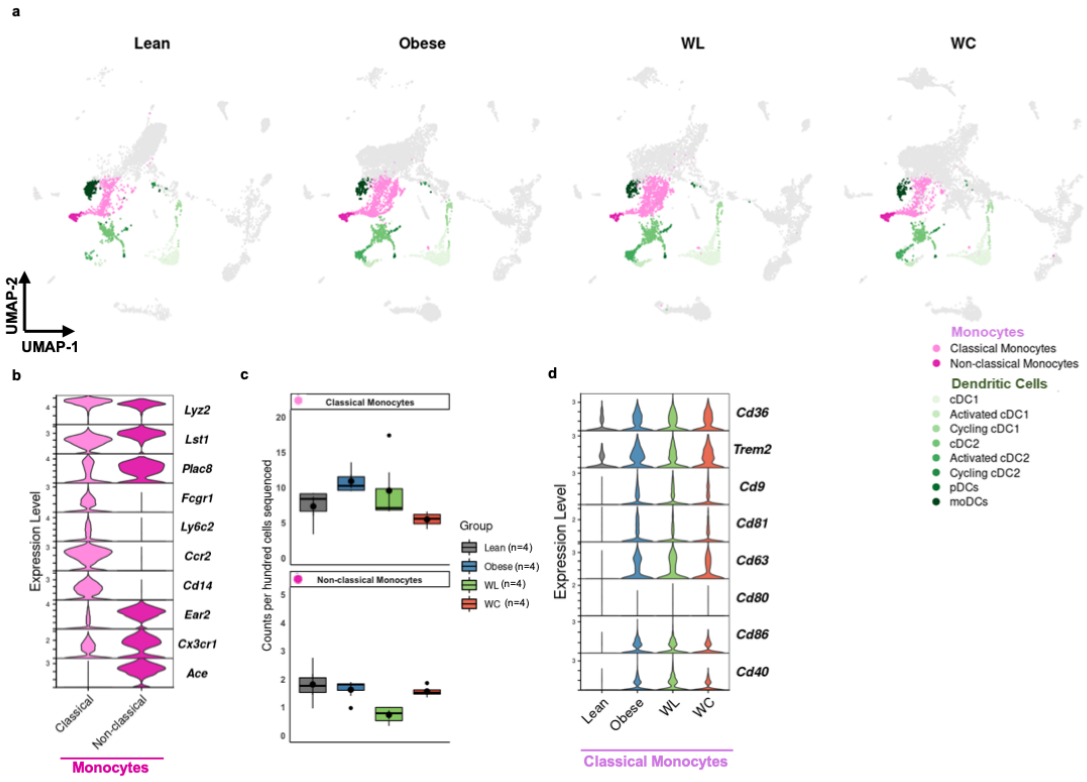

Figure 3.11: Monocytes upregulate features of lipid handling during obesity, weight loss, and weight regain. **a** Uniform Manifold Approximation and Projection (UMAP) of highlighted monocyte and DC subclusters by diet group for lean (grey), obese (blue), weight loss (WL; green), and weight cycled (WC; orange) mice. **b** Expression of genes associated with monocyte subclusters. **c** Monocyte counts per 100 cells sequenced by diet group (mean $\pm$ SEM; n=4 mice; n.s.d.). **d** Lipid-handling, activation, adhesion, and co-stimulation genes by diet group for classical monocytes. Pairwise two-tailed t-tests with Bonferroni correction for multiple comparisons were used to compare groups against the Lean reference group for cell counts with significant p values shown. For panel **c**, box indicates interquartile range (25th-75th percentile) with 50th percentile indicated by solid line and mean indicated by large circle. Range of whiskers indicates largest and smallest values within 1.5 times the interquartile range and values outside of the range are indicated by small circles.

high levels of key immunoregulatory ligands *Cd274*, *Pdcd1lg2*, and *Cd200* associated with coinhibitory T cell receptors (Fig. 3.12e). Taken together, these data suggest that DCs in AT shift towards an activated immunoregulatory status with onset of obesity and that these features are retained long-term through WL and WC.

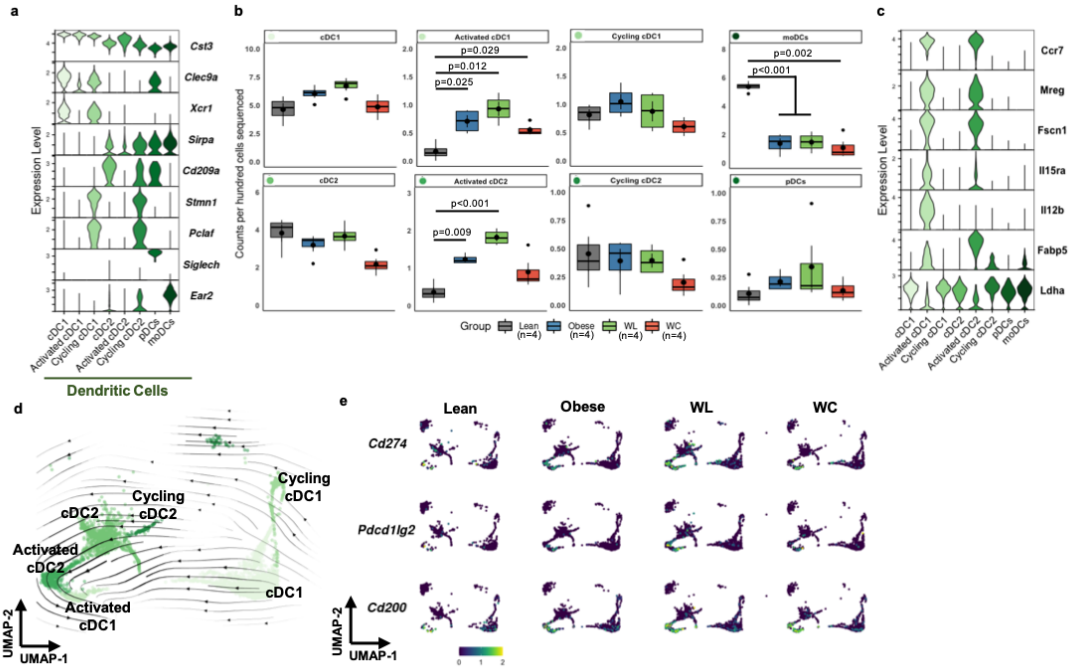

Figure 3.12: Dendritic cells shift towards a mature, activated status in mice that have gained, lost, and regained weight a Expression of genes enriched in DC subsets. **b** DC counts per 100 cells sequenced by diet group (mean ± SEM; n=4 mice). **c** Expression of genes associated with DC activation. **d** Embedding of RNA velocity displayed on the UMAP for conventional (c)DC subsets. **e** Expression of immunoregulatory ligands *Cd274*, *Pdcd1lg2*, and *Cd200* in DCs by diet group. Pairwise two-tailed t-tests with Bonferroni correction for multiple comparisons were used to compare groups against the Lean reference group for cell counts with significant p values shown. For panel **c**, box indicates interquartile range (25th-75th percentile) with 50th percentile indicated by solid line and mean indicated by large circle. Range of whiskers indicates largest and smallest values within 1.5 times the interquartile range and values outside of the range are indicated by small circles.

3.2.7 Macrophage populations are highly adaptable to change in dietary status

Macrophages make up the largest proportion of immune cells in AT and are highly responsive to changes initiated by caloric excess. Dimensional reduction and clustering of macrophage subsets highlights the dramatic changes that occur during AT adaptation to HFD (Fig. 3.13a). Common markers of tissue macrophages, *Lyz2*, *Cst3*, *Adgre1* (coding for F4/80), *Cd68*, and *Lgals3* (coding for MAC2) were highly expressed by all macrophage subclusters and robust protein expression for conventional AT macrophage markers CD64

and CD11b was observed (Fig. 3.13b). TRMs were enriched for expression of *Klf4*, *Cbr2*, and *Stab1* [276], while LAMs highly expressed various genes associated with lipid interactions (*Trem2*, *Cd9*, *Lpl*) [116], and cycling macrophages expressed cell cycle genes (*Stmn1, Pclaf*) [261] (Fig. 3.13c). In addition, we identified a subset of cycling macrophages and another small subset of macrophages that expressed very high levels of *Saa3* and *Slpi*, which are defining features of efferocytes [277].

The changes in macrophage subclusters largely persist after weight gain, even following 9 weeks of WL or WC. TRMs decreased with obesity and even more with WL and WC (Fig. 3.13d). Importantly, while LAMs increase with obesity, they do not return to lean levels with WL and increase even more with WC; thus, levels are not directly correlated with AT mass. Cycling macrophages are increased with obesity, recovered with WL, but again worsen with WC and frequency of efferocytes was similar between diet groups.

3.2.8 Alterations in macrophage phenotype remain unresolved with WL

A great challenge in classification of AT macrophages is that conventional markers are often not exclusive or only poorly describe cell function. We observed that TRMs retained high expression of the M2-associated *Mrc1* gene (coding for the mannose receptor CD206). However, these same cells completely lost expression of the M2-associated *Cd163* gene with the onset of obesity (Fig. 3.13e). The persistence of this transcriptional change, which lasted for at least 9 weeks following WL and into subsequent WC, compelled us to further investigate if TRMs could be transitioning towards a LAM-like profile. Based on RNA velocity estimates, the majority of LAMs are likely derived from tissue infiltrating monocytes, as previously suggested [116], that acquire features of lipid handling prior to differentiation (Fig. 3.11d). However, RNA velocity also indicates that some TRMs are projected to become LAMs (Fig. 3.13f). MacSpectrum, a tool that uses macrophage differentiation (MDI) and polarization indexes (MPI) previously generated using in vitro systems [114], was utilized to further interrogate changes in tissue-resident and LAM phenotypes (Fig. 3.13g).

We observed that obesity shifted both subpopulations of macrophages towards a more pro-inflammatory phenotype that was not recovered following WL, indicated by a higher MPI which signifies gene expression patterns associated with M1-like phenotypes. Specifically, WC LAMs appeared to be even more inflammatory compared to cells from other conditions, indicating that these cells may be an important target for subsequent studies seeking to improve outcomes of WL and weight regain.

3.2.9 Open access interactive data portal

Importantly, we believe the immunophenotyping conducted using CITE-seq in our models of obesity, WL, and WC, has broad applicability, which can be hypothesis-generating for models of cancer, infection, or metabolic disease in other tissues. Moreover, our dataset is a resource for identifying targets for focused investigations in clinical human AT samples. To facilitate discovery and to broaden accessibility of this data, we have created an open-access online interactive portal called MAIseq (Murine Adipose Immune sequencing) with our preprocessed data for the research community using modified source code from Shiny-Cell [278] at https://hastylab.shinyapps.io/MAIseq/. Users can utilize a variety of built-in visualization approaches that span beyond what we could report in this manuscript. For instance, we also identified γ/δ T cells, NK and NKT cells, multiple B cell subsets and plasma cells, and even some CD45+ stromal cells that were not discussed herein. Users can explore our cell cluster annotations, identify potential genes of interest, plot gene expression by diet groups, clusters, or subclusters, and plot expression of surface markers from CITE-seq. We provide clear instructions for use and options to download figures and tables in a variety of formats. Collectively, our data provides critical groundwork for understanding the causes of WC-accelerated metabolic disease.

3.3 Discussion

WL improves obesity-associated insulin resistance in humans and mouse models; however, as highlighted here and by others [15, 252, 279, 280], WL does not normalize AT immune

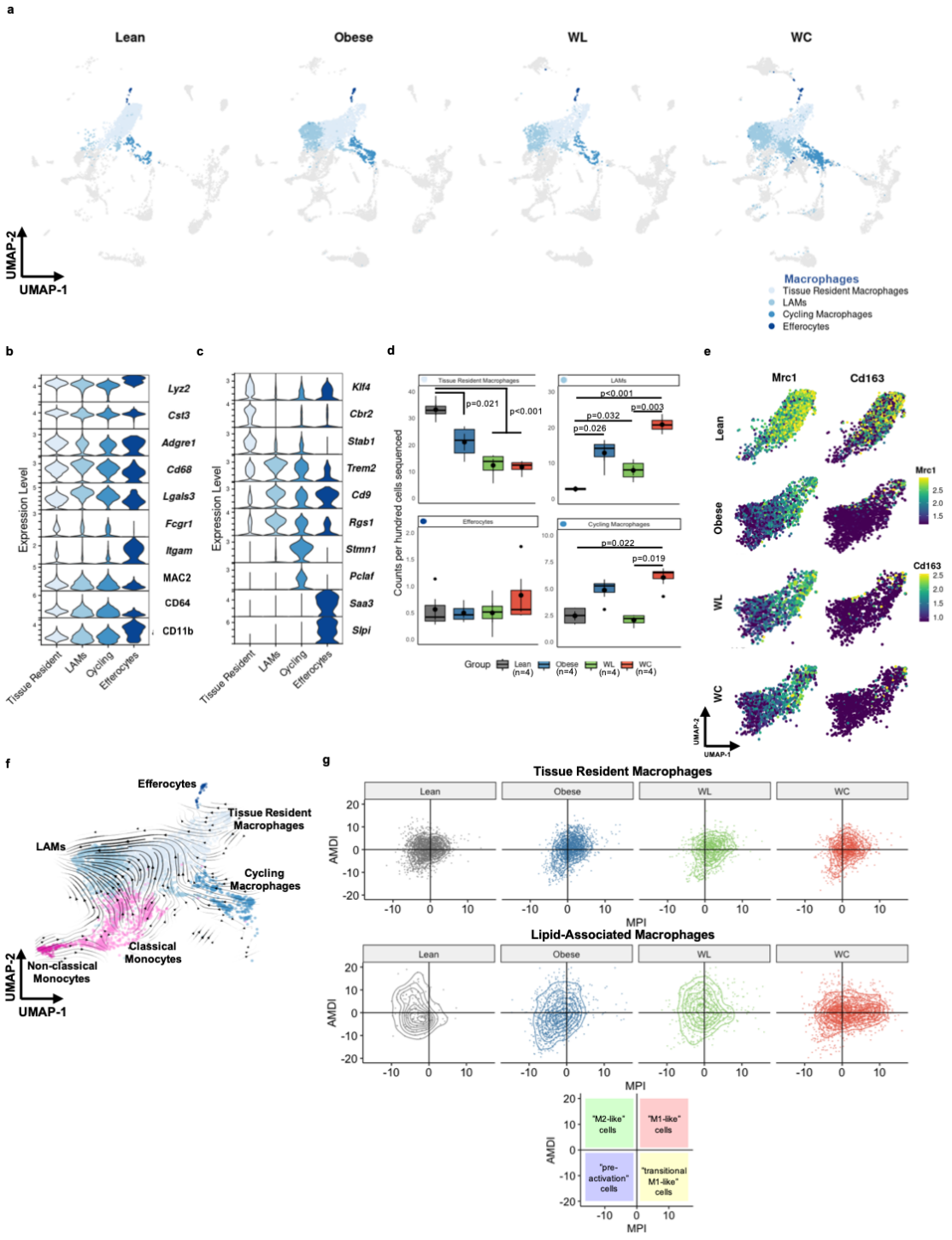

Figure 3.13

populations in murine models of WC. Previous research shows that AT immune cells increase during early stages of WL [279, 281], presumably functioning as lipid handlers

Figure 3.13: Diet-induced obesity causes persistent changes in adipose tissue macrophages, even after weight loss and regain. **a** Uniform Manifold Approximation and Projection (UMAP) of macrophage subclusters plotted by diet groups for lean (grey), obese (blue), weight loss (WL; green), and weight cycled (WC;orange) mice. **b** Expression levels for genes (*Lyz2, Cst3, Adgre1, Cd68, Lgals3*, and *Itgam*) and proteins (CITE-seq; MAC2, CD64, and CD11b) associated with macrophages. **c** Expression of genes that associate with macrophage subclusters. **d** Counts per hundred cells sequenced for macrophage subclusters (mean $\pm$ SEM; n=4 mice). Box indicates interquartile range (25th-75th percentile) with 50th percentile indicated by solid line and mean indicated by large circle. Range of whiskers indicates largest and smallest values within 1.5 times the interquartile range and values outside of the range are indicated by small circles. **e** UMAP visualization of *Mrc1* and *Cd163* expression in tissue resident macrophages (TRMs) by diet group. **f** Embedding of RNA velocity displayed on the UMAP for macrophage and monocyte subsets. **g** TRMs and LAMs plotted on based on the macrophage polarization index (MPI) and the activation-induced macrophage differentiation index (AMDI) calculated using MacSpectrum. A shift to the right indicates a more M1-like phenotype. Each macrophage subset indicated with a different shade of blue. Pairwise two-tailed t-tests with Bonferroni correction for multiple comparisons were used to compare groups for cell counts; significant p values shown.

---

during lipolysis. Following WL in our model, male mice still retain many of the changes associated with prior obesity. We speculate that this obesity-associated immunophenotypic imprinting, which does not recover with WL, may ultimately be an underlying contributor to the detrimental impact of weight regain on metabolic health that is observed in both mice and humans. Supporting this, many inflammatory phenotypes are exacerbated in the WC group compared to the obese group. Indeed, given the frequency and risks associated with weight regain [11, 14–16, 24, 26, 27], understanding the cell types and/or mechanisms in AT that are not fully recovered following WL is critical.

In the T cell compartment, the greatest change in abundance occurs in T_{regs}, which decrease with obesity and do not rebound with WL. Interestingly, obese AT Tregs have decreased expression of *Il1rl*, which codes for the receptor ST2, and *Il1rl1* expression remains low with WL and WC. This is consistent with *Gata3*-expressing ILC2s, which are reduced with obesity and produce IL33 – a type 2 cytokine that promotes glucose tolerance in mice and is the primary ligand for ST2 [282]. AT Treg ST2 expression is regulated by

Pparg in response to insulin in a HIF-1α and Med23 dependent manner, and impairments in this signaling reduce stimulated proliferation of T_{regs} [283]. The persistent loss of ST2 expression in AT T_{regs} during WL and WC suggests a cell-intrinsic Treg imprinting induced by obesity that ultimately reduces their long-term maintenance for protection against glucose intolerance during future weight regain. Interestingly, mast cells are increased with WC, but also have reduced *Il1lr* expression and increased expression of lipid-associated genes, such as *Trem2* and *Fabp5*. While the role of mast cells in AT is unclear due to lack of specific knockout models, this suggests that the demand to handle excess lipid in obese AT occurs concomitantly with reductions in availability and response to type 2 cytokines, such as IL-33, and that these changes are not resolved with WL.

$CD8^+$ T cells are elevated in obesity and WC and are most enriched after WL. Moreover, obesity increases expression of exhaustion-associated genes in $CD8^+$ T cells that is not normalized by WL. T cell exhaustion has been recently noted in human and mouse AT $CD8^+$ T cells, which were shown to have impaired stimulation and increased markers of T cell exhaustion following obesity [224, 284, 285]. This transcriptional phenotype was further validated in our model by comparing T cells identified in our study to previously published exhausted T cell atlases generated in models of viral infection and cancer [265]. We also previously reported that AT T cell clonality is increased during obesity and that the T cell repertoire likely responds to positively charged, non-polar antigens [286]. It is plausible that APCs accumulate and present lipid-adducted proteins during lipid clearance following weight gain but also WL. Thus, chronic $CD8^+$ T cell stimulation via antigen presentation may drive T cell exhaustion and warrants further investigation. In support of this, AT DCs shift to a mature, activated state with the onset of obesity and persist during WL and WC. This activated status is characterized by increased expression of *Ccr7*, *Mreg*, and *Fscn1*, which have all been previously reported as critical features of immunoregulatory DCs that are enriched in non-small-cell lung cancer and uptake of anti-tumor antigens [287]. Furthermore, expression of the immunoregulatory proteins *Cd274*, *Pdcd1lg2*, and

Cd200 on activated AT DCs suggests these cells may be important regulators of T cell function and exhaustion in AT.

Macrophages are the most abundant immune cell type in our analysis. TRMs decrease with obesity and do not recover with WL. We also noticed a remarkable change in transcriptomic profile of this subcluster with obesity. Expression of *Mrc1*, coding for the M2-like macrophage marker CD206, is maintained during obesity, WL, and WC. However, expression of *Cd163*, another M2-like marker, is lost with the onset of obesity and the loss persists during WL and WC. These findings support divergence from the classical M1-M2 terminology, particularly in disease-associated microenvironments like obese AT, in favor of functional phenotyping or high-dimensional cell phenotyping [288]. Moreover, LAMs increase with obesity and only partly resolve with WL, supporting the notion that WL alone is insufficient to correct the AT immune landscape. Upon weight regain, LAMs and cycling macrophages tend to increase compared to obese animals. This shift in proportions of TRMs and LAMs, and increased lipid handling genes in the classical monocyte population, suggests a critical role for lipid regulation following weight gain, however, the role of macrophage lipid handling is not fully understood [289, 290]. LAM depletion via *Trem2* knockout has been reported to worsen insulin resistance during HFD feeding, suggesting macrophages may help buffer lipid overload [116]. Additionally, loss of TREM2 via global knockout or anti-TREM2 neutralizing antibodies improves T cell responses, similar to anti-PD-1 immunotherapy, and ultimately reduced tumor size in a macrophage-dependent manner [291]. Thus, lipid handling may be delicately linked to antigen presentation and T cell exhaustion in both metabolic disease and cancer. Interestingly, the tetraspanins CD9, CD63, and CD81 which were increased by gene expression in classical monocytes with weight cycling have been suggested to play a role in multinucleate giant cell formation [292]. Giant multinucleated cells have been found in obese adipose tissue and contribute to the clearance of dead adipocytes [293, 294]. However, in our studies, these large cells were likely filtered out during cell isolation, and thus it is not known if they change with

WC.

In summary, we identified obesity-associated immune imprinting of multiple distinct cell subsets that likely contribute to WC-accelerated metabolic disease in our mouse model, and potentially in humans. Unfortunately, the role of many of these cell types and functions in regulating adipose homeostasis during weight gain are not well understood, and even less is known in WL and WC. However, our results suggest critical areas of interest for future studies. Increases in activated DCs, LAMs, and exhausted T cells suggest that antigen presentation is a critical point of regulation, or dysregulation, in obese AT. Additional studies reported in Chapter IV improve our understanding of AT antigen presentation by utilizing single cell T cell receptor sequencing to uncover clonal responses associated with AT during obesity. Macrophage lipid handling also appears to be important for AT regulation; however, whether this process reaches capacity or is dysregulated in obesity is not known. Moreover, dysregulation of macrophage lipid handling and the lipid scavenger receptor, TREM2, have been implicated as key features in numerous diseases, such as Alzheimer's, cancer, and infection – expanding the importance of our findings to additional immunological diseases. Finally, the loss of type 2 immune subsets, IL-33 responsiveness, and changes in the TRM transcriptional phenotype along with a concomitant increase in M1-like cells, support an increase in inflammation, which has been previously linked to insulin resistance. Taken together, these findings support continued investigation into AT immune cells during obesity, WL, and WC in both murine models and humans. Understanding which processes are critical for adipose homeostasis may help suggest pharmacological interventions that can be used during WL or weight regain to mitigate future metabolic disease risk. Additionally, studies utilizing other models of WL, such as exercise or bariatric surgery, could greatly improve our understanding of immunometabolism and will help to identify advantageous immunotherapeutic targets.

CHAPTER 4

Obesity-induced acceleration of adipose tissue CD8$^+$ T cell aging that persist during WL and weight regain.

4.1 Preface

Part of the work performed for this dissertation utilized paired single cell α and β TCR sequencing. These preliminary results are the foundation of an expanded study further identifying clonal T cell populations that contribute to AT inflammation and that may play an extended role in the pathogenesis of other diseases, such as T2D and cancer. Here, in Chapter IV, this preliminary data will be discussed along with additional approaches carried out to understand AT T cell characteristics. Furthermore, future directions for this work are outlined and the relevance of such findings is discussed with the hope that future trainees will continue this work.

4.2 Introduction

Marked inflammation in AT has been a central focus of primary obesity literature for over a decade. Many of the inflammatory mediators detected systemically and within AT are produced by effector CD8$^+$ T cells and it has long been known that CD8$^+$ T cells are enriched in obese AT compared to lean AT [154]. At the same time, T_{regs} are highly effective at suppression of effector CD8$^+$ T cells and are reduced in AT during diet-induced obesity (DIO) [145–148]. However, it remains unclear whether CD8$^+$ are the primary producers of inflammatory cytokines like IFN-γ and TNFα or whether they have the capacity to induce destruction of stressed cells in the local AT milieu.

In Chapter III, we confirmed that T_{regs} do not return to normal abundance that CD8$^+$ T cells remained enriched following WL. We also identified that most CD8$^+$ T_{EM} have an exhausted gene signature. Previously, our group had reported that CD8$^+$ T cells were clonally enriched in AT during obesity and other groups have determined that T_{regs} have

reduced clonality in AT following DIO [148]. However, very little work has been reported to explore clonality in the context of WL or weight regain, and even less has been completed to investigate specific T cell clones.

In this chapter, $CD8^+$ T cells in AT during WL and WC are explored using common surrogate surface markers as well as functional assessments of T cell cytokine production. Furthermore, two different experimental paradigms were used to characterize and identify the contribution of $CD8^+$ in the setting of DIO. Finally, clonality of AT $CD8^+$ T cells and T_{regs} is explored using paired α and β TCR sequencing and was used to generate retrogenic TCR constructs for future experiments.

4.3 Results

4.3.1 Effector memory T cells persist in AT after WL

In Chapter III, expression of transcripts associated with long-term survival and T cell memory formation were used to identify $CD8^+$ T_{EM}. Because preparation for CITE-seq requires cell capture, lysis, and reverse transcription of antibody-conjugated oligos and poly-A mRNA, it is possible for some cell types to be excluded. For example, it is difficult to maintain RNA integrity in RNase-rich cells, like eosinophils as discussed in Chapter I [124]. To confirm differences in abundance of AT $CD8^+$ T cells during obesity, WL, and WC, we performed flow cytometry for markers associated with $CD8^+$ T_{EM}. However, it is still necessary to liberate cells from the AT matrix using enzymatic digestion. We tested the effects of collagenase on T cell surface marker identification by treating T cells isolated from both AT and spleen with three different collagenase formulations followed by flow cytometry. We observed that AT T cells are sensitive to collagenase and, as a result, many TCR-β^+ cells appear as expressing neither CD4 or CD8α (Fig. 4.1a). While some of these double-negative cells are likely TCR expressing NKT cells, this data largely suggests AT T cell numbers are underestimated by flow cytometry. Regardless, we selected the least damaging collagenase, Type IV, and utilized fluorescence-minus one (FMO) controls to guide

our gating for CD8$^+$ T_{EM} markers (Fig. 4.1b).

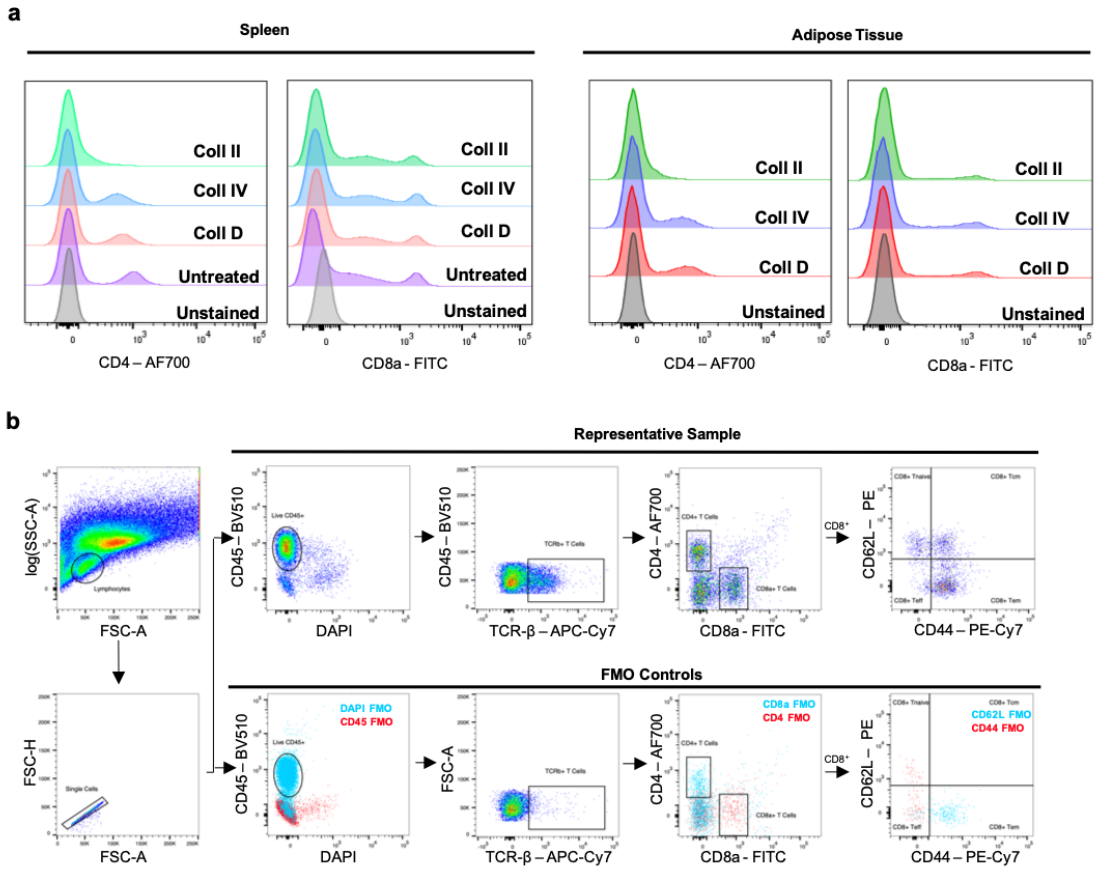

Figure 4.1: Surface T cell markers are sensitive to collagenase digestion. **a** Representative fluorescence intensity of CD4 (Alexafluor-700) and CD8α (FITC) for spleen (left) and adipose tissue (right) using collagenases type IV, II, and D. Unstained indicates control samples that were not treated with antibody and untreated indicates samples that were not enzymatically digested with any collagenase. **b** Gating schema for CD8$^+$ T_{EM} markers showing fluorescence-minus one (FMO) controls and a representative fully stained sample.

Flow cytometry reproduces many of the observations that were described using CITE-seq. Normalized to the AT mass collected for cell isolation (i.e. cells per gram of tissue collected), number of CD4$^+$ was significantly increased in eAT from WL mice. Number of CD8$^+$ T cells per gram of tissue was increased in obese and WC eAT compared to lean eAT and even further increased in WL eAT (Fig. 4.2a). Because we report that there are differences in adipocyte size between lean and WL groups in Chapter III, and therefore the relative cellularity of AT, the relative proportion of CD4$^+$ and CD8$^+$ T cells of all viable

leukocytes (% of live CD45$^+$) was also determined (Fig. 4.2b). Percent of CD4$^+$ T cells was slightly elevated in WL mice compared to lean mice, but were not significantly different from obese or WL mice. Percent of CD8$^+$ T cells was increased in obese and WC eAT compared to lean eAT and even further increased in WL eAT. No statistically significant differences were observed between groups for the number of naïve CD8$^+$ T cells ($T_{naïve}$) or CD8 $^+$ T_{CM} normalized to eAT mass (Fig. 4.2c). Effector CD8$^+$ T cells (T_{eff}) number normalized to eAT mass were slightly elevated in the WL mice compared to lean mice. Number of CD8 $^+$ T_{EM} normalized to eAT mass were increased in obese and WC eAT compared to lean eAT and even further increased in WL eAT. The relative proportion of each CD8$^+$ T cell subset of total CD8$^+$ T cells suggests that progressive enrichment for CD8$^+$ T_{EM} occurs during obesity and WL, while there is an overall reduction in percent of CD8$^+$ $T_{naïve}$ cells (Fig. 4.2d).

4.3.2 Depletion of CD8$^+$ T cells during weight regain does not protect against WC-associated impairment of glucose tolerance.

Since CD8$^+$ T_{EM} are most enriched during the transitions from lean to obese and obese to WL in AT, we utilized an antibody-based depletion approach to acutely deplete all CD8$^+$ T cells systemically. This approach allows us to remove memory CD8$^+$ T cells, but allows for reinfiltration of newly generated CD8$^+$ $T_{naïve}$ once circulating antibodies have been cleared. We first performed a pilot study to test whether CD8α-targeted antibodies would effectively deplete CD8$^+$ T cells in multiple tissues and to identify at which point CD8$^+$ began to recover. We placed C57BL/6J mice on HFD for 8 weeks at which point mice received 100 μg of either CD8-depleting antibody (anti-CD8) or an IgG matched control antibody via intraperitoneal injection three times over 1 week (Fig. 4.3a). Half of the mice were sacrificed 1 week following beginning of treatment (9 weeks on diet) while the remaining mice were sacrificed 4 weeks after completion of treatment (12 weeks on diet). Thymus, blood, spleen, eAT, and sAT were collected and CD8$^+$ T cells were measured

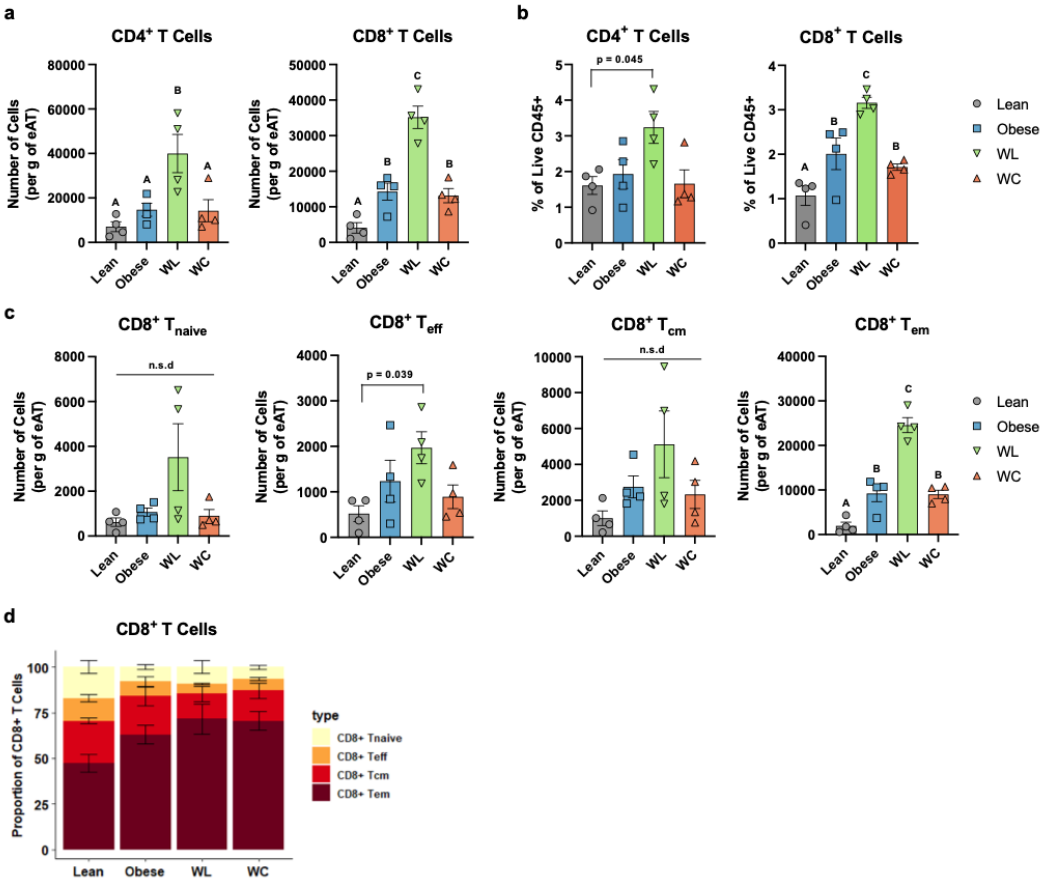

Figure 4.2: AT CD4$^+$ and CD8$^+$ are enriched after WL. a CD4$^+$ and CD8$^+$ normalized to total adipose tissue (AT) mass for lean (grey), obese (blue), WL (green) and WC (orange) mice. **b** Proportion of CD4$^+$ and CD8$^+$ of total CD45$^+$ leukocytes. **c** Relative abundance normalized to total AT mass for $T_{naïve}$, T_{eff}, T_{CM}, and T_{EM} CD8$^+$ T cell subsets for each diet group. **d** Proportion of each CD8$^+$ T cell subset of total CD8$^+$ T cells. Mean $\pm$ SEM shown, *p$<$0.05 using T tests with Tukey correction for multiple comparisons, n=4. Significant differences between pairwise comparisons are indicated by different letters, by reported adjusted p value, or as no significant difference (n.s.d).

by flow cytometry (Fig. 4.3b). After 1 week of anti-CD8 treatment, mice had reduced CD8$^+$ T cell numbers in all tissues except for the thymus. Thymic CD8$^+$ trended towards a reduction, but was non-significant, suggesting that the ability to generate and mature CD8$^+$ T cells in the thymus was not impaired by depleting antibody treatment. Following 3 weeks of recovery (weeks 9-12), CD8$^+$ T cell numbers were incompletely recovered in the blood, spleen, and sAT, and fully recovered in the thymus and eAT.

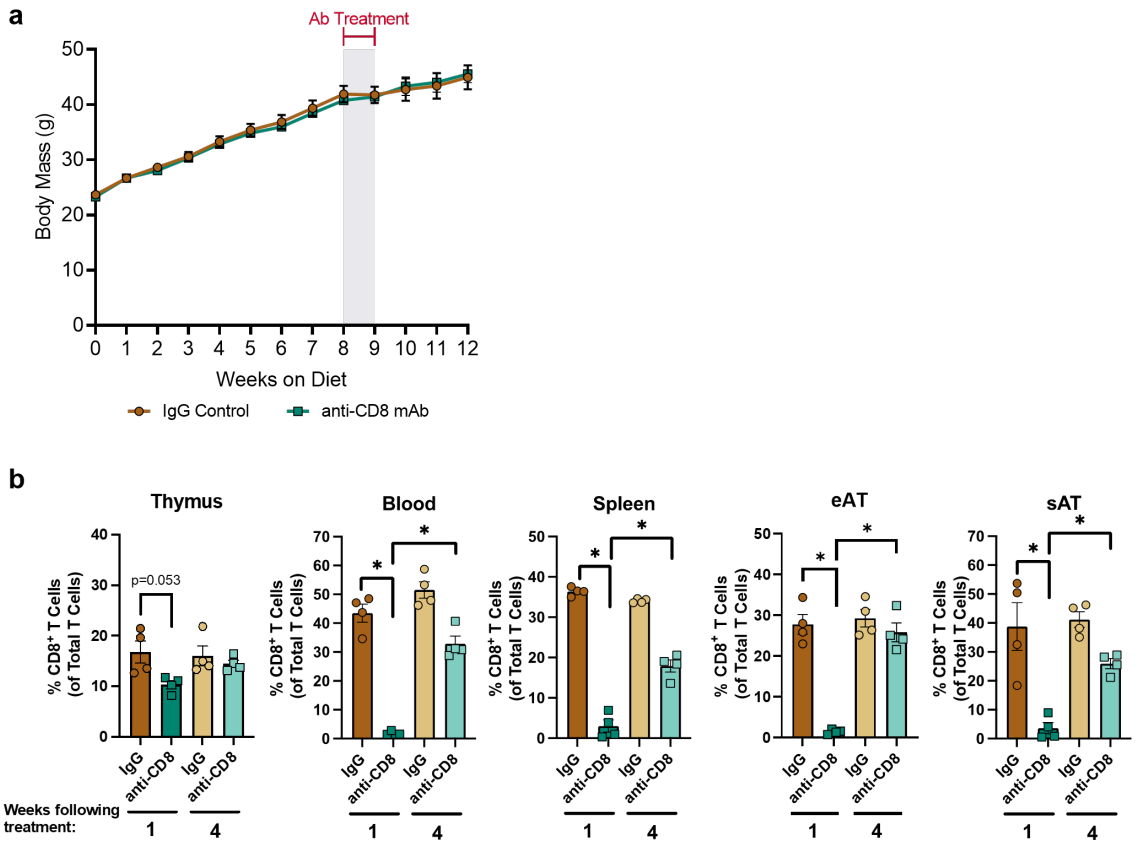

Figure 4.3: CD8$^+$ T cells recover within 3 weeks of antibody-mediated CD8$^+$ T cell depletion. a Body mass curve for mice over 12 weeks on HFD. 1 week antibody treatment is indicated by gray overlay for mice treated with with IgG control (brown) or anti-CD8 (teal) monoclonal antibodies. **b** Proportion of CD8$^+$ T cells of total T cells in thymus, blood, spleen, epididymal adipose tissue (eAT), and subcutaneous adipose tissue (sAT) 1 and 4 weeks following beginning of treatment measured by flow cytometry. Mean $\pm$ SEM displayed, *p$<$0.05 or as indicated by t-test with Bonferroni correction for multiple comparisons.

To determine if memory CD8$^+$ T cells were necessary for WC-associated glucose intolerance, we utilized CD8-targeted monoclonal depleting antibodies to deplete CD8$^+$ T cells for the final week of WL (weeks 17-18). We hypothesized that, following depletion, naïve T cells would infiltrate eAT during weight regain, but also that naïve T cells were insufficient to result in impaired glucose tolerance. Therefore, we expected to see improved glucose tolerance in WC mice that received depleting monoclonal antibodies (mAbs) compared to control antibodies, with no change in obese groups. We observed that CD8$^+$ T

cell depletion had no effect on rate of weight regain, but obese mice treated with depleting antibody had slightly elevated body mass compared to obese mice treated with IgG control antibody during the final 9 weeks of diet (Fig. 4.4a). Lean mass was similar between groups, but fat mass was slightly increased in groups receiving anti-CD8 mAb compared to obese IgG treated mice (Fig. 4.4b). Anti-CD8 mAb treatment had no effect on glucose tolerance in obese mice by ipGTT only a mild, non-significant effect on glucose disposal in WC mice (Fig. 4.4c). However, anti-CD8 mAb treated WC mice had increased fasting glucose following a 5 hour fast. Taken together, this data suggests that memory formation in AT CD8$^+$ T cells is not essential for WC-associated impairments in glucose tolerance.

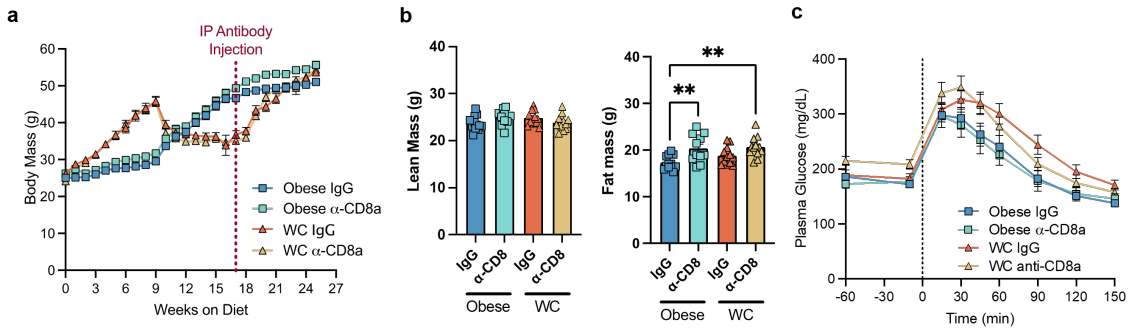

Figure 4.4: CD8$^+$ T cell depletion prior to weight regain does not protect glucose tolerance in mice. **a** Body mass of obese (blue) and WC (orange) mice receiving either IgG control mAb or anti-CD8 mAb. Initiation of treatment lasting one week is indicated by the red dashed line. **b** Lean mass (left) and fat mass (right) after 27 weeks of diet. **c** Intraperitoneal glucose tolerance test following a 5 hour fast with a 2 g/kg lean mass dose of 20% dextrose solution. Mean ± SEM shown, **p<0.01.

4.3.3 Anti-PD-1 immunotherapy does not reduce obesity-associated impaired glucose tolerance

Using CITE-seq in Chapter III, we identified that AT T cells express an exhausted T cell transcriptional phenotype and also express high levels of PD-1 on their surface. We utilized flow cytometry to further confirm that AT CD8$^+$ T cells express PD-1 and observed that PD-1 surface expression was elevated by obesity and remained high during WL and WC (Fig. 4.5).

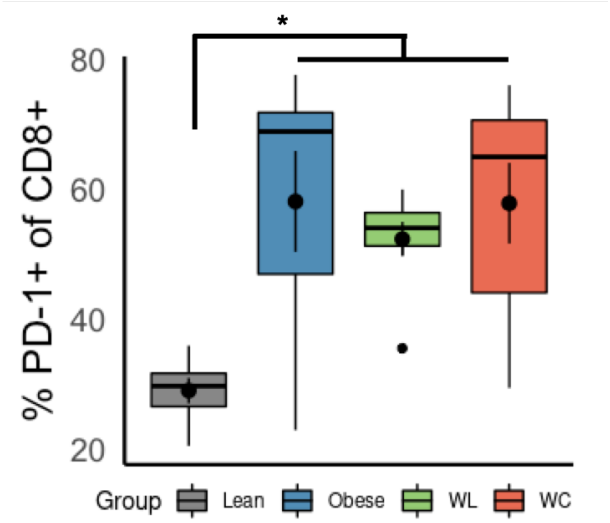

Figure 4.5: PD-1 expression in AT T cells during WL and WC. Proportion of adipose tissue (AT) $CD8^+$ T cells expressing PD-1. Boxes represent 50th percentile with median indicated by solid black line and the average indicated by the large black circle within the box. Small black circles indicate outliers. Significant differences detected by t-tests with Tukey correction for multiple comparisons, *$p<0.05$, n=8.

Therefore, it is possible that T cells in AT become exhausted during obesity, thereby having impaired effector function and failing to induce inflammation in AT during WC. To test this hypothesis, we utilized an anti-PD-1 neutralizing monoclonal antibody. This antibody blocks interactions between PD-1 and its ligands PD-L1 and PD-L2. C57BL/6J male mice were placed on HFD for 12 weeks. Between weeks 8 and 12, mice were treated three times per week with either 200 μg of anti-PD-1 or control IgG. Anti-PD-1 treatment did not have an effect on body mass (Fig. 4.6a) or food intake (Fig. 4.6b). Lean mass (Fig. 4.6c) and fat mass (Fig. 4.6d) prior (week 8) and following treatment (week 12) were also not different between treatment groups. No differences in fasting glucose (Fig. 4.6e), glucose tolerance prior to treatment (Fig. 4.6f), glucose tolerance after treatment (Fig. 4.6g), or ipGTT AUC (Fig. 4.6h) were observed between treatment groups. Overall, these data suggests that anti-PD-1 neutralizing antibodies in the context of obesity do not impair glucose tolerance.

To address the possibility that T cell driven immune cell expansion and infiltration in the

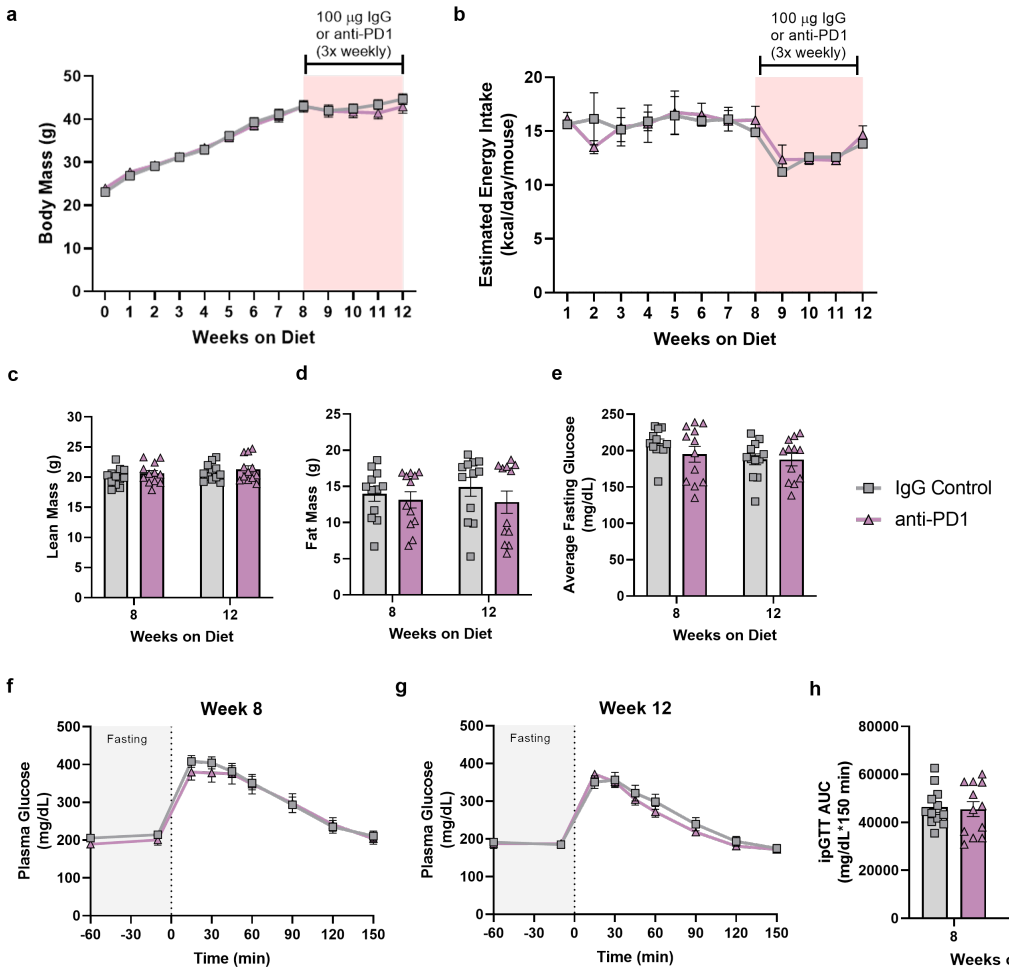

Figure 4.6: PD-1 neutralizing antibodies do not affect weight gain or protect obese mice against impaired glucose tolerance. a Body mass curves and **b** food intake of mice placed HFD for 12 weeks and challenged with IgG control (gray) or neutralizing PD-1 antibodies (purple). Light red shading indicates duration of treatment. **c** Lean and **d** fat mass at 8 weeks (prior to treatment) and 12 weeks (post treatment) on diet. **e** Average fasting glucose, **f, g** intraperitoneal glucose tolerance test (ipGTT), and **h** area under the curve (AUC) after 8 and 12 weeks on diet. Two-way ANOVA with bonferroni correction for multiple comparisons performed for body mass, food intake, and ipGTT (factors = time x treatment). T-tests performed for lean mass, fat mass, average fasting glucose, and ipGTT AUC. No significant differences observed, n=12.

context of anti-PD-1 treatment occured without disrupting glucose tolerance, we isolated sAT, liver, and pancreas and performed histology on tissue sections. Hematoxylin and eosin staining, which has previously been used to identify immune cell infiltration during anti-PD-1 treatment in mice [295], did not suggest anti-PD-1 mediated immune cell infiltration

into any of the tissues we assessed (Fig. 4.7).

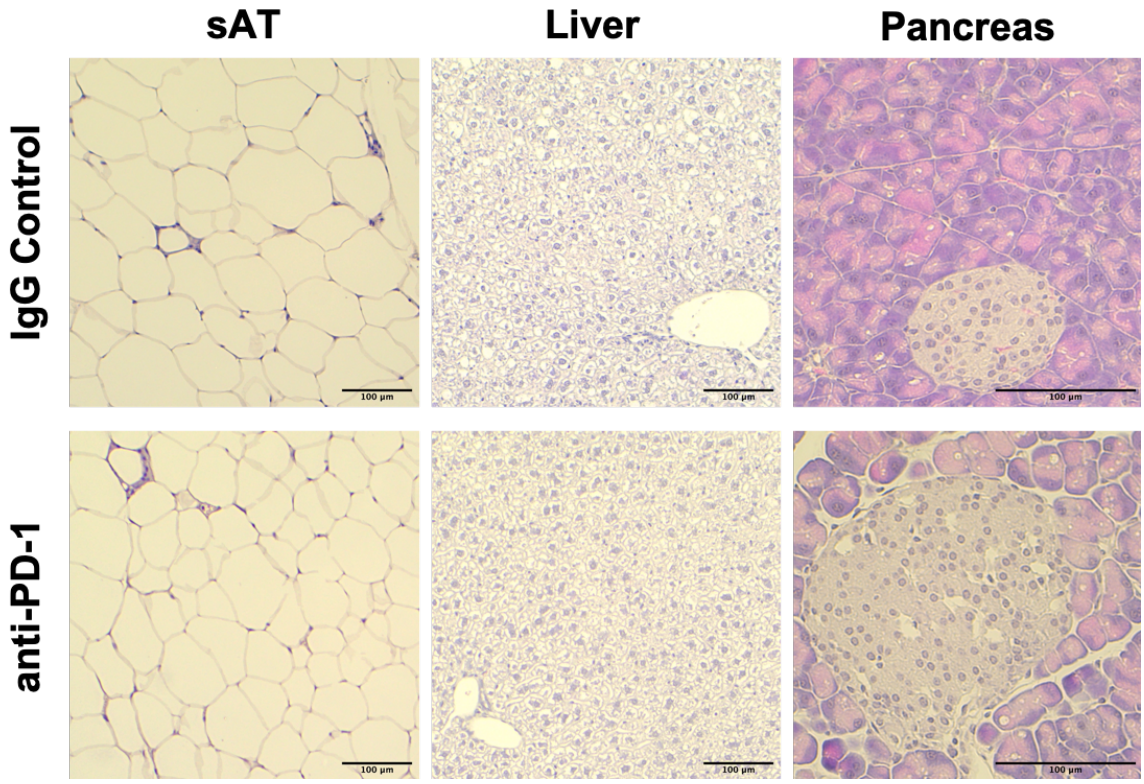

Figure 4.7: PD-1 neutralizing antibodies do not induce leukocyte infiltration during HFD. Representative hematoxylin and eosin staining of 5 μm sections of subcutaneous adipose tissue (sAT; 20x), liver (20x), and pancreas (40x) for IgG control treated (top) and anti-PD-1 treated (bottom) obese mice. Scale bar represents 100 μm.

4.3.4 AT CD8$^+$ T_{EM} acquire an age-associated phenotype during obesity that is retained with WL.

Although PD-1 is often used as a marker of T cell exhaustion, it has many functions and is expressed very early during T cell activation. Because no T cell expansion or overt AT inflammation was observed in anti-PD-1 treated obese mice, we used an *ex vivo* stimulation approach to determine if AT T cells are dysfunctional during WL and WC. Intracellular IFN-γ and IL-2 following stimulation was measured by flow cytometry (Fig. 4.8a). Paired unstimulated controls were included to determine baseline cytokine levels. Stimulation of CD8$^+$ T cells induced production of IFN-γ in cells isolated from lean and WL eAT, but

cells isolated from obese or WC AT had an impaired response (Fig. 4.8b). Additionally, while IL-2 production was robustly stimulated in lean CD8$^+$ T cells, obese, WL, and WC CD8$^+$ T cells did not increase production of IL-2 during stimulation (Fig. 4.8c). Taken together, this data suggests that AT CD8$^+$ T cells do have dysfunctional cytokine response to stimulation during obesity and that this effect may be persistent during WL and weight regain.

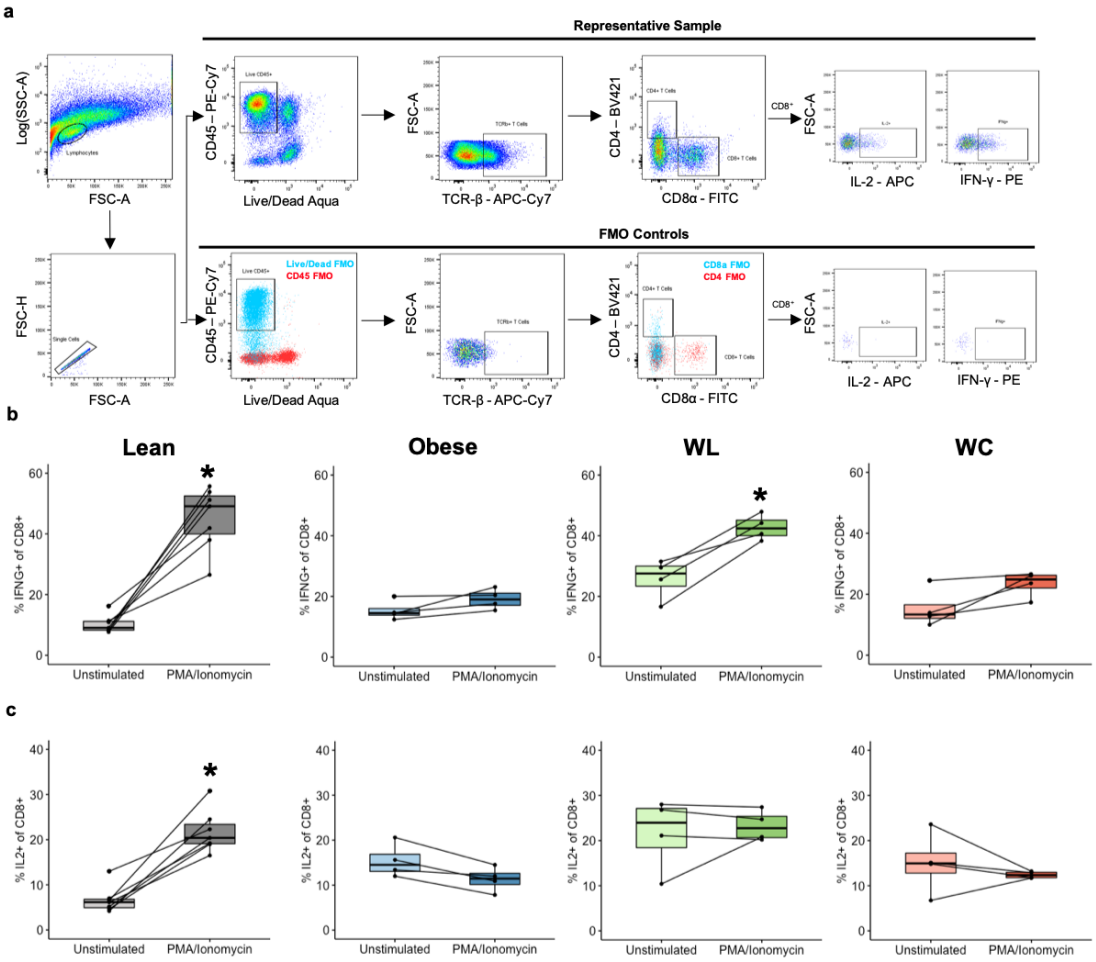

Figure 4.8: CD8$^+$ T cells have impaired cytokine response to stimulation following obesity. **a** Flow gating schema for a representative sample and fluorescence minus one (FMO) controls. Proportion of CD8$^+$ T cells expressing IFN-γ **b** and IL-2 **c** following 6 hours of stimulation. Lines connect paired unstimulated/stimulated samples that were isolated from the same mouse. T-tests were performed to compare unstimulated and stimulated samples, *$p<0.05$, n=4.

Since we previously identified elevated expression of exhaustion-associated transcripts in obese, WL, and WC CD8$^+$ AT T cells, but observed no response to anti-PD-1 treatment, we returned to our published scRNA-seq data to identify other potential mechanisms of impaired CD8$^+$ T cell response in AT. Interestingly, genes associated with typical cytotoxic proteins, such as granzyme B, were low or absent in most AT $^+$ T cells (Fig. 4.9a). However, expression of the non-cytolytic peptide granzyme K was very high in obese, WL, and WC CD8$^+$ T_{EM} (Fig. 4.9b).

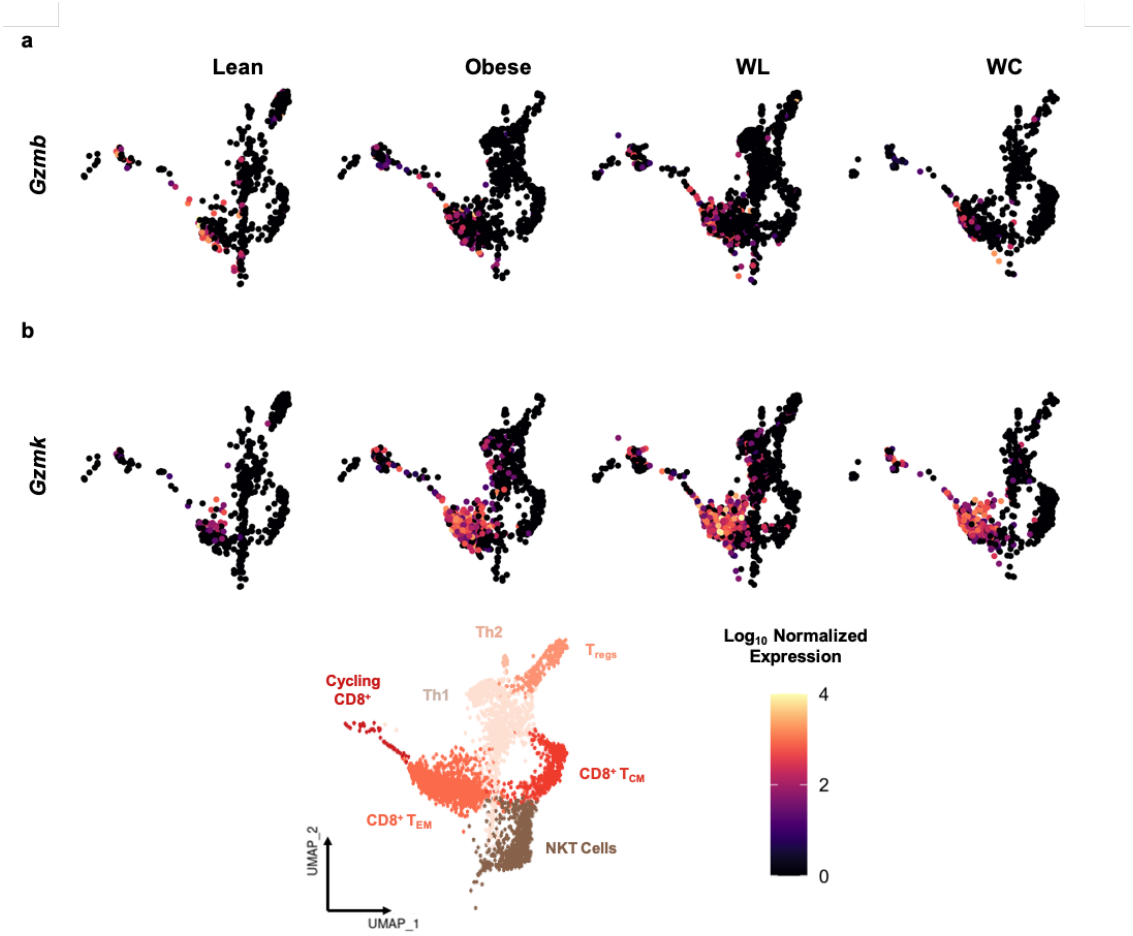

Figure 4.9: AT CD8$^+$ T_{EM} highly express granzyme K during obesity. Log normalized gene expression of **a** granzyme B (*Gzmb*) and **b** granzyme K (*Gzmk*) in AT T cells. Cell clusters and annotations are shown for reference.

Reduced expression of granzyme B, increased expression of granzyme K, and expression of exhaustioon-associated transcripts has been previously described as an age-

associated phenotype [216]. Therefore, it is possible that obesity results in accelerated immune aging that can contribute to disease progression.

4.3.5 AT CD8$^+$ T cells are clonally enriched during WL and WC.

One common feature of age-associated CD8$^+$ T cells in multiple tissues is increased TCR clonality [216]. Therefore, we performed V(D)J sequencing on our CITE-seq samples to recover paired α and β TCR chain information. To visualize clonal enrichment, cells were binned into groups based on their clonal size (i.e the number of cells with a matching clone). Clonal bins were determined as either single clones (only one cell with a given clonotype) or into one of four quartiles (2, 3-5, 6-15, or >16). Immunosuppressive AT T_{regs} had reduced clonality in obese, WL, and WC mice compared to lean mice (Fig. 4.10a). In addition, CD8$^+$ T_{EM} clonality was most enriched in WL and WC mice (Fig. 4.10b).

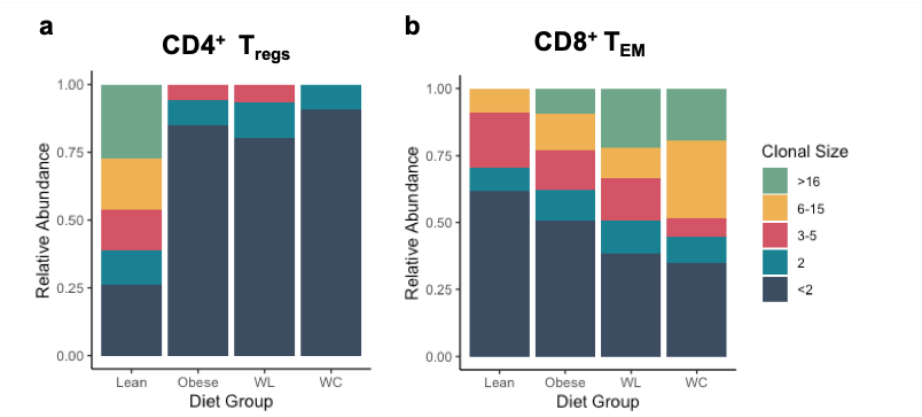

Figure 4.10: Lean adipose is enriched for clonal T_{regs} while obese, weight loss, and weight cycled adipose are enriched for clonal CD8$^+$ T_{EM} Clonotype enrichment binned by clone size and reported as relative abundance of each bin per diet group for **a** CD4$^+$ T_{regs} and **b** CD8$^+$ T_{EM}.

To determine if any clones detected in our V(D)J sequencing have been previously described, we utilized the public TCR database, TCRdb. Three clonotypes that were enriched in WL and WC CD8$^+$ T_{EM} have been previously associated with T1D (Table 4.1).

Clonotypes that have been previously associated with T1D express very little Gzmb or Prf1 (coding for perforin) and instead express Gzmk (Fig. 4.11). These data suggest

Group Enrichment	Chain	V Gene	J Gene	CDR3
WL	α	TRAV7N-4	TRAJ52	CAVSEHGANTGKLTF
	β	TRBV5	TRBJ2-7	CASSQEGLVSYEQYF*
Obese	α	TRAV3D-3	TRAJ15	CAVSARQGGRALIF
	β	TRBV31	TRBJ1-1	CAWSLSPGGTEVFF
WC	α	TRAV3D-3	TRAJ26	CAVSPNNYAQGLTF
	β	TRBV3	TRBJ2-4	CASSLAGQGQNTLYF*
WL	α	TRAV13N-1	TRAJ6	CATSGGNYKPTF
	β	TRBV3	TRBJ2-7	CASSPTFSSYEQYF*
WL	α	TRAV4-4/DV10	TRAJ34	CAAVSSNTNKVVF
	β	TRBV3	TRBJ2-2	CASRGGRRTGQLYF

*Previously associated with T1D

Table 4.1: Top 5 most enriched AT CD8$^+$ T cell clonotypes.

that autoreactive *Gzmk*$^+$ T cells are enriched during obesity and persist during settings of WL, potentially contributing to peripheral inflammation and impairing systemic glucose regulation.

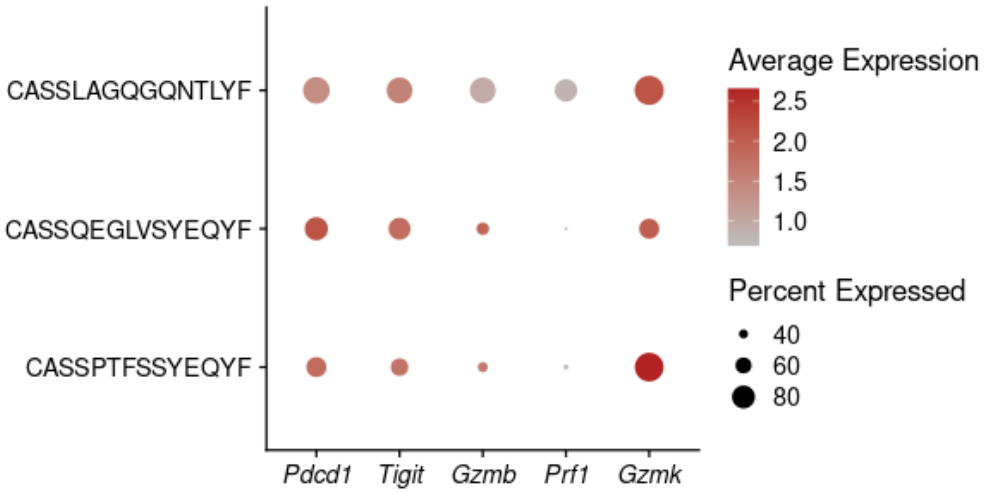

Figure 4.11: T1D-associated T cell clonotypes found in WL and WC express Gzmk. Averaged expression of *Pdcd1, Tigit, Gzmb, Prf1, and Gzmk* in cells expressing TCR-β CDR3s previously associated with T1D in TCRdb.

4.4 Discussion

AT CD8$^+$ T cells are challenging to measure using traditional markers of memory and effector cells. It is clear that tissue processing has a significant effect on the surface repertoire

of T cells, with many protein epitopes altered in the presence of collagenases. More importantly, most T cells, regardless of transcriptional profile, express proteins associated with effector memory subpopulations that were originally defined in the blood and secondary lymphoid organs. The tissue specificity of T cell markers has recently been highlighted in studies showing critical differences in T cell surface protein expression in the skin, liver, and intestines [296, 297]. Therefore, complimentary approaches utilizing surface protein markers, patterns of gene expression, and functional assays are necessary to accurately characterize AT $CD8^+$ T cells. In Chapter III, CITE-seq was used to characterize $CD8^+$ AT T cells and it was observed that $CD8^+$ T_{EM} were enriched in WL and WC AT. Using flow cytometry, we show here that $CD8^+$ T_{EM} are most enriched in WL AT, but are also elevated in obese and WC AT.

To determine if these $CD8^+$ T cells play a role in impaired glucose disposal, we utilized an antibody depletion approach. Antibody depletion effectively depletes most $CD8^+$ T cells in blood, spleen, sAT, and eAT. Furthermore, $CD8^+$ numbers recover within approximately 3 weeks in AT. When cells were acutely depleted prior to weight regain, only fasting plasma glucose was elevated compared to IgG control treated mice. These data suggest that $CD8^+$ memory may not be a necessary component of the glucose disposal phenotype observed in WC mice. In other settings, such as aging, some $CD8^+$ T cells highly express markers of memory. However, naïve T cells from a young (”young T cells”) mouse transplanted into an old mouse phenotypically match the original T cells found in the recipient (”old T cells”) [216]. Therefore, it is likely that the phenotype of AT T cells and their contribution to disease progression does not require antigen-induced memory and expansion.

Previously, anti-PD-1 neutralizing antibodies in AT did not affect AT T cell activation during obesity after 10 days of treatment [224]. In our hands, PD-1 neutralizing antibody treatment for 4 weeks also did not induce T cell infiltration into peripheral tissues and did not affect glucose tolerance. However, T cells isolated from eAT of obese, WL, and WC mice did have impaired production of cytokines in response to stimulation. Taken

together, these findings suggest that PD-1 derived signaling is not likely to be the driver of dysfunctional T cell response in AT.

Surprisingly, AT T cells isolated during WL and WC transcriptionally match T cells observed in very old mice. For reference, the mice in this study are only 35-weeks old while those in aging study are >2 years old. Marked reductions in expression of *Gzmb* and increased expression of *Gzmk* suggest that obesity accelerates immune cell aging in AT. In contrast to GZMB and perforin, GZMK is not believed to cause cell lysis. Instead, GZMK promotes inflammatory cytokine production by other cells in the same microenvironment. For example, GZMK stimulates production of IL-6, CCL2, and CCL5 in senescent fibroblasts [216].

We also observed clonal enrichment of $CD8^+$ T_{EM} in obese, WL, and WC AT using V(D)J sequencing. Further analysis identified a T cell clonotype that has been reported as being insulin-responsive. However, WC mice do not undergo T1D-associated β cell destruction as we discuss in the next chapter. At least in the AT where we measured these clonotypes, the clonal insulin-responsive T cells do not express GZMB or perforin. Therefore, autoreactive T cells that may recognize β cells are unlikely to directly induce β cell death, but may impair β cell function and contribute to dysregulation of glucose homeostasis in the context of body weight variability.

4.5 Future Directions

The observations highlighted in this chapter revealed many new unanswered questions. First, the direct effects of $CD8^+$ T cells in AT remain unclear. While these cells do not appear to induce cell lysis through delivery of GZMB or perforin, they do still retain the potential to induce inflammation through GZMK. However, GZMK has not yet been studied in the context of obesity or T2D. It is not also known if stromal cells, such as adipocytes and β cells, respond directly to GZMK stimulation. However, 3T3-L1 fibroblasts do respond to GZMK stimulation and 3T3-L1 fibroblasts are often differentiated into preadipocyte-

like cells *in vitro*. Therefore, preliminary studies could identify the effects of recombinant GZMK on inflammatory cytokine production and lipid storage or lipolysis in culture. Additional studies would characterize primary adipocytes, other adipose tissue leukocytes (e.g macrophages) and isolated islets treated with recombinant GZMK or co-cultured with $CD8^+$ T cells from obese mice.

Another question that remains is what antigens might activate clonal AT T cells. By V(D)J sequencing, we have already identified numerous enriched $CD8^+$ T cell clones in WL and WC eAT. To assess if these clones are specifically recruited to AT, a retrogenic approach can be used. Stem cells treated with retroviruses that induce expresssion of paired α/β TCR chains can be generated from the gene usage information we have collected from V(D)J sequencing. The method to generate these retrogenic constructs is described in Chapter II and an example plasmid construct has already been generated using the most enriched TCR in WL eAT (Fig. 4.12).

TCR retrogenic studies could determine whether T cells with a selected TCR have the capacity to migrate and proliferate in AT or other peripheral tissues (e.g pancreatic islets), but retrogenic T cells delivered to a naïve mouse may not experience the same environment as obese, WL, or WC T cells do. Therefore, subsequent adoptive cell transfer studies are likely to be essential for determining if AT is a specific reservoire for $GZMK^+$ T cells in the context of obesity.

Most importantly, it remains unclear how obesity induces an age-associated phenotype. Similarities between obesity and aging have already been established for multiple diseases, including cardiovascular disease, T2D, and Alzheimer's. If obesity does accelerate expression of an age-associated transcriptional profile, as our data suggests, then $CD8^+$ T cells may be a critical contributor to inflammaging. It is already known that obese individuals have improved response to immunotherapy in the context of many cancers. However, it remains unknown whether age-associated T cells can be induced to express classical $CD8^+$ cytotoxic proteins. This question may also improve our understanding of the pathogen re-

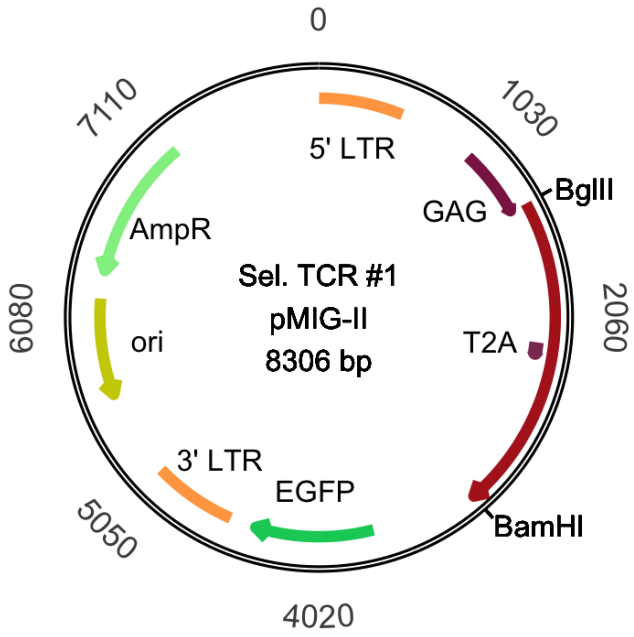

Figure 4.12: Example retrogenic TCR construct. Plasmid construct containing a 1,805 bp nucleotide sequence encoding for a paired α and β TCR (red arrow) linked by a T2A peptide. Construct also contains expression vectors for AmpR for antibiotic selection and eGFP for positive fluorescence selection by FACS.

sponse during infection in obese individuals, who likely already have a pool of enriched memory cells in AT. Therefore, continued work to elucidate the mechanisms that induce the GZMB to GZMK shift (and vise-versa) in $CD8^+$ T cells has broad applicability.

CHAPTER 5

WC impairs pancreatic insulin secretion but does not perturb whole-body insulin action in diet-induced obese mice

Adapted from Winn, N.C., Cottam, M.A., Bhanot, M., Caslin, L.H., Garcia, J.N., Arrojo e Drigo, R., and Hasty A.H. Revisions submitted to *Diabetes*, May 2022.

5.1 Introduction

Blood glucose is controlled within a narrow window, minute-to-minute, through the integration of multiple organ systems and tissues. The balance between endogenous glucose production and blood glucose clearance defines glycemic control – each of which rely on the peripheral actions of pancreatic insulin. Chronic obesity is characterized by impaired glucose tolerance and hyperinsulinemia [298, 299]. The combination of elevated blood glucose and hyperinsulinemia promotes the expansion of pancreatic β cell mass [300], which is considered a compensatory adaptation to worsening glycemia. Although hyperinsulinemia is typically considered a consequence of peripheral insulin resistance [301], a growing body of evidence suggests it may be a driver of – or at least a significant contributor towards – worsening insulin resistance that accompanies obesity [298–300, 302, 303]. Nonetheless, prolonged hyperglycemia/hyperinsulinemia causes β cell fatigue and ultimately β cell failure, defined clinically as T2D [304].

Caloric restriction (CR) is known to improve obesity-evoked insulin resistance in humans and rodents; whereas one or more bouts of weight regain (e.g., WC) is linked with increased risk of a cluster of cardiometabolic diseases as compared to obesity alone [24, 26, 27]. As discussed in Chapter II, our group developed a murine model of WC whereby mice undergo periods of diet-induced weight gain, WL, and weight regain, which accelerates glycemic dysfunction compared with weight-matched obese controls [250, 305]. Though our prior work establishes that WC augments glucose intolerance, it is unclear whether

this is principally attributable to decreased insulin action (i.e., defined in this context as decreased suppression of endogenous glucose production and decreased insulin-mediated glucose clearance), impaired pancreatic islet function, or a combination of both. Uncovering the mechanisms for impaired glucose regulation caused by WC may have clinical implications given that most obese individuals regain lost weight within 1-2 years [11, 14–16].

In this study, we aimed to systematically pinpoint the major control points and mechanisms by which glycemic deterioration manifests in WC mice using rigorous in vivo and ex vivo functional tests. We hypothesized that WC worsens peripheral insulin action and glucose clearance. Instead, we report that WC-induced glucose intolerance is not explained by worsened whole-body insulin action but rather attributable to inadequate insulin secretion that is directly linked to loss of β cell identity and adaptive plasticity. Taken together, our results suggest that repeated bouts of WL and weight regain impair pancreatic compensation to body weight variability and, by consequence, insulin secretion in mice.

5.2 Results

5.2.1 WC-induced glucose intolerance is not attributable to impaired insulin action.

Body mass was not different between obese and WC mice (Fig. 5.1a). Arterial glucose was clamped at 120 mg/dl via variable (GIR. Neither clamped glucose nor GIR were different between groups (Fig. 5.1b & 5.1c). In addition, endogenous glucose rate of appearance ($EndoR_a$) and glucose turnover (R_d) were not different between groups during basal or clamp conditions (Fig. 5.1d & 5.1e), respectively. Compared to obese mice, clamped, but not fasting insulin concentrations were significantly lower in WC mice (Fig. 5.1f). Importantly, exogenously infused insulin (human) was not different between WC and obese mice (Fig. 5.1g), suggesting that the differences are due to endogenous insulin secretion or insulin processing. Consistent with a secretion phenotype, clamp c-peptide levels were lower in WC animals (Fig. 5.1h). To demonstrate the relationship between glucose flux and in-

sulin, arterial insulin was plotted as a function of glucose turnover and EndoR_a (Fig. 5.1i & 5.1j). In this representation, decreased insulin action would be indicated by a right-shifted trendline with a decreased slope. Thus, it appears that WC mice do not have decreased insulin action compared to obese controls. During hyperinsulinemia, a bolus of [^{14}C]2DG was administered to determine the glucose metabolic index (i.e., estimate of tissue glucose uptake; R_g). Muscle (gastrocnemius, vastus lateralis, and soleus) and eAT R_g, were decreased in WC mice (Fig. 5.1k). However, whole-body glycolysis and glucose storage (computed from the detritiation of [3-^{3}H]-glucose) were not different between groups (Fig. 5.1l).

There were no detectible differences in liver glycogen between groups (Fig. 5.2a), whereas liver triglycerides were lower in WC versus obese mice (Fig. 5.2b). The latter may be related to the effect of chronic hyperinsulinemia on liver steatosis [306, 307]. Given that insulin concentrations were lower in WC mice during the hyperinsulinemic-euglycemic clamp, we performed ex vivo insulin stimulation and assessed phosphorylation of AKT(ser473) to determine insulin responsiveness in an isolated system. Gastrocnemius and sAT explants isolated from lean controls, obese, and WC mice were incubated in the absence or presence of insulin (low, 10nM; high, 100nM) and subsequently immunoblotted for total AKT and pAKT(ser473) (Fig. 5.2b). Compared to lean animals, pAKT(ser473) was decreased in obese and WC groups in sAT with no differences between obese and WC groups (Fig. 5.2d). In gastrocnemius muscle, there were also no differences in pAKT(ser473) between WC and obese mice (Fig. 5.2c). However, a trend for greater pAKT(ser473) in WC versus obese muscle was observed after high dose insulin. These data suggest that when insulin concentrations are matched *ex vivo*, WC animals do not have worsened proximal insulin signaling than obese controls. Taken together, data from hyperinsulinemic-euglycemic clamp and ex vivo insulin responsiveness experiments indicate that lower endogenous insulin rather than impaired insulin action contributes to delayed glucose clearance in WC mice.

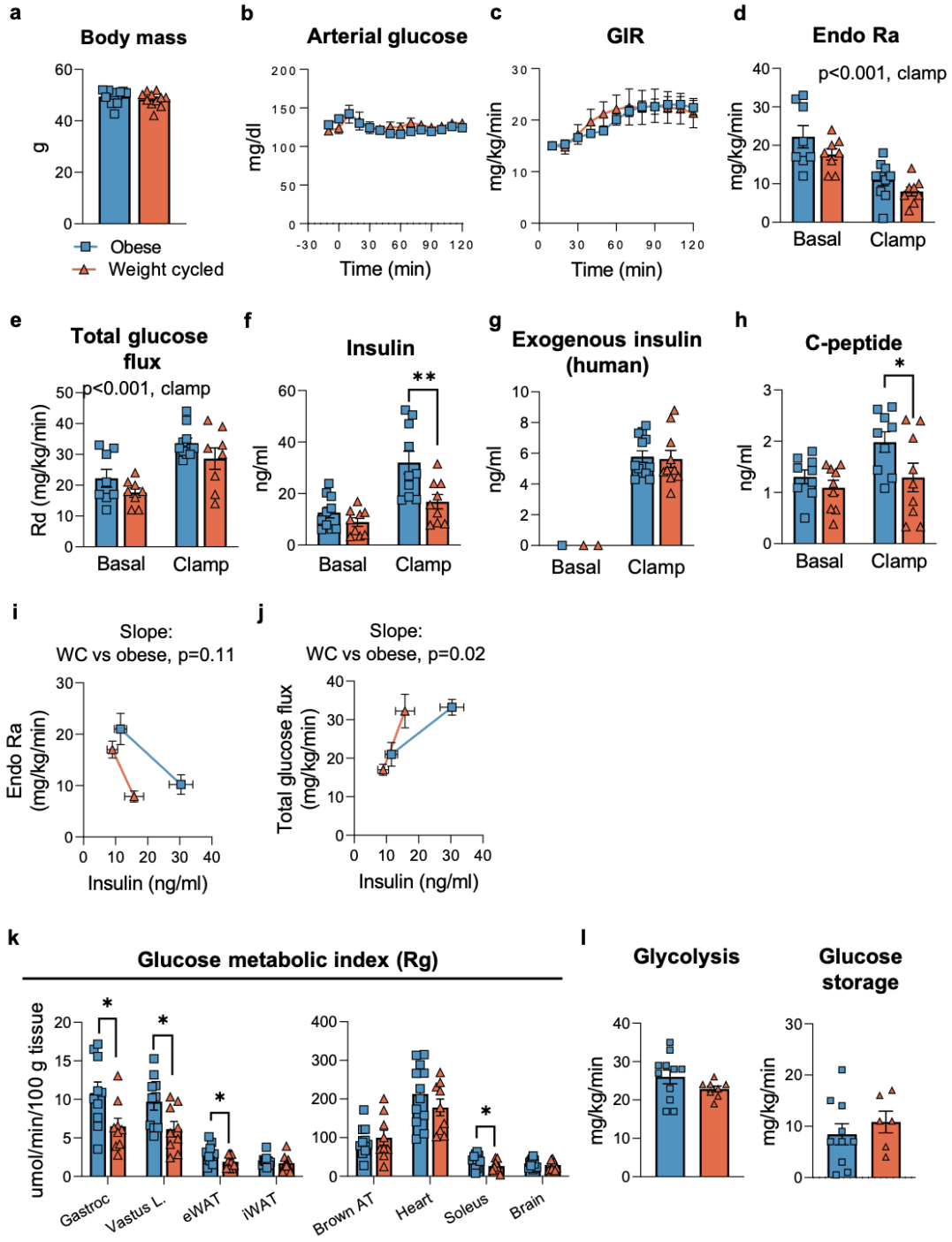
a
Body mass
g
Obese
Weight cycled
b
Arterial glucose
mg/dl
Time (min)
c
GIR
mg/kg/min
Time (min)
d
Endo Ra
p<0.001, clamp
mg/kg/min
Basal
Clamp
e
Total glucose flux
p<0.001, clamp
Rd (mg/kg/min)
Basal
Clamp
f
Insulin
**
ng/ml
Basal
Clamp
g
Exogenous insulin (human)
ng/ml
Basal
Clamp
h
C-peptide
*
ng/ml
Basal
Clamp
i
Slope:
WC vs obese, p=0.11
Endo Ra (mg/kg/min)
Insulin (ng/ml)
j
Slope:
WC vs obese, p=0.02
Total glucose flux (mg/kg/min)
Insulin (ng/ml)
k
Glucose metabolic index (Rg)
umol/min/100 g tissue
Gastroc
Vastus L.
eWAT
iWAT
Brown AT
Heart
Soleus
Brain
l
Glycolysis
mg/kg/min
Glucose storage
mg/kg/min

Figure 5.1

Figure 5.1: WC-induced glucose intolerance is not attributable to impaired insulin action. **a** Body weight was collected followed by catheter hook-up, priming infusions, and clamped infusions prior to clamp. **b** Arterial glucose was measured frequently with a target concentration of 120 mg/dl. **c** Arterial glucose was maintained by exogenous glucose infusion rate (GIR). **d** Endogenous glucose rate of appearance ($EndoR_a$) and **e** glucose turnover (R_d) were assessed during basal and clamp conditions. **f** Total insulin, **g** exogenous human insulin, and **h** C-peptide concentrations were measured at baseline (t=-10) and during steady state (120 min) clamped conditions. Basal and clamp **i** $EndoR_a$ and **j** glucose turnover (R_d) were presented a function of respective insulin concentrations. **k** A bolus of [^{14}C]2DG was infused at 120 min and blood was sampled frequently to assess exponential isotopic decay. Mice were anesthetized at 155 min and tissues harvested and snap frozen. The glucose metabolic index (R_g) was assessed from ^{14}C radioactivity and presented per 100 g of tissue. (**l** the rate of whole-body glycolysis was determine from the detritiation of [3-^{3}H]-glucose and glucose storage was estimated from the difference in steady state glucose flux (R_d) and glycolysis. Independent t-tests were used to assess statistical differences between groups for panels **a**, **k**, and **l**. Two-way repeated measures ANOVA with time and group (obese vs WC) as factors were conducted for panels **b-h**. Multiple comparisons were assessed using Tukey post hoc testing. Differences in slopes were determined via simple linear regression for panels **i** and **j**. n=8-11/group. Data presented as mean $\pm$ SE.

5.2.2 WC impairs *in vivo* glucose stimulated insulin secretion independent of diet composition

To uncover if WC impairs *in vivo* pancreatic function, we conducted hyperglycemic clamps on a second cohort of animals. To control for the possibility that diet composition during WL alters pancreatic response to subsequent weight regain, we included a third group of mice that underwent WC while maintained on HFD throughout the entire experimental period (Fig. 5.3A). These mice were pair fed (PF) to the WC group during the WL phase. This PF group is termed 'WC-PF'. Body weight curves, energy intake, and body composition between WC and WC-PF groups were not different (Fig. 5.3b-f). In addition, there were no differences in fasting glucose, insulin, or NEFA concentrations following the WL period or the weight regain period between WC and WC-PF animals, respectively (Fig. 5.3g-i). These data indicate that each WC group was well-matched, but also reveal that consuming diets with different macronutrient (HFD versus LFD) composition during WL did not differentially alter fasting indices of glucoregulation after 9 weeks of WL or 9

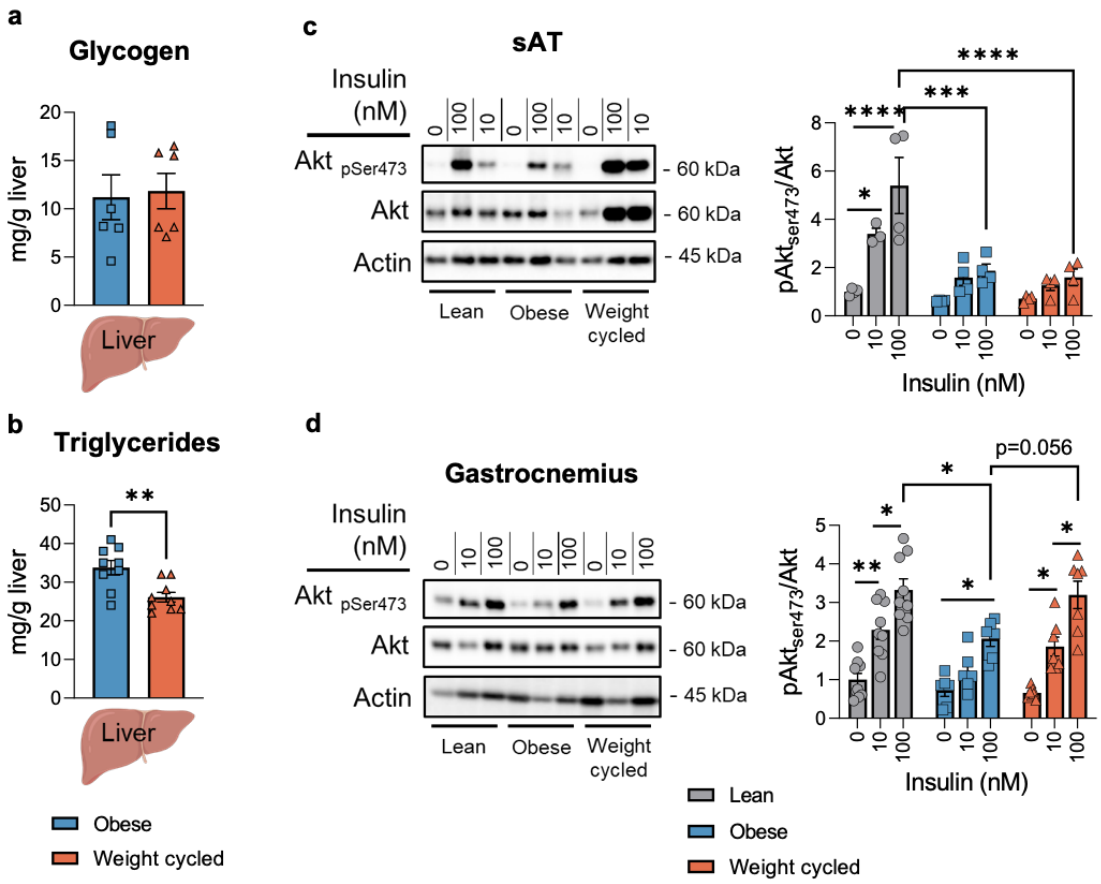

Figure 5.2: Obese and WC sAT and skeletal muscle have similar response to *ex vivo* insulin stimulation. **a** Liver glycogen and **b** liver triglycerides were measured after 27 week feeding period. Phosphorylation of AKT at ser473 was used as a proxy readout for insulin responsiveness in **c** subcutaneous adipose tissue (sAT) and **d** gastrocnemius muscle. Independent t tests were used to assess statistical differences between groups for panel **b** and **c**. Two-way ANOVA with group (lean, obese, WC) and insulin dose (0nM, 10nM, 100nM) as factors was used to assess statistical differences for panels **c** and **d**. Pairwise comparisons were adjusted Tukey test. Data presented as mean ± SE.

weeks of weight regain.

The three groups of mice undergoing hyperglycemic clamps did not differ in body weight (Fig. 5.4a). Arterial glucose was clamped at 250 mg/dl via exogenous glucose, which was not different between groups (Fig. 5.4b). A 25% reduction in GIR AUC (Fig. 5.4c, ANOVA, p=0.1) manifested in both WC groups compared to obese mice, suggesting reduced glucose clearance. Compared to obese animals, arterial insulin AUC was reduced in WC groups during hyperglycemia (Fig. 5.4d). To approximate early phase

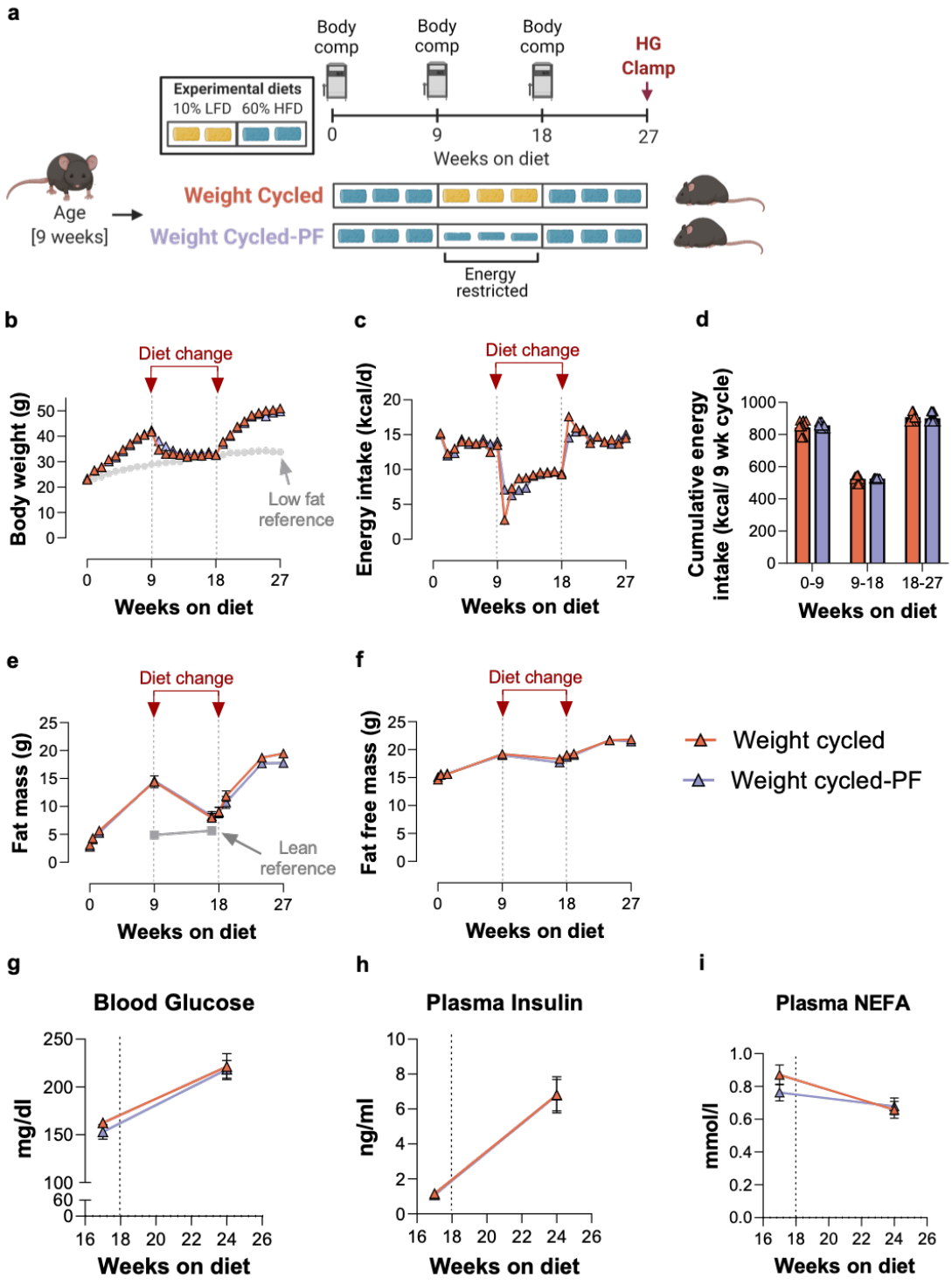
a
Body comp
Body comp
Body comp
HG Clamp
Experimental diets
10% LFD 60% HFD
0
9
18
27
Weeks on diet
Age
[9 weeks]
Weight Cycled
Weight Cycled-PF
Energy restricted
b
Diet change
Body weight (g)
Low fat reference
Weeks on diet
c
Diet change
Energy intake (kcal/d)
Weeks on diet
d
Cumulative energy intake (kcal/ 9 wk cycle)
0-9
9-18
18-27
Weeks on diet
e
Diet change
Fat mass (g)
Lean reference
Weeks on diet
f
Diet change
Fat free mass (g)
Weeks on diet
Weight cycled
Weight cycled-PF
g
Blood Glucose
mg/dl
Weeks on diet
h
Plasma Insulin
ng/ml
Weeks on diet
i
Plasma NEFA
mmol/l
Weeks on diet

Figure 5.3

Figure 5.3: Differences in diet composition does not alter body composition or blood biochemistry during WC. a WC mice undergoing 9 weeks of ad lib HFD feeding followed by 9 weeks of ad lib LFD and subsequently 9 weeks of ad lib HFD (regain) are compared with WC mice who are energy restricted (pair fed; PF-WC) during the WL phase. **b** Weekly body weight was not different between WC and WC-PF mice over time. **c** Weekly energy intake and **d** cumulative energy intake during each 9 week block of diet feedings. **e** Fat mass and **f** fat free mass were assessed before and after each diet change. After a 5 h fast, tail blood was collected, processed, and assessed for **g** plasma glucose, **h** insulin, and **i** non-esterified fatty acid (NEFA) concentrations at week 17 and week 24. Two-way repeated measures ANOVA with time and group (WC vs WC-PF) as factors were conducted with Tukey adjustment for pairwise comparisons. n=10-14/group. A lean reference group (grey) from Chapter III is included. Data presented as mean ± SE.

---

insulin secretion, the insulin change from basal to peak glucose concentration, which occurred within 10 minutes of glucose infusion, was computed. The percent increase from basal to peak glucose was not statistically different between groups (Obese: 95±10%; WC: 98±11%; WC-PF: 75±8%). However, the percent increase in insulin was approximately 3-fold higher in obese animals than either WC groups (Fig. 5.4e). Basal but not clamped NEFA concentrations were higher in WC groups relative to obese mice, whereas the percent NEFA suppression during hyperglycemia was not different between groups (Fig. 5.4f & 5.4g). Together these data reveal that during clamped hyperglycemia, WC – independent of preceding diet composition – decreases insulin secretion and tends to decrease glucose clearance.

To complement the hyperglycemic clamp studies, a subset of arterial catheterized mice were challenged with an oral mixed meal to determine whether perturbed glucose metabolism in WC manifests in response to oral delivery of mixed nutrients (Fig. 5.5a). Following oral gavage, a trend for decreased mixed-meal glucose clearance was noted in both WC groups relative to obese controls (Fig. 5.5b). Insulin excursions showed a time dependent response, whereby arterial insulin progressively increased in obese animals from t=0 min to t=60 min while WC groups displayed a plateau in insulin concentrations between 30 min and 60 min post gavage (Fig. 5.5c). Compared with obese mice, there was a trend for

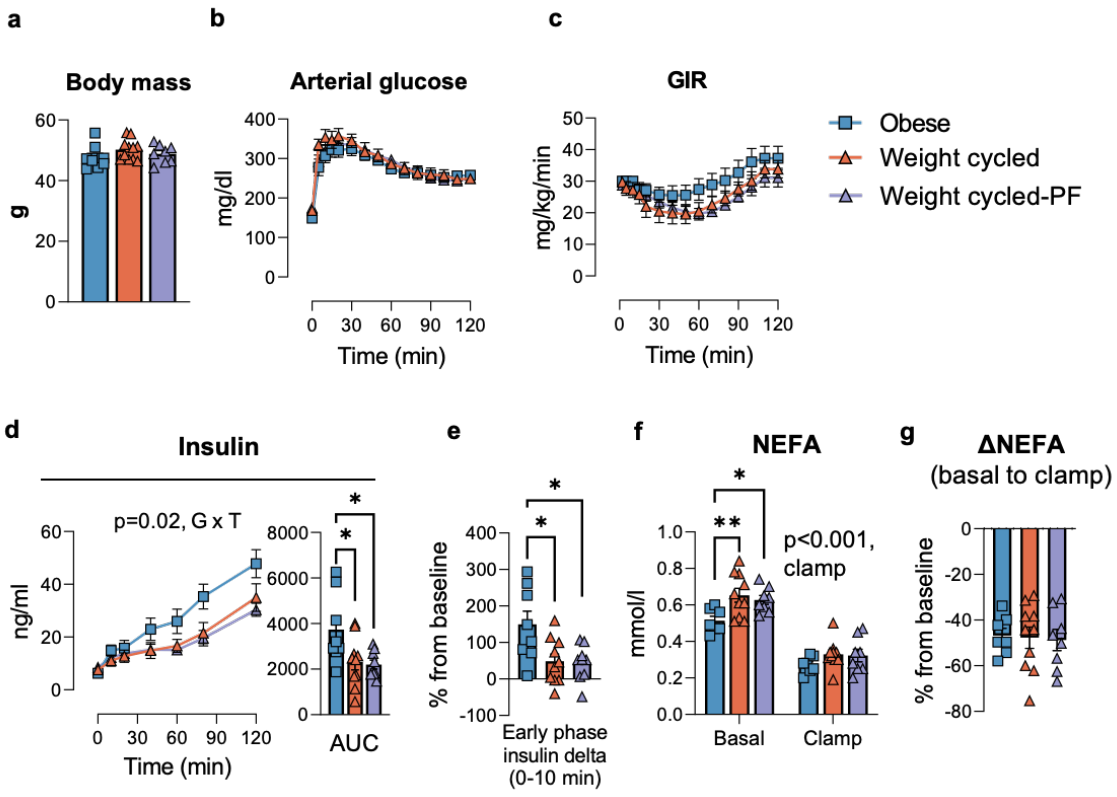

Figure 5.4: WC impairs in vivo glucose stimulated insulin secretion independent of diet composition. a Body weight collected at time of hyperglycemic clamp. **b** During the hyperglycemic clamp, arterial glucose was measured frequently with a target concentration of 250 mg/dl. **c** Target glucose concentration was achieved and maintained via exogenous GIR. **d** Plasma insulin was assessed every 10-40 minutes during the clamp procedure and presented as AUC. **e** Early phase insulin secretion is presented as the percent increase from basal to 10 minutes of glucose infusion. **f** Basal (-10 min) and clamp (110 min) NEFA concentrations were assessed. **g** The percent suppression of plasma NEFA levels during the clamp was computed. One-way ANOVA was used to assess main effect of group for panels **a**, **e**, and **g** with Tukey adjusted pairwise comparisons. Two-way ANOVA with time and group (obese, WC, WC-PF) as factors was used to assess statistical differences for panels **b-d** and **g**. Pairwise comparisons were evaluated via Tukey adjustment. n=8-10/group. Data presented as mean ± SE.

increased NEFA concentrations in animals that underwent either model of WC (Fig. 5.5d; ANOVA, p=0.06). For WC-PF mice, liver and sAT mass were elevated compared to obese mice, but eWAT and pancreas mass were not different (Fig. 5.5e). In sum, these data imply that WC animals have decreased glucose clearance in response to an oral mixed meal.

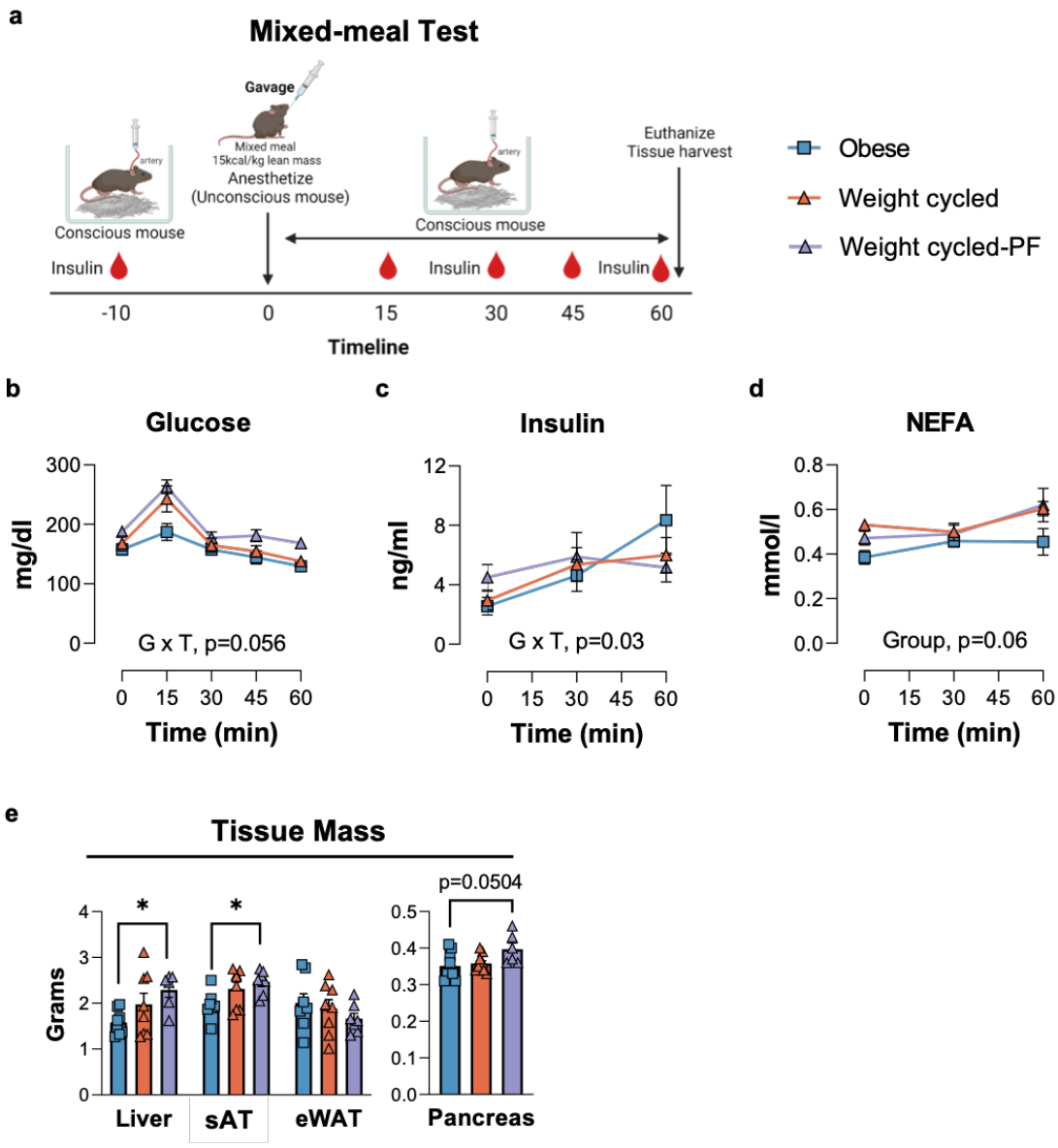

Figure 5.5: WC deceases nutrient clearance in response to a mixed meal. **a** After 27 weeks of LFD or HFD feeding, obese, WC, and WC-PF mice underwent a mixed meal tolerance test via oral gavage (Ensure, 15 kcal/kg FFM or 2.5% of total daily energy intake). **b** Arterial glucose, **c** insulin, **d** and NEFA were measured in the fasted state (5 h fast) and during the meal. **e** Tissues were harvested post meal challenge and weighed. For panels **b-d** two-way repeated measures ANOVA with time and group (obese, WC vs WC-PF) as factors were conducted with Tukey adjustment for pairwise comparisons. One-way ANOVA was used to assess main effect of group for panel **e** with Tukey adjusted pairwise comparisons. n=4-7/group. Data presented as mean ± SE. Fig 5.5a was generated using BioRender.

5.2.3 Insulin secretion is suppressed in WC islets

Next, we determined whether the reduction in *in vivo* insulin secretion in WC mice manifested in isolated pancreatic islets. Isolated islets were perifused with insulin secretagogues (e.g., glucose, IBMX, KCl) *ex vivo* to determine dynamic insulin secretion (Fig. 5.6a). No differences in insulin secretion were detected during low (5.6 mM) or high glucose (16.7 mM) perfusion between obese and WC islets (Fig. 5.6b). However, compared to obese controls, WC islets showed a diminished insulin response to non-specific phosphodiesterase inhibition using IBMX, suggesting that cAMP-supported insulin secretion is impaired or less sensitive to stimulation in WC islets. Membrane depolarization induced insulin secretion using KCl was similar between groups. Insulin content per islet equivalent (i.e., islet of 150 μm diameter) was approximately 40% lower in WC vs obese mice (Fig. 5.6c). Immunofluorescence imaging revealed a modest reduction in insulin immunolabeling pixel intensity in contrast-matched images from the WC islets compared to lean and obese islets, respectively (Fig. 5.6d). Islet area (as a percent of total pancreas area) was increased in obese mice compared to lean mice (Fig. 5.6e), whereas WC islets failed to compensate for hyperglycemia by increasing insulin$^+$ β cell area. Furthermore, obese islets appeared larger than lean and WC islets (Fig. 5.5f). Obese islets contained about twice as many β cells than WC or lean islets (Fig. 5.5g). However, the ratio of α:β cells was not different between obese and WC mice (Fig. 5h).

5.2.4 Components of β-cell transcriptional identity are downregulated by WC

To identify the mechanism behind impaired stimulated insulin secretion caused by WC, we collected islets from obese and WC mice for bulk RNA-sequencing. Obese and WC islet transcriptomes were segregated by unbiased linear dimensional reduction using multidimensional scaling (Fig. 5.7a). Differential expression comparing obese and WC samples detected 361 significantly different genes with 114 upregulated genes and 247 downregulated genes (Fig. 5.7b). Gene ontology of differentially expression genes identified up-

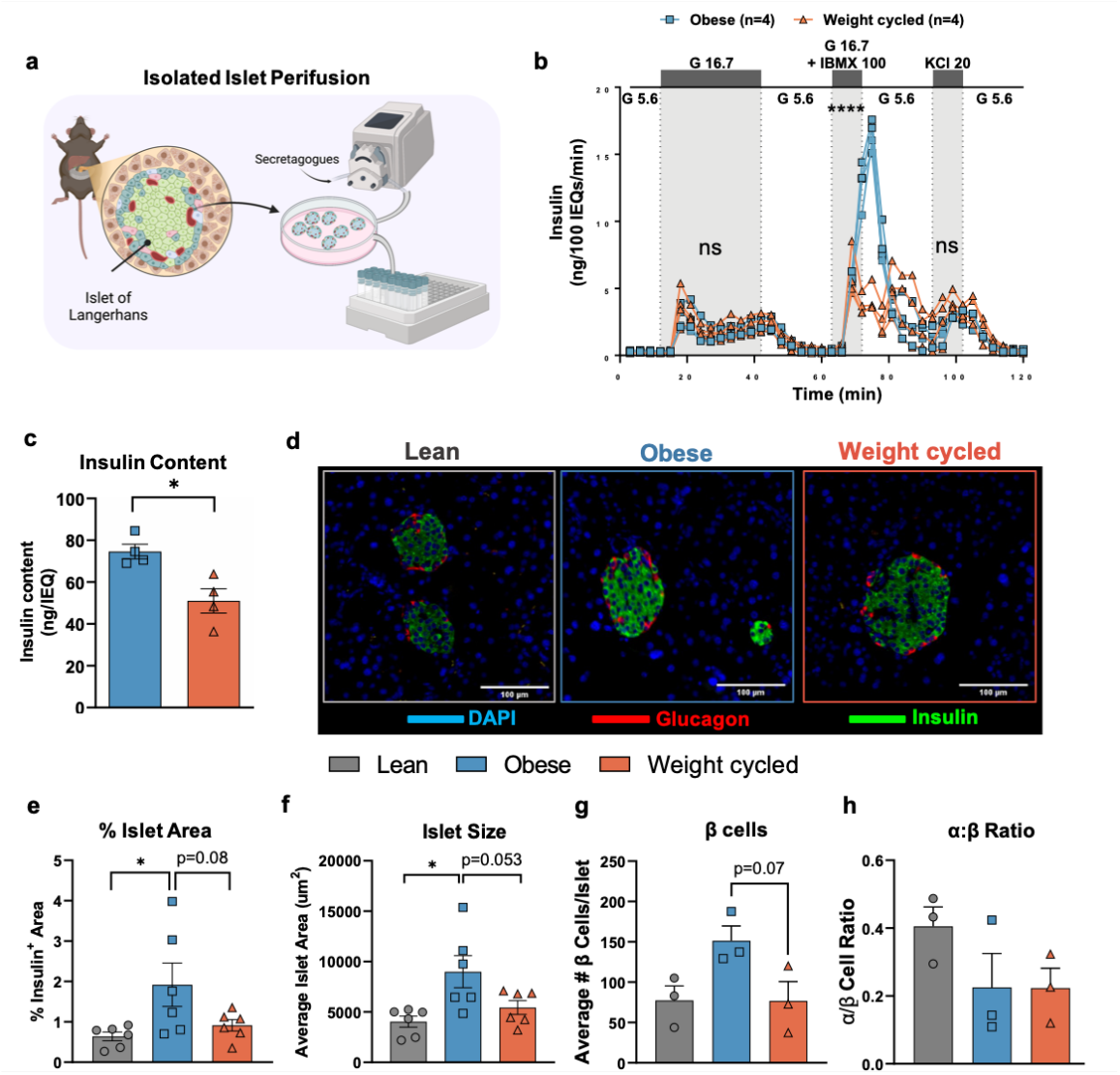

Figure 5.6: ***Ex vivo*** **insulin secretion is reduced in WC mice.** **a** Pancreatic islets were isolated and handpicked from obese and WC mice for islet perifusion (n=4). **b** Islets were perifused with insulin secretagogues (glucose 5.6 mM and 16.7 mM, IBMX, and KCl) to determine dynamic insulin secretion, n=4. **c** Insulin content was determined by normalizing insulin concentration in media containing islets to an islet equivalent (islet of 150 μm diameter). **d** Representative images of fixed paraffin embedded pancreata from lean, obese, and WC mice immunolabeled for DAPI (blue), insulin (green), and glucagon (red). **e** Insulin$^+$ area relative to total pancreas area per tissue section (n=6 mice, mean $\pm$ SE of 3 slides/mouse), **f** average islet size (n=6 mice, mean $\pm$ SE of 3 slides/mouse), **g** number of β cells per islet (n=3 mice, mean $\pm$ SE of 30 islets/mouse) and **h** ratio of α:β cells was quantified. Fig5.6a was generated using BioRender.

regulation of cell-cycle related pathways and downregulation of pathways associated with organization and protein localization in WC islets compared to obese islets (Fig. 5.7c). Total normalized counts for genes included in cell-cycle pathways were low, but significantly different between obese and WC islets (Fig. 5.7d). To investigate potential differences in β-cell proliferation, we performed immunofluorescence imaging and quantification for the nuclear marker Ki-67. However, Ki-67^{+}Insulin^{+} cells were sparse in islets and frequency did not differ between groups (lean = 0.46%, obese = 0.23%, and WC = 0.16% of intraislet cells).

Multiple drivers of β cell identity and function, *Nkx6.1*, *Mafa*, *Pdx1*, *Ucn3*, and *Slc2a2*, were also downregulated in WC islets compared to obese islets (Fig. 5.8a). Conversely, transcripts for insulin (*Ins1* and *Ins2*) and *G6pc2* were elevated in WC islets. Therefore, we determined whether posttranscriptional changes occurred between groups using immunofluorescence imaging. Immunolabeling for NKX6.1 revealed a qualitative reduction in NKX6.1 expression of WC islets (Fig. 5.8b). Likewise, nuclear MAFA was also reduced in islets from WC mice (Fig. 5.8c). Because markers of β cell identity were reduced, we also immunolabeled for GLUT2, a β-cell specific glucose transporter. GLUT2 localized to the plasma membrane of insulin^{+} cells but was less uniform and had reduced signal intensity in WC mice (Fig. 5.8d).

To further identify if changes in drivers of β cell function impaired insulin granule formation in WC animals, transmission electron microscopy was utilized (Fig. 5.9a). The percentage of cytoplasmic insulin-loaded granules was 22% lower ($p<0.05$) in β cells from WC compared to obese mice (Fig. 5.9b), despite no differences in the average number of total vesicles per field of view (FOV) (Fig. 5.9c). The percentage of empty vesicles was 30% higher ($p=0.053$) in WC compared to obese islets (Fig. 5.9d). Taken together, experiments on isolated islets support that reduced insulin secretion observed in WC mice, compared to those from obese mice, is linked with both an insufficient transcriptional/post-transcriptional response to weight regain and impaired insulin granule loading.

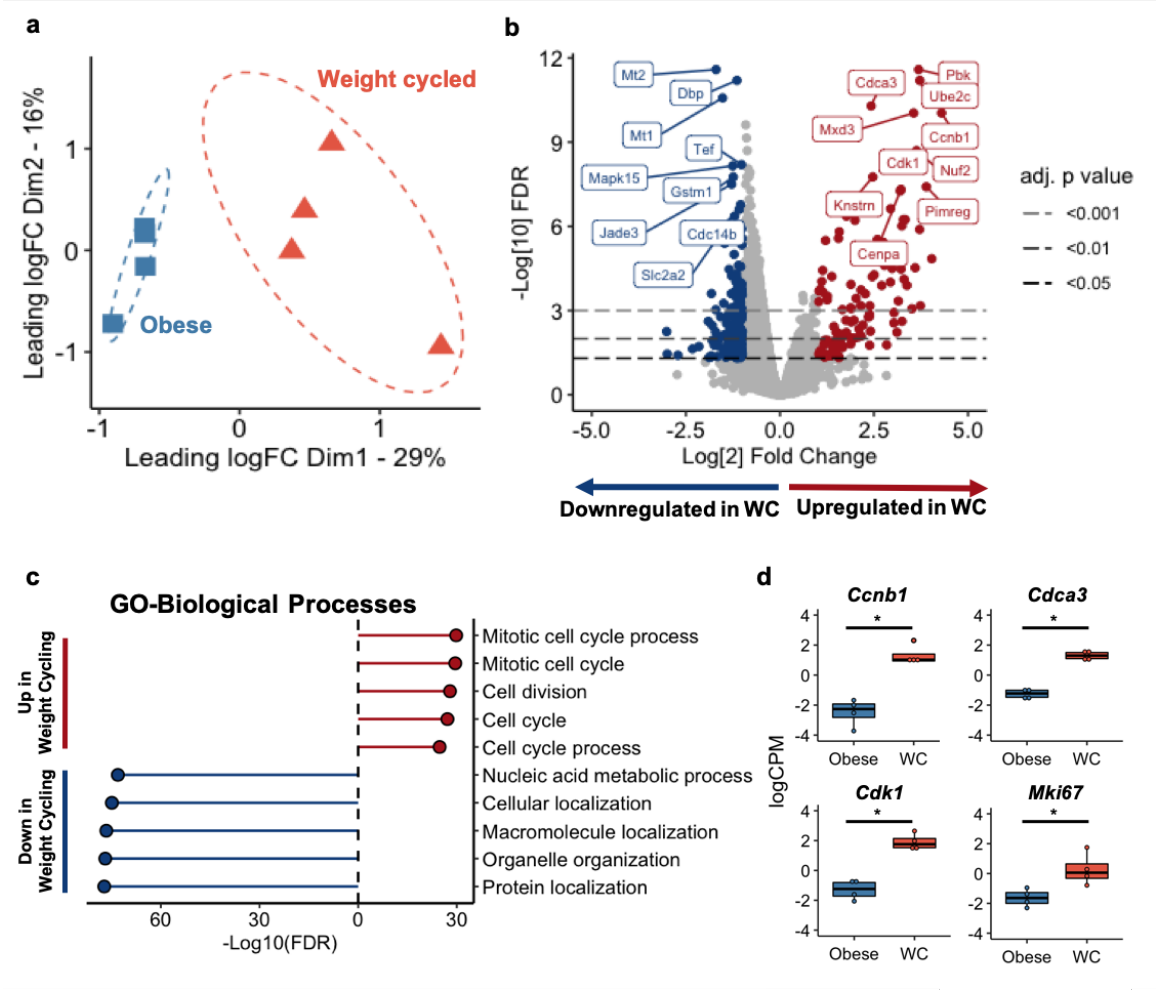

Figure 5.7: WC islets are transcriptionally distinct from obese islets. Bulk RNA-sequencing was performed on isolated islets from obese and WC male mice (n=4). **a** Multidimensional scaling analysis reveals two clusters of samples, which discriminate based on diet. **b** Top 10 significantly upregulated (red) and downregulated (blue) genes ($p<0.5$) and ($\log_2$ fold-change<1) shown on a volcano plot. **c** Gene ontology for biological processes of significantly upregulated and downregulated genes organized by false discovery rate (FDR). **d** Log counts per million from bulk RNAseq for selected genes associated with cell proliferation (*$p<0.05$).

5.3 Discussion

WC has been identified as a risk factor for T2D in humans [26], yet the mechanism(s) by which WC alters nutrient flux and/or insulin resistance (compared to obesity alone) is incomplete. Along these lines, it is unclear whether repeated fluctuations in body weight accelerates β-cell fatigue and associated hyperglycemia. Peripheral insulin resistance, de-

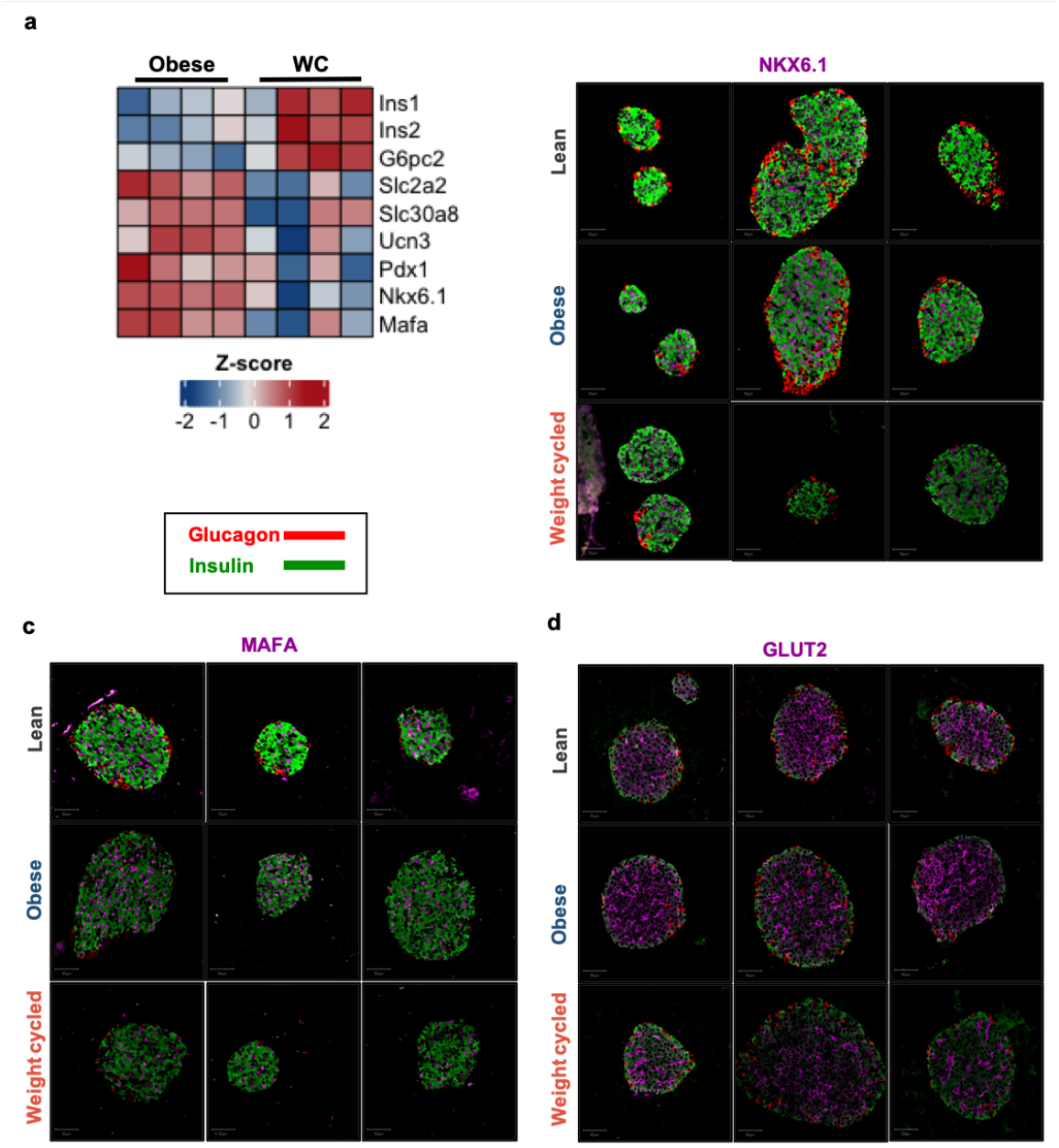

Figure 5.8: Expression of β–cell transcription factors and glucose transporter 2 are reduced in pancreatic islets by WC. a Heatmap of selected genes related to β-cell function for each individual sample where upregulated genes are shown in red and downregulated genes are shown in blue. Immunofluorescence for **b** NKX6.1, **c** MAFA, and **d** GLUT2 (magenta; n=3 islets from independent mice). Insulin (green) and glucagon (red) immunolabeling is also shown for each image.

fined as liver, muscle, and AT resistance to insulin action, precedes diabetes development. Similarly, β cell insulin resistance can also precede T2D [308]. Long-term WL has repeat-

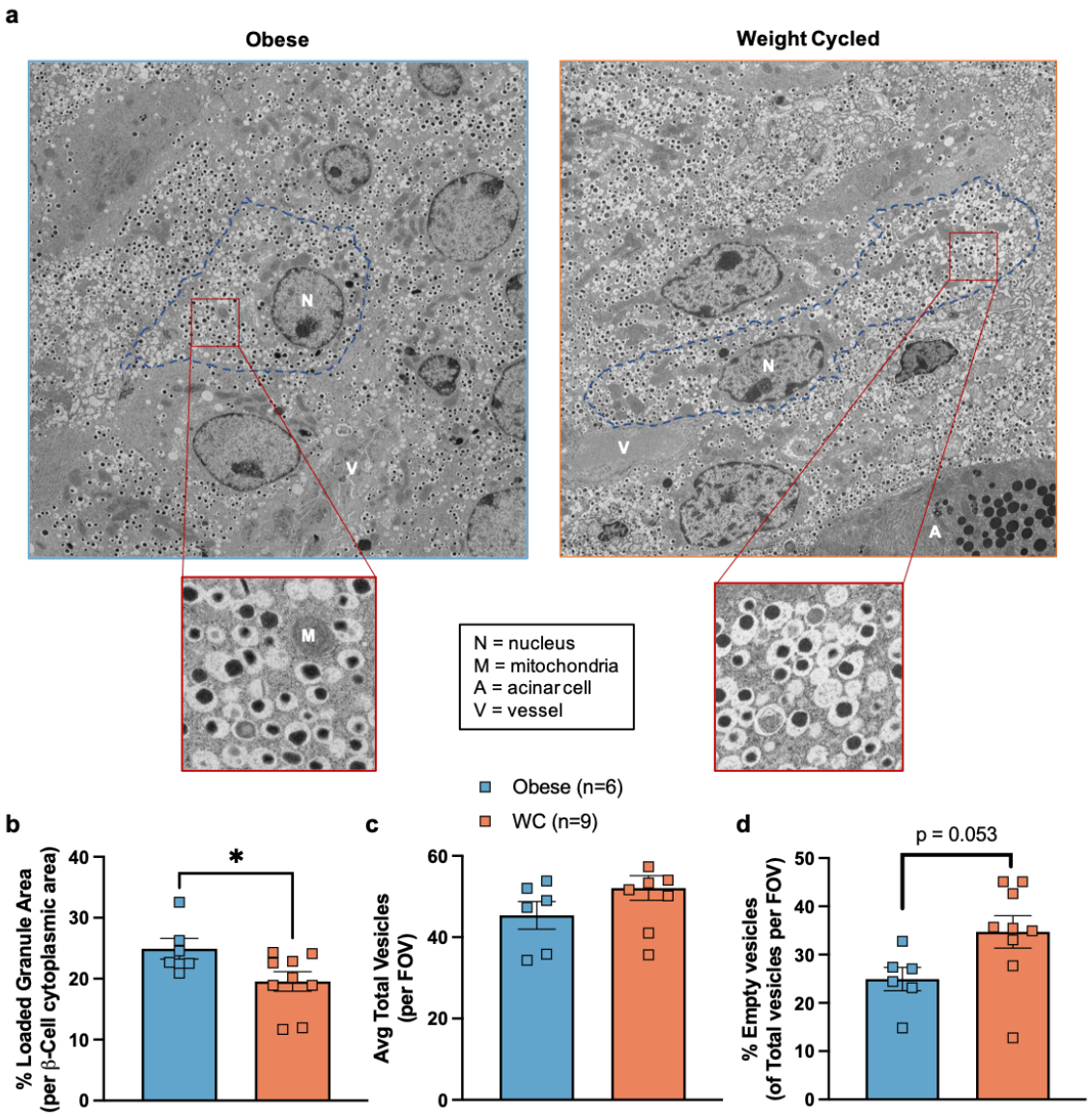

Figure 5.9: Insulin granule loading is impaired by WC. After the 27 week HFD or WC feeding protocol, pancreata were isolated from obese and WC mice and immediately fixed for transmission electron microscopy. **a** Representative images for obese and WC islets including an outlined β cell (blue, dashed lines) and zoomed field of view (FOV; red) of insulin granules. **b** Percent of loaded granule area per total β-cell cytoplasmic area. **c** Average total number of empty or loaded vesicles counted per FOV (FOV = 2.99 μm x 2.99 μm). **d** Percentage of empty vesicles of total vesicles counted per FOV. 6 FOVs were measured per mouse, n=6-9 mice. Data presented as mean $\pm$ SEM, *p$<$0.05.

edly shown to improve glucose homeostasis by increasing peripheral insulin sensitivity and by maintaining tight pancreatic insulin-to-glucose balance [309–315]. Despite these

findings, the effects of weight regain on glucose fluxes and insulin action are not clear.

In this chapter, we used our mouse model of diet-induced WC to systematically interrogate the metabolic phenotype of glucose-intolerant WC mice with two primary objectives: i) pinpoint the organ/tissue site of glycemic dysfunction caused by WC and ii) begin to uncover the mechanisms evoking impaired glucoregulation in WC mice. We hypothesized that WC would worsen peripheral insulin action and glucose clearance. This hypothesis was founded in part by prior evidence that WC mice have attenuated insulin signaling in AT and liver compared to obese controls following intraperitoneal insulin administration [250]. In contrast to our hypothesis, WC does not worsen whole-body insulin action compared with obesity alone, but rather decreases pancreatic insulin secretion. These findings suggest that inadequate pancreatic adaptation to fluctuations in body weight is a central player in the deterioration of glycemic control caused by WC in mice.

It is well established that pancreatic β cells adapt to chronic over nutrition by increasing β cell mass and hyperinsulinemia [301, 316]. Yet, it is unclear the extent to which islets are adaptable to multiple bouts of weight gain and WL. The pattern of nutrient loading (weight gain), unloading (WL), and reloading (weight regain) may invoke a state of pancreatic inflexibility. This stimulus of nutrient loading/unloading is important and relevant to the human condition given that many individuals transition through multiple bouts of caloric excess and caloric restriction during their lifespan – the latter of which is challenging to maintain for reasons discussed elsewhere [317]. Nonetheless, uncovering the molecular mechanisms attributing to pancreatic flexibility or loss thereof is of clinical relevance and importance.

We find that during in vivo hyperglycemia (clamped), WC mice secrete less insulin and require lower GIR (generally indicative of lower glucose clearance) to maintain clamped hyperglycemia. The relative reduction in GIR may be affected by possible differences in the suppression of endogenous glucose production. However, we are not able to make conclusions regarding EndoR_a given that glucose was not isotopically labelled during the

hyperglycemic clamp. On the other hand, whole-body insulin action (determined from hyperinsulinemic-euglycemic clamp) does not appear to be different between obese and WC animals. Indeed, glucose fluxes (R_a and R_d) assessed during euglycemia – and clamped hyperinsulinemia – did not differ between WC and obese animals. Though arterial insulin levels were lower in WC mice. This latter effect likely explains the decrease in tissue R_g in WC mice, which disappears when R_g is normalized to its respective insulin concentration. Yet, it should be noted that the relationship between insulin concentrations and tissue R_g are likely non-linear. Nonetheless, *ex vivo* insulin responsiveness is not different between obese and WC animals when equal amounts of insulin are present.

With regards to isolated islets, glucose stimulated insulin secretion (GSIS) alone is not dampened by WC. In contrast, cAMP driven insulin secretion during exposure to a non-specific phosphodiesterase inhibitor (i.e., IBMX) and high glucose was reduced in WC compared to obese mice. This impairment in islet functional capacity is linked with reductions in insulin content (per islet equivalent), less insulin positive immunostaining, and reduced percentage of insulin loaded granules in WC mice. Numerous factors can drive altered insulin secretion in β cells, such as signaling by inflammatory cytokines, endoplasmic reticulum stress, apoptosis, loss of specific endocrine identity, and cellular metabolism [reviewed in [318]]. Our transcriptomics approach revealed reductions in key transcription factors from lean, obese, and WC mice. *Mafa*, *Nkx6.1*, and *Pdx1* are involved in regulating β cell proliferation and expansion in response to nutrients and are decreased in models of T2D [319]. Pathway analysis from RNAseq suggested increased proliferation. However, few cells positively stained for Ki-67 within islets, suggesting that β cell proliferation is low in obese and WC mice after 27 weeks of diet. Genes associated with proliferation are typically also associated DNA-damage repair. We did not identify differences in expression for additional genes associated with DNA repair (such as *Xrcc2, Xrcc3, Rad52*) in the RNAseq dataset between obese and WC mice, but our data do not rule out DNA-damage as a mechanism for impaired insulin synthesis or secretion in WC.

β cell specific deletion of one or more of the 'identity' transcription factors (*Mafa*, *Nxk6.1*, or *Pdx1*, among others) causes overt hyperglycemia due in part to decreased insulin synthesis/secretion [320]. Glycemic control can be improved by sustained expression of *Mafa* in the hyperglycemic Db/Db mouse model [321]. Haploinsufficiency for *Pdx1* is linked with increased β cell apoptosis [322, 323] and *Pdx1* insufficient mice have impaired glucose tolerance despite having relatively normal GSIS in perifused islets [322]. Our model of WC closely mimics the metabolic phenotype and β cell characteristics of *Pdx1* haploinsufficient mice, which display decreased expression of *Slc2a2*, islet area, and adaptation to diet-induced obesity. Collectively, these findings are in line with the idea that β cell proliferation and expansion is stalled in previously obese mice such that when challenged with a second bout of nutrient excess are unable to mount a sufficient response (i.e., β cell fatigue).

WC decreases several β cell transcription factors critical to maintaining pancreatic flexibility, yet the molecular mechanisms causing the downregulation of these β cell identity markers is not inherently clear. Prior research reveals that increased oxidative stress decreases expression of *Mafa*, *Nkx6.1*, and *Pdx1* in human islets [319]. Similarly, Db/Db mice exhibit a reduction in these markers that is restored via transgenic expression of the glutathione peroxidase-1 antioxidant enzyme [319]. Transcriptionally, we did not find clear evidence for increased oxidative stress between WC and obese islets. However, it is possible that functional differences could manifest. In addition, evidence demonstrates that intermediary metabolism of glucose and other substrates contribute to insulin secretion and proliferative activity in islets. Thus, rapid changes in nutrient load during diet transitions may pose a significant burden on β cells which are highly susceptible to increased oxidative stress [324–326]. Interestingly, the expression of *Ins1* and *Ins2* were increased in WC mice; however, this was accompanied with lower insulin content and decreased secretion *in vivo* and *ex vivo*. Moreover, the percentage of insulin-loaded granules was lower in WC β cells, together suggesting posttranscriptional insulin gene regulation is implicated in the

functional loss of insulin secretion. Whether insulin granule formation/trafficking or membrane docking are impaired in WC islets awaits further testing. Whilst the present findings do not pinpoint the precise molecular signal or mechanism(s) responsible for insufficient β cell responsiveness, we unveil a model in which β cells in mice that WC fail to effectively compensate for increased insulin demand during chronic hyperglycemia. This in turn results in reduced peripheral insulin availability and impaired glucose tolerance.

In summary, we report that WC-induced glucose intolerance is unlikely attributable to worsened peripheral insulin resistance in mice, but rather linked with inadequate insulin secretion. Our findings support the notion that repeated bouts of weight gain challenge pancreatic flexibility. Specifically, reductions at both the transcript and protein levels of the β cell transcription factors NKX6.1 and MAFA in WC mice suggest a loss of adequate β cell compensation normally observed with obesity alone. Additional mechanistic studies are needed to confirm whether restoration of these β cell transcription factors causally resolve worsened glucose homeostasis evoked by WC.

CHAPTER 6

Conclusions and Future Work

6.1 Progress in understanding obesity and T2D

Each year, the reported prevalence of both obesity and T2D increase. Obesity is strongly correlated with reduced life expectancy, increased healthcare costs, and has been mechanistically linked to many comorbidities. Therefore, interest in effective therapeautic approaches to treat obesity remains high. Treatment for obesity can be broadly binned into three categories, all of which also greatly improve glycemic control: 1) life-style modification, 2) medical WL, and 3) surgical WL. Life-style modifications can occur in various forms, but usually include management of food intake and efforts to improve fitness through exercise. To support WL, medical approaches including pharmaceuticals can be used. However, effective and safe pharmaceuticals are limited and often have concerning side-effects. For example, agents that reduce absorption of fat by the intestines (e.g. Orlistat) are only marginally improve long-term WL and can cause gastrointestinal discomfort [327]. Many therapeutics used to improve glycemic control are also implicated in treatment of obesity. For example, sodium glucose transport inhibitors (SGLTIs) that reduce reuptake of glucose in the kidneys to reduce blood sugar levels also cause mild WL (i.e 2-3 kg) [328]. Another class of drugs that improve insulin secretion, glucagon-like peptide receptors (GLP-1Rs) agonists, also cause clinically significant WL. While the exact mechanism GLP-1R agonist induced WL remains unclear, evidence supports a central mechanism of food intake regulation [329]. Bariatric surgery, which dramatically reduces food intake by decreasing the size of the stomach, is in many cases a last resort. Regardless of approach, successful WL is dependent on a simple formula: energy absorbed and metabolized must be lower than the systemic energy demand.

Associations between obesity and inflammation are numerous. In fact, almost all known

immune cell subsets have been identified in both mouse and human AT. As discussed in Chapter I and shown in Chapter III, obesity-associated changes in AT immune cell populations include both loss of immunoregulatory cells and enrichment for pro-inflammatory populations. Therefore, the potential for management of obesity-associated inflammation to reduce risk of comorbidities, such as T2D, is enormous. However, despite significant efforts, no effective therapeutics targeting systemic or AT inflammation have shown efficacy by reducing progression of comorbidities or improving long-term WL. Importantly, our lack of understanding of AT immune cells and mechanisms driving their recruitment, activation, and function likely limit our ability to effectively target obesity-associated inflammation.

6.2 WL and WC in basic research

Understanding WL and WC in humans is paramount to generating effective laboratory models. However, both WL and WC are challenging to identify in humans for numerous reasons. Survey based approaches attempt to identify WL or weight regain by asking questions about ongoing weight management efforts, or those attempted in the past, and use that information to generate population-level estimates. For example, the National Health and Nutrition Examination Survery conducted by the Centers for Disease Control asks: ”What kind of diet are you on? Is it a weight loss or low calorie diet: low fat or cholesterol diet; low salt or sodium diet; sugar free or low sugar diet; low fiber diet; high fiber diet; diabetic diet; or another type of diet?”. Overall, survey based approaches can give insight into frequency of WL attempts, but rarely improve our understanding of WL management. Managed care studies, on the other hand, provide metrics for WL (e.g changes in BMI or waist-to-hip ratio) over time. However, these studies are often small or with limited focus due to the significant time and costs associated with recurring clinical visits. With increasing availability of deidentified electronic medical records, our ability to accurately estimate WL and weight regain events (i.e WC) will improve. Furthermore, the abundance

of associated data will provide enormous clarity into behaviors, available therapeutics, and even genetic differences that can be utilized to improve clinical WL. For example, a recent study exemplified the utility of large medical records coupled with exome sequencing to identify a single nucleotide polymorphism (SNP) associated with protection from obesity [330]. While development of these exciting avenues continues, many basic research groups (including the Hasty laboratory), have attempted to generate laboratory models that effectively replicate components of human WL and WC.

6.3 Caveats of WL and WC mouse models

Our lab and others have utilized mouse models that replicate features of WL and WC in humans. The primary mouse model utilized in this work and shown in Figure 3.1 was developed based on a 6-year follow-up study of participants on The Biggest Loser television show [331]. In this study, participants taking part in an extreme WL management program very successfully lost weight, but the majority of participants were found to have regained lost weight after 6 years. Authors originally attributed this to reductions in caloric demand at decreased body weight (i.e metabolic adaptation limiting long-term WL). Using *ad libitum* access to either LFD or HFD, we are able to accurately measure and control body weight over time. Thorough analysis of this model identified two important contributors to impaired glucose tolerance: 1) Persistent changes in AT immune cells and 2) Impaired insulin secretion.

However, our diet-induced model of WL and WC also has many important caveats. Foremost is that, although mice are fed *ad libitum*, the diet composition is controlled and does not perfectly match western-style consumption. However, unique mouse models seeking to address these differences are being developed for diet-induced obesity models, but have not yet been established for WL or WC [332]. Change in dietary composition alters the texture, palatability, and caloric density of food pellets. Therefore, it remains unknown whether the balance or choice of carbohydrates (simple and complex), fat, and protein

contribute to WC-associated metabolic disease. The HFD formulation used in our work contains fat primarily from lard. Other groups have begun to explore differences between dietary lipids (e.g olive oil, lard, butter, and palm oil) and their effects on immune cells [333]. In addition, rodent diets high in fructose (as opposed to sucrose) often result in worsened liver disease [334]. However, we have shown that limited caloric intake (i.e CR) without switching from HFD to LFD does not improve glucose tolerance in WC mice (Fig. 5.3), suggesting that WC-associated metabolic dysfunction is not due to composition of diet during WL.

One of the strengths of our mouse model is that obese and WC mice are weight-matched (as are lean and WL mice). In other models of WC in which multiple repeated cycles are used, WC mice eventually gain more weight than obese controls [335–337]. However, neither of these approaches mimic human behavior. For example, WC-like behavior may appear due to seasonal behavior in humans (i.e weight gain during the winter holidays and WL in late Spring). Likewise, the timescale of bouts of WL and weight regain are variable in humans and the effects of different cycle interval lengths are unknown.

Another important consideration is that diet is only one of many components of WL. Our group has begun to explore the effects of exercise on AT immune cells before and during diet-induced obesity, as well as following WL. In addition, WL induced by GLP-1R agonists provide a potential alternative approach to induce WL without altering diet composition. Although many questions remain unanswered in regards to WL, and by extension WC, rodent models allow us to interrogate specific components of metablic disease in a robust, reproducible fashion. Therefore, many of the findings highlighted in this work are opportunities for subsequent discovery in clinical research.

In humans, women are thought to WC more frequently than men. However, male mice more readily gain weight than female mice and are used throughout the majority of this dissertation. We have taken female mice through our WC protocol before (Fig. 3.4) and noted a non-significant defect in glucose tolerance. However, female mice have a very

low rate of weight gain during the initial 9-wk HFD interval. During the second bout of HFD, when mice are much older, female mice gain weight at a much greater rate. It is possible that a better model for WC in female mice would start diet later in life so that the initial HFD interval has a greater impact on overall body weight. Interestingly, this data also suggests that impact of weight gain (i.e the degree of AT remodeling or inflammatory injury during obesity) is reflected in the final WC metabolic phenotype.

6.4 WL, AT remodeling, and weight regain

Chronic low-grade inflammation is a feature of obese AT and coincides with incidence of AT insulin resistance. Inflammatory cytokines interfere with signaling through the insulin receptor. In tandem, insulin itself may induce inflammatory cytokine production by immune cells during settings of hyperinsulinemia. Furthermore, uncontrolled lipolysis during settings of insulin resistance can release fatty acids that alter immune cell phenotype and activity (e.g LAMs). Because significant WL does improve most features of glycemic control in both humans and rodent models, it has long been assumed that WL also recovers the AT mileu from immune cell infiltration occuring during obesity. However, efforts by others and shown in this work have challenged that notion, highlighting the persistence of inflammatory immune cells in AT even after WL [15, 252, 279, 280].

Many of the immune cells present in AT are thought to play roles in tissue remodeling. Adipocytes are highly adaptable and can expand or proliferate to meet the demands of lipid storage. At the same time, the extracellular matrix surrounding adipocytes must also be remodeled to support tissue expansion, or contraction in settings of WL. For example, macrophages express a variety of matrix metalloproteinases and can also clear dying adipocytes [338]. During settings of obesity, $CD11c^{+}$ macrophages, which we have identified by CITE-seq to be primarily LAMs, express very high levels of *Mmp12*. Highlighting the importance of matrix remodeling, *Mmp12* deficient mice gain more weight than wild-type controls, but have improved insulin sensitivity [339]. Likewise, LAMs also highly

express *Spp1* (coding for osteopontin), which binds integrin receptors on many immune cells to promote migration, adhesion, tissue residency, and activation. As discussed in Chapter III, LAMs do not decrease in number following WL. We also showed that while fat mass was similar between lean and WL mice, adipocytes in WL tended to be smaller (Fig. 3.3), suggesting that clearance of small adipocytes and remodeling of the tissue extracellular matrix by macrophages is impaired during WL. Osteopontin is also a high affinity ligand for the CD44 receptor used to mark memory T cells and likely plays a role in long-term survival and suppressed activity of T cells in AT [284, 340, 341]. Of note, osteopontin also alternatively activates (i.e reduces IL-4 production and increasing IFN-γ production) iNKT cells and induces degranulation of mast cells [342, 343]. Taken together, these data suggest that immune cells that persist in AT following WL are likely to contribute to the rate of weight regain and the metabolic consequences of WC. However, this notion also generates numerous avenues for exploring therapeutic targets. For example, it is unknown whether therapies that promote macrophage eggress from AT would support weight maintenance and AT remodeling. Likewise, while CD44-targeted neutralizing antibodies have failed to show efficacy in phase II clinical trials for treatment of cancer, it is unknown if immunotherapy would reduce $CD4^+$ Th1 and $CD8^+$ cell accumulation in AT to restore the T_{reg} enriched niche [341].

6.5 The complex role of T cells in AT

Due to the observation that inflammatory $CD8^+$ T cells were enriched in obese AT, we originally hypothesized that the $CD8^+$ T cell compartment would contract to form memory $CD8^+$ T cells during WL [154, 250]. Our CITE-seq approach and follow-up V(D)J sequencing supports that AT is indeed enriched for clonal $CD8^+$ T_{EM} during WL. However, we were suprised to find that total $CD8^+$ T_{EM} number (and proportion of total immune cells) was very high following WL, suggesting that this lymphocyte compartment does not contract during WL. Paradoxically, the clonal $CD8^+$ T_{EM} observed during WL and WC

had impaired production of cytokine in response to stimulation and expressed markers of exhaustion. Therefore, focus has been shifted to better understand how these $CD8^+$ T cells contribute to metabolic dysfunction observed in WC. Yet, many questions remain unanswered. First, how do $CD8^+$ T cells survive in AT and does AT act as a unique reservoire for these cells? Furthermore, can $CD8^+$ T cells migrate out of AT and infiltrate other tissues, such as pancreas or liver? We observed reduced expression of *Gzmb* and reduced production of cytokines, but are there different roles for these cells in AT inflammation (e.g GZMK production)? Most importantly, is signaling through the TCR required for AT $CD8^+$ T cell recruitment and survival, and if so, what antigens are they responding to? We have begun to address these questions using a variety of paradigms. For example, we have identified TCRs associated with T1D and have begun to generate retrogenic models to identify if TCR signaling during obesity drives these cells to AT and pancreas. In addition, we have collected preliminary data suggesting that immune cells can migrate from transplanted AT to distant sites (e.g subcutaneous tumors). While the exact role of $CD8^+$ T_{EM} remains unclear, the potential for these cells to contribute to systemic immunity is an exciting avenue for continued research with applications in cancer biology, infection (e.g in HIV), and metabolism.

6.6 WL and WC in the pancreatic islet

In Chapter V, we identified that impaired β cell insulin secretion may be the driving force behind WC-associated impaired glucose tolerance. However, it is also important to note that there was a decrease in β cell area (by $insulin^+$ immunolabeling) in WC compared to obese mice. Because we did not observe differences in total pancreatic mass, these data suggests WC mice have decreased total β cell mass in addition to impaired insulin secretion. One caveat of this approach is that the total time for pancreatic compensation to occur in the last 9-wk HFD interval for WC mice is shorter than the two 9-wk HFD intervals (18-wk total) the obese control group is exposed to. Interestingly, in experiments

not shown in Chapter V, we found that WL mice have greater β cell mass than WC mice. This data suggests that β cell mass may further decrease during weight regain rather than rebound to compensate for metabolic demand.

In Chapter V, using a bulk RNAseq approach, we identified reductions in multiple β cell transcription factors. While these data suggest a link between WC and a defect in insulin secretion, the molecular mechanisms driving these effects remains unknown. However, it is important to remember that pancreatic tissue is surrounded by peritoneal fat during obesity and chronic free-fatty acid exposure leads to lipotoxicity in β cells, suggesting that inability of AT to recover during WL may contribute to subsequent islet damage [344]. Our CITE-seq AT data may also provide insight into potential mechanisms that could contribute to islet defects. For example, we observed enrichment for LAMs in obesity that persists during WL and WC in AT. LAMs, unlike other macrophage subpopulations, also highly express inflammatory cytokines like IL-1β, which are known to impair β cell proliferation and function [345]. Other cells, like T_{regs}, had a markedly altered transcriptional profile, characterized by loss of sensitivity to anti-inflammatory cytokines like IL-33, during obesity that was not recovered by WL. It is likely these changes are not limited to the AT milieu and therefore loss of T_{reg} function in islets could result exacerbated inflammatory response during WC [346]. Finally, we identified a subset of $GZMK^+$ $CD8^+$ T cells with a TCR repertoire associated with T1D. It remains unknown if or how GZMK can alter β cell survival or function. However, expression of many senescence associated secreted proteins (induced by GZMK in other cells) is correlated with T1D, suggesting that CD^+ T cell derived GZMK may play a role in islet dysfunction as well [347–349]. All of these possibilities require additional experiments, but are important for understanding WC-associated metabolic disease and may be critical for the identification of novel targetable pathways to prevent obesity-associated β cell stress.

6.7 Future Directions

The overarching finding of this work was that WL failed to resolve AT immune infiltration, which preceeds further enrichment of type I immune cells after WC. However, changes in many immune cell subtypes were only briefly explored in this work and the mechanisms driving these changes remain untested. One unexplored area is the epigenetic regulation of the transcriptional landscape of immune cells in AT during obesity. Multiple type II immune cells observed in lean AT decrease in number and have altered phenotype after WL. This suggests that there is a persistent change in transcriptional regulation, which could be explained by epigenetic modifications, in these cells that are not as rapidly recruited to the local tissue microenvironment as type I immune cells. Specifically, downregulation of surface receptors important for sensing local cues (e.g the IL-33 receptor in T_{regs} and ILC2s; CD163 in TRMs) suggest that these cells have long-term impairments in their classical functions. Multiple lipid-responsive transcription factors (e.g CEPBP or LXR) regulate immune cell function and therefore it is possible that a compromise between lipid handling and immunoregulatory functions persists after WL [350, 351]. New developments in single cell assays for transposase-accessible chromatin (ATAC-seq) would offer clear insight into chromatin accessibility within these cells and, coupled with predictive transcription factor binding motif models, may identify targetable transcription factors that limit immunoregulatory capacity. Fortunately, there are many available transgenic mouse models that could facilitate further exploration in this area. For example, a tamoxifen-inducible Cre driven by the CD206 promoter has already been described, offering both temporal and cell-type specific control of gene depletion in TRMs if crossed with appropriate floxed models (e.g *Cebpb*$^{fl/fl}$ mice; Jax Strain #:032282) [352].

Another area of burgeoning research is modeling cellular cross-talk. We have known for many years that cell-to-cell communication is essential for multiple biological processes (e.g antigen presentation, costimulation, cytokine response, cell migration). These models rely largely on known relationships between ligands, receptors, and downstream signal-

ing. By identifying patterns of cells expressing ligands (i.e communicators) and those receiving signals to produce transcription factors (i.e receivers), the delicate relationships between and within cell types can be identified. Tools such as CellChat and CellPhoneDB provide the foundational networks for identifying these communications and the scientific community is already exploring crosstalk between immune cell subsets [353, 354]. However, it may be more interesting to investigate the relationship between immune cells and nearby stromal cells (e.g adipocytes) to better understand changes in cellular communication that correlate with insulin resistance, apoptosis, and inflammation. Larger data sets that include both adipocytes and immune cells may already offer an opportunity to test these ideas [355]. Moreover, as cellular resolution of spatial transcriptomics improves, we will be able to identify critical processes that occur during specific cellular communication events. For example, we still have little insight into the mechanisms that signal and promote clearance of dying adipocytes by macrophages (i.e in CLS) and what, if any, effects that rapid lipid-uptake has on macrophage phenotype. Would improved recruitment, phagocytosis, or lysosomal degredation of dying adipocytes by macrophages reduce obesity-associated AT insulin resistance? Currently, the transcriptional changes that are involved in adipocyte clearance during early (recognition), middle (containment), and late (engulfment and metabolism) stages are unknown. Fortunately, CLS are easy to recognize and can be captured at multiple stages across a large tissue section. For example, PLIN-1 surrounding the lipid droplet is rapidly degraded upon adipocyte cell death, giving an early indicator (prior to recognition by macrophages). Actively processed CLS are covered in macrophages and in late stages macrophage expression of PLIN-2 increases. This relative time-scale of adipocyte clearance, coupled with spatial transcriptomics and modeling of cell-to-cell communications, would give incredible insight into this critical homeostatic process.

Another unexplored area of research, highlighted by the work in Chapters III and IV, is how systemic immunity is altered during settings of obesity and WL. We identified in-

creased numbers of activated DCs, which express both immunoregulatory genes/proteins and multiple genes associated with cellular migration. Therefore, it is like that these cells egress from AT where they present AT-derived antigens within secondary lymphoid organs. It is possible that these cells suppress acute immune responses peripherally, which may explain why obese individuals have impaired pathogen clearance. For example, DCs found in the lung transport influenza to lymphnodes where it is presented to activate T cells [356]. It was previously identified that impaired T cell memory formation to influenza infection during obesity was not improved by WL [357]. While it remains unknown whether AT-derived activated DCs migrate into the lung, it raises the question of whether immunoregulatory obesity-derived DCs could impair systemic response to infection. In the tumor microenvironment, PD-L1$^+$ DCs also suppress T cells and promote tumor survival. Because obese individuals have increased risk of tumor progression and, paradoxically, respond better to immunotherapy (e.g anti-PD-1) in some cases, it is possible that immunoregulatory AT-derived DCs migrate and contribute to tumor growth. Moreover, whether T cells can migrate directly from AT to tumors (e.g in breast cancer) remains unclear, but an expanded pool of PD-1$^+$ T cells found in obese, WL, and WC AT may be therapeutically valuable in the context of anti-PD-1 immunotherapy.

In regards to pancreatic islets, one of the most striking unanswered questions is whether formation of autoreactive T cells occurs during settings of chronic hyperinsulinemia. In our data, it appears that cells likely to respond to insulin do not produce cytolytic proteins found in similar cells that cause β cell death in T1D. However, these data do not exclude the possibility that GZMK$^+$ T cells could also contribute to β cell stress. The question of whether these cells are able to migrate out of AT and reach islets remains unanswered. Moreover, is it possible to block GZMK signaling through the use of immunotherapy and reduce islet inflammation? Alternatively, do these cells directly contribute to insulin resistance in the liver, skeletal muscle, and AT? If so, GZMK could be implicated in increased insulin demand that ultimately leads to β cell fatigue. To address these questions, a trans-

genic GZMK knockout mouse could be utilized to assess whether GZMK is important for obesity-associated insulin resistance [358]. To date, GZMK remains one of the few "orphan" granzymes with unknown substrates and therefore any discoveries regarding GZMK, and particularly its contribution to metabolic disease, would be valuable to the immunology research community.

6.8 Summary

In summary, the completion of my dissertation work has shown that WC modeled through diet-induced WL and weight regain in mice causes a defect in pancreatic insulin secretion. There is also a significant shift in AT immune cell phenotype, abundance, and activity that occurs during obesity amd remains unresolved with subsequent diet-induced WL. As a result, populations like LAMs and $CD8^+$ T_{EM} may contribute to subsequent weight regain through a complex system of cross-talk (e.g immunoregulatory signaling and inflammatory cytokines). Among these cells, α/β TCRs previously identified in T1D patients were observed, suggesting a link between AT T cells and β cell dysfunction. As part of this work, a web-based tool was made available to future investigators (hastylab.shinyapps.io/MAIseq), allowing free access to our CITE-seq data for discovery. Future studies will seek to identify if AT $CD8^+$ T cells contribute to metabolic disease through alternative mechanisms (e.g GZMK secretion) and if these cells rely on TCR-mediated signaling to migrate, proliferate, and survive in metabolic tissues.

Bibliography

1. *Global action plan for the prevention and control of NCDs 2013-2020* 2013. https://www.who.int/publications/i/item/9789241506236.
2. Blüher, M. Obesity: global epidemiology and pathogenesis. en. *Nature Reviews Endocrinology* **15,** 288–298. ISSN: 1759-5029, 1759-5037. http://www.nature.com/articles/s41574-019-0176-8 (2022) (May 2019).
3. Haththotuwa, R. N., Wijeyaratne, C. N. & Senarath, U. *Worldwide epidemic of obesity* 3–8 (Elsevier, 2020).
4. Wang, Y. *et al.* Has the prevalence of overweight, obesity and central obesity levelled off in the United States? Trends, patterns, disparities, and future projections for the obesity epidemic. *International Journal of Epidemiology* **49,** 810–823. ISSN: 0300-5771 (3 June 2020).
5. Finkelstein, E. A., Trogdon, J. G., Cohen, J. W. & Dietz, W. Annual medical Sspending attributable to obesity: payer-and service-specific estimates. *Health Affairs* **28,** w822–w831. ISSN: 0278-2715 (Supplement 1 Jan. 2009).
6. Wirth, A., Wabitsch, M. & Hauner, H. The prevention and treatment of obesity. *Deutsches Ärzteblatt international.* ISSN: 1866-0452 (Oct. 2014).
7. Foster, G. D., Makris, A. P. & Bailer, B. A. Behavioral treatment of obesity. *The American Journal of Clinical Nutrition* **82,** 230S–235S. ISSN: 0002-9165 (1 July 2005).
8. Kushner, R. F. Weight loss strategies for treatment of obesity: lifestyle management and pharmacotherapy. *Progress in Cardiovascular Diseases* **61,** 246–252. ISSN: 00330620 (2 July 2018).
9. Ruban, A., Stoenchev, K., Ashrafian, H. & Teare, J. Current treatments for obesity. *Clinical Medicine* **19,** 205–212. ISSN: 1470-2118 (3 May 2019).
10. Haase, C. L. *et al.* Weight loss and risk reduction of obesity-related outcomes in 0.5 million people: evidence from a UK primary care database. *International Journal of Obesity* **45,** 1249–1258. ISSN: 0307-0565 (6 June 2021).
11. Stunkard, A. The results of treatment for obesity. *A.M.A. Archives of Internal Medicine* **103,** 79. ISSN: 0888-2479 (1 Jan. 1959).
12. Stunkard, A. J. Behavior modification in the treatment of obesity. *Archives of General Psychiatry* **36,** 801. ISSN: 0003-990X (7 July 1979).
13. Ayyad, C. & Andersen, T. Long-term efficacy of dietary treatment of obesity: a systematic review of studies published between 1931 and 1999. *Obesity Reviews* **1,** 113–119. ISSN: 1467-7881 (2 Oct. 2000).
14. Crawford, D., Jeffery, R. W. & French, S. A. Can anyone successfully control their weight? Findings of a three year community-based study of men and women. *International journal of obesity and related metabolic disorders : journal of the International Association for the Study of Obesity* **24,** 1107–10 (9 Sept. 2000).

15. Wing, R. R. & Phelan, S. Long-term weight loss maintenance. *The American Journal of Clinical Nutrition* **82,** 222S–225S. ISSN: 0002-9165 (1 July 2005).

16. Fildes, A. *et al.* Probability of an obese person attaining normal body weight: cohort study using electronic health records. *American Journal of Public Health* **105,** e54–e59. ISSN: 0090-0036 (9 Sept. 2015).

17. MacLean, P. S., Bergouignan, A., Cornier, M.-A. & Jackman, M. R. Biology's response to dieting: the impetus for weight regain. *American Journal of Physiology-Regulatory, Integrative and Comparative Physiology* **301,** R581–R600. ISSN: 0363-6119 (3 Sept. 2011).

18. Sumithran, P. & Proietto, J. The defence of body weight: a physiological basis for weight regain after weight loss. *Clinical Science* **124,** 231–241. ISSN: 0143-5221 (4 Feb. 2013).

19. Greenway, F. L. Physiological adaptations to weight loss and factors favouring weight regain. *International Journal of Obesity* **39,** 1188–1196. ISSN: 0307-0565 (8 Aug. 2015).

20. Williams, G. C., Grow, V. M., Freedman, Z. R., Ryan, R. M. & Deci, E. L. Motivational predictors of weight loss and weight-loss maintenance. *Journal of Personality and Social Psychology* **70,** 115–126. ISSN: 1939-1315 (1 1996).

21. Wing, R. R. & Hill, J. O. Successful weight loss maintenance. *Annual Review of Nutrition* **21,** 323–341. ISSN: 0199-9885 (1 July 2001).

22. Corral, P. D., Bryan, D. R., Garvey, W. T., Gower, B. A. & Hunter, G. R. Dietary adherence during weight loss predicts weight regain. *Obesity* **19,** 1177–1181. ISSN: 19307381 (6 June 2011).

23. Lissner, L. *et al.* Variability of body weight and health outcomes in the Framingham population. *New England Journal of Medicine* **324,** 1839–1844. ISSN: 0028-4793 (26 June 1991).

24. Rzehak, P. *et al.* Weight change, weight cycling and mortality in the ERFORT Male Cohort Study. *European Journal of Epidemiology* **22,** 665–673. ISSN: 0393-2990 (10 Sept. 2007).

25. Oh, T. J. *et al.* Body-weight fluctuation and incident diabetes mellitus, cardiovascular disease, and mortality: a 16-Year prospective cohort study. *The Journal of Clinical Endocrinology& Metabolism* **104,** 639–646. ISSN: 0021-972X (3 Mar. 2019).

26. Delahanty, L. M. *et al.* Effects of weight loss, weight cycling, and weight loss maintenance on diabetes incidence and change in cardiometabolic traits in the Diabetes Prevention Program. *Diabetes care* **37,** 2738–45. ISSN: 1935-5548 (10 Oct. 2014).

27. Bangalore, S. *et al.* Body-weight fluctuations and outcomes in coronary disease. *New England Journal of Medicine* **376,** 1332–1340. ISSN: 0028-4793 (14 Apr. 2017).

28. Choi, D., Choi, S. & Park, S. M. Impact of weight variability on mortality among Korean men and women: a population based study. *Scientific Reports* **9,** 9543. ISSN: 2045-2322 (1 Dec. 2019).

29. Flannick, J., Johansson, S. & Njølstad, P. R. Common and rare forms of diabetes mellitus: towards a continuum of diabetes subtypes. *Nature Reviews Endocrinology* **12,** 394–406. ISSN: 1759-5029 (7 July 2016).

30. Knip, M. & Simell, O. Environmental triggers of type 1 diabetes. *Cold Spring Harbor Perspectives in Medicine* **2,** a007690–a007690. ISSN: 2157-1422 (7 July 2012).

31. Van der Werf, N., Kroese, F. G., Rozing, J. & Hillebrands, J.-L. Viral infections as potential triggers of type 1 diabetes. *Diabetes/Metabolism Research and Reviews* **23,** 169–183. ISSN: 15207552 (3 Mar. 2007).

32. Lombardi, A., Tsomos, E., Hammerstad, S. S. & Tomer, Y. Interferon alpha: The key trigger of type 1 diabetes. *Journal of Autoimmunity* **94,** 7–15. ISSN: 08968411 (Nov. 2018).

33. Classification and diagnosis of diabetes: standards of medical Care in diabetes. *Diabetes Care* **45,** S17–S38. ISSN: 0149-5992 (Supplement$_1$ Jan. 2022).

34. Gunasekaran, U. & Gannon, M. Type 2 diabetes and the aging pancreatic beta cell. *Aging* **3,** 565–575. ISSN: 1945-4589 (6 June 2011).

35. Sirdah, M. M. & Reading, N. S. Genetic predisposition in type 2 diabetes: A promising approach toward a personalized management of diabetes. *Clinical Genetics* **98,** 525–547. ISSN: 0009-9163 (6 Dec. 2020).

36. Herder, C. & Roden, M. Genetics of type 2 diabetes: pathophysiologic and clinical relevance. *European Journal of Clinical Investigation* **41,** 679–692. ISSN: 00142972 (6 June 2011).

37. Hasson, B. R., Apovian, C. & Istfan, N. Racial/ethnic differences in insulin resistance and beta cell function: relationship to racial disparities in type 2 diabetes among African Americans versus caucasians. *Current Obesity Reports* **4,** 241–249. ISSN: 2162-4968 (2 June 2015).

38. Harris, M. I., Eastman, R. C., Cowie, C. C., Flegal, K. M. & Eberhardt, M. S. Racial and ethnic differences in glycemic control of adults with type 2 diabetes. *Diabetes Care* **22,** 403–408. ISSN: 0149-5992 (3 Mar. 1999).

39. Cossrow, N. & Falkner, B. Race/ethnic issues in obesity and obesity-related comorbidities. *The Journal of Clinical Endocrinology& Metabolism* **89,** 2590–2594. ISSN: 0021-972X (6 June 2004).

40. Sobngwi, E. *et al.* Effect of a diabetic environment in utero on predisposition to type 2 diabetes. *The Lancet* **361,** 1861–1865. ISSN: 01406736 (9372 May 2003).

41. Portha, B., Chavey, A. & Movassat, J. Early-life origins of type 2 diabetes: fetal programming of the beta-cell mass. *Experimental Diabetes Research* **2011,** 1–16. ISSN: 1687-5214 (2011).

42. Gannon, M. High fat diet regulation of β-cell proliferation and β-cell mass. *The Open Endocrinology Journal* **4,** 66–77. ISSN: 18742165 (1 Nov. 2010).

43. Mosser, R. E. *et al.* High-fat diet-induced β-cell proliferation occurs prior to insulin resistance in C57Bl/6J male mice. *American Journal of Physiology-Endocrinology and Metabolism* **308,** E573–E582. ISSN: 0193-1849 (7 Apr. 2015).

44. Cox, A. R. *et al.* Extreme obesity induces massive beta cell expansion in mice through self-renewal and does not alter the beta cell lineage. *Diabetologia* **59,** 1231–1241. ISSN: 0012-186X (6 June 2016).

45. Buchanan, T. A. & Xiang, A. H. Gestational diabetes mellitus. *Journal of Clinical Investigation* **115,** 485–491. ISSN: 0021-9738 (3 Mar. 2005).

46. Xu, Y. *et al.* Prolactin-stimulated survivin induction is required for beta cell mass expansion during pregnancy in mice. *Diabetologia* **58,** 2064–2073. ISSN: 0012-186X (9 Sept. 2015).

47. Gummesson, A., Nyman, E., Knutsson, M. & Karpefors, M. Effect of weight reduction on glycated haemoglobin in weight loss trials in patients with type 2 diabetes. *Diabetes, Obesity and Metabolism* **19,** 1295–1305. ISSN: 1462-8902 (9 Sept. 2017).

48. Penn, L. *et al.* Importance of weight loss maintenance and risk prediction in the prevention of type 2 diabetes: analysis of European Diabetes Prevention study RCT. *PLoS ONE* **8,** e57143. ISSN: 1932-6203 (2 Feb. 2013).

49. Schauer, P. R., Mingrone, G., Ikramuddin, S. & Wolfe, B. Clinical outcomes of metabolic surgery: efficacy of glycemic control, weight loss, and remission of diabetes. *Diabetes Care* **39,** 902–911. ISSN: 0149-5992 (6 June 2016).

50. Pandol, S. J. The exocrine pancreas. *Colloquium Series on Integrated Systems Physiology: From Molecule to Function* **3,** 1–64. ISSN: 2154-560X (1 Feb. 2011).

51. Steiner, D. J., Kim, A., Miller, K. & Hara, M. Pancreatic islet plasticity: interspecies comparison of islet architecture and composition. *Islets* **2,** 135–145. ISSN: 1938-2014 (3 May 2010).

52. Cabrera, O. *et al.* The unique cytoarchitecture of human pancreatic islets has implications for islet cell function. *Proceedings of the National Academy of Sciences* **103,** 2334–2339. ISSN: 0027-8424 (7 Feb. 2006).

53. E Drigo, R. A. *et al.* New insights into the architecture of the islet of Langerhans: a focused cross-species assessment. *Diabetologia* **58,** 2218–2228. ISSN: 0012-186X (10 Oct. 2015).

54. Aamodt, K. I. & Powers, A. C. Signals in the pancreatic islet microenvironment influence β-cell proliferation. *Diabetes, Obesity and Metabolism* **19,** 124–136. ISSN: 14628902 (Sept. 2017).

55. MacDonald, P. E., Joseph, J. W. & Rorsman, P. Glucose-sensing mechanisms in pancreatic β-cells. *Philosophical Transactions of the Royal Society B: Biological Sciences* **360,** 2211–2225. ISSN: 0962-8436 (1464 Dec. 2005).

56. O'Neill, C. M. *et al.* Circulating levels of IL-1β+IL-6 cause ER stress and dysfunction in islets from prediabetic male mice. *Endocrinology* **154,** 3077–3088. ISSN: 0013-7227 (9 Sept. 2013).

57. Eizirik, D. L., Miani, M. & Cardozo, A. K. Signalling danger: endoplasmic reticulum stress and the unfolded protein response in pancreatic islet inflammation. *Diabetologia* **56,** 234–241. ISSN: 0012-186X (2 Feb. 2013).

58. Paula, F. M. M. *et al.* Exercise training protects human and rodent β cells against endoplasmic reticulum stress and apoptosis. *The FASEB Journal* **32,** 1524–1536. ISSN: 0892-6638 (3 Mar. 2018).

59. Christensen, A. A. & Gannon, M. The beta cell in type 2 diabetes. *Current Diabetes Reports* **19,** 81. ISSN: 1534-4827 (9 Sept. 2019).

60. Jansson, L. *et al.* Pancreatic islet blood flow and its measurement. *Upsala Journal of Medical Sciences* **121,** 81–95. ISSN: 0300-9734 (2 Apr. 2016).

61. Farmer, T. D. *et al.* Comparison of the physiological relevance of systemic vs. portal insulin delivery to evaluate whole body glucose flux during an insulin clamp. *American Journal of Physiology-Endocrinology and Metabolism* **308,** E206–E222. ISSN: 0193-1849 (3 Feb. 2015).

62. Field, J. B. Extraction of insulin by liver. *Annual Review of Medicine* **24,** 309–314. ISSN: 0066-4219 (1 Feb. 1973).

63. Meier, J. J., Veldhuis, J. D. & Butler, P. C. Pulsatile insulin secretion dictates systemic insulin delivery by regulating hepatic insulin extraction in humans. *Diabetes* **54,** 1649–1656. ISSN: 0012-1797 (6 June 2005).

64. Williams, I. M. *et al.* Insulin exits skeletal muscle capillaries by fluid-phase transport. *Journal of Clinical Investigation* **128,** 699–714. ISSN: 0021-9738 (2 Jan. 2018).

65. McClatchey, P. M. *et al.* Perfusion controls muscle glucose uptake by altering the rate of glucose dispersion in vivo. *American Journal of Physiology-Endocrinology and Metabolism* **317,** E1022–E1036. ISSN: 0193-1849 (6 Dec. 2019).

66. Williams, I. M. & Wasserman, D. H. Capillary endothelial insulin transport: the rate-limiting step for insulin-stimulated glucose uptake. *Endocrinology* **163.** ISSN: 0013-7227 (2 Feb. 2022).

67. Wasserman, D. H., Wang, T. J. & Brown, N. J. The vasculature in prediabetes. *Circulation Research* **122,** 1135–1150. ISSN: 0009-7330 (8 Apr. 2018).

68. Schaffer, L. A model for insulin binding to the insulin receptor. *European Journal of Biochemistry* **221,** 1127–1132. ISSN: 0014-2956 (3 May 1994).

69. Jiráček, J. & Žáková, L. Structural perspectives of insulin receptor isoform-selective insulin analogs. *Frontiers in Endocrinology* **8.** ISSN: 1664-2392 (July 2017).

70. Whitehead, J. P., Clark, S. F., Ursø, B. & James, D. E. Signalling through the insulin receptor. *Current Opinion in Cell Biology* **12,** 222–228. ISSN: 09550674 (2 Apr. 2000).

71. Hopkins, B. D., Goncalves, M. D. & Cantley, L. C. Insulin–PI3K signalling: an evolutionarily insulated metabolic driver of cancer. *Nature Reviews Endocrinology* **16,** 276–283. ISSN: 1759-5029 (5 May 2020).

72. Hotamisligil, G. S. The role of TNFα and TNF receptors in obesity and insulin resistance. *Journal of Internal Medicine* **245,** 621–625. ISSN: 0954-6820 (6 June 1999).

73. Wu, H. & Ballantyne, C. M. Metabolic inflammation and insulin resistance in obesity. *Circulation Research* **126,** 1549–1564. ISSN: 0009-7330 (11 May 2020).

74. Rui, L., Yuan, M., Frantz, D., Shoelson, S. & White, M. F. SOCS-1 and SOCS-3 block insulin signaling by ubiquitin-mediated degradation of IRS1 and IRS2. *Journal of Biological Chemistry* **277,** 42394–42398. ISSN: 00219258 (44 Nov. 2002).

75. Ueki, K., Kondo, T. & Kahn, C. R. Suppressor of cytokine signaling 1 (SOCS-1) and SOCS-3 Cause insulin resistance through inhibition of tyrosine phosphorylation of insulin receptor substrate proteins by discrete mechanisms. *Molecular and Cellular Biology* **24,** 5434–5446. ISSN: 0270-7306 (12 June 2004).

76. Hurrel, D. G., Pedersen, O. & Kahn, C. R. Alterations in the hepatic insulin receptor kinase in genetic and acquired obesity in rats. *Endocrinology* **125,** 2454–2462. ISSN: 0013-7227 (5 Nov. 1989).

77. Wells, H. G. Adipose tissue, a neglected subject. *Journal of the American Medical Association* **114.** ISSN: 0002-9955 (22 June 1940).

78. Cinti, S. *Obesity, type 2 diabetes and the adipose organ* ISBN: 978-3-319-40520-9 (Springer International Publishing, 2018).

79. Frontini, A. & Cinti, S. Distribution and development of brown adipocytes in the murine and human adipose organ. *Cell Metabolism* **11,** 253–256. ISSN: 15504131 (4 Apr. 2010).

80. Fischer, A. W., Schlein, C., Cannon, B., Heeren, J. & Nedergaard, J. Intact innervation is essential for diet-induced recruitment of brown adipose tissue. *American Journal of Physiology-Endocrinology and Metabolism* **316,** E487–E503. ISSN: 0193-1849 (3 Mar. 2019).

81. Herz, C. T. & Kiefer, F. W. Adipose tissue browning in mice and humans. *Journal of Endocrinology* **241,** R97–R109. ISSN: 0022-0795 (3 June 2019).

82. Verboven, K. *et al.* Abdominal subcutaneous and visceral adipocyte size, lipolysis and inflammation relate to insulin resistance in male obese humans. *Scientific Reports* **8,** 4677. ISSN: 2045-2322 (1 Dec. 2018).

83. Cheong, L. Y. & Xu, A. Intercellular and inter-organ crosstalk in browning of white adipose tissue: molecular mechanism and therapeutic complications. *Journal of Molecular Cell Biology* **13,** 466–479. ISSN: 1759-4685 (7 Oct. 2021).

84. Tanaka, M. *et al.* Intraperitoneal, but not retroperitoneal, visceral adipose tissue is associated with diabetes mellitus: a cross-sectional, retrospective pilot analysis. *Diabetology& Metabolic Syndrome* **12,** 103. ISSN: 1758-5996 (1 Dec. 2020).

85. Boyko, E. J., Fujimoto, W. Y., Leonetti, D. L. & Newell-Morris, L. Visceral adiposity and risk of type 2 diabetes: a prospective study among Japanese Americans. *Diabetes Care* **23,** 465–471. ISSN: 0149-5992 (4 Apr. 2000).

86. Wajchenberg, B. L. Subcutaneous and visceral adipose tissue: their relation to the metabolic syndrome. *Endocrine Reviews* **21,** 697–738. ISSN: 0163-769X (6 Dec. 2000).

87. Fukuda, T. *et al.* Ratio of visceral-to-subcutaneous fat area predicts cardiovascular events in patients with type 2 diabetes. *Journal of Diabetes Investigation* **9,** 396–402. ISSN: 20401116 (2 Mar. 2018).

88. Sun, K., Kusminski, C. M. & Scherer, P. E. Adipose tissue remodeling and obesity. *Journal of Clinical Investigation* **121,** 2094–2101. ISSN: 0021-9738 (6 June 2011).

89. Govers, R. Molecular mechanisms of GLUT4 regulation in adipocytes. *Diabetes& Metabolism* **40,** 400–410. ISSN: 12623636 (6 Dec. 2014).

90. Obradovic, M. *et al.* Leptin and obesity: role and clinical implication. *Frontiers in Endocrinology* **12.** ISSN: 1664-2392 (May 2021).

91. Elmquist, J. K., Ahima, R. S., Elias, C. F., Flier, J. S. & Saper, C. B. Leptin activates distinct projections from the dorsomedial and ventromedial hypothalamicnuclei. *Proceedings of the National Academy of Sciences* **95,** 741–746. ISSN: 0027-8424 (2 Jan. 1998).

92. Bouret, S. G. *et al.* Hypothalamic neural projections are permanently disrupted in diet-induced obese rats. *Cell Metabolism* **7,** 179–185. ISSN: 15504131 (2 Feb. 2008).

93. Ingalls, A. M., Dickie, M. M. & Snell, G. D. Obese, a new mutation in the house mouse. *Journal of Heredity* **41,** 317–318. ISSN: 1465-7333 (12 Dec. 1950).

94. Funcke, J.-B. *et al.* Monogenic forms of childhood obesity due to mutations in the leptin gene. *Molecular and Cellular Pediatrics* **1,** 3. ISSN: 2194-7791 (1 Dec. 2014).

95. Farooqi, I. S. *et al.* Effects of recombinant leptin therapy in a child with congenital leptin deficiency. *New England Journal of Medicine* **341,** 879–884. ISSN: 0028-4793 (12 Sept. 1999).

96. Farooqi, I. S. *et al.* Beneficial effects of leptin on obesity, T cell hyporesponsiveness, and neuroendocrine/metabolic dysfunction of human congenital leptin deficiency. *Journal of Clinical Investigation* **110,** 1093–1103. ISSN: 0021-9738 (8 Oct. 2002).

97. Nakamura, K., Fuster, J. J. & Walsh, K. Adipokines: A link between obesity and cardiovascular disease. *Journal of Cardiology* **63,** 250–259. ISSN: 09145087 (4 Apr. 2014).

98. Kadowaki, T. & Yamauchi, T. Adiponectin and adiponectin receptors. *Endocrine Reviews* **26,** 439–451. ISSN: 0163-769X (3 May 2005).

99. Ma, X., Wang, D., Zhao, W. & Xu, L. Deciphering the roles of PPARγ in adipocytes via dynamic change of transcription complex. *Frontiers in Endocrinology* **9.** ISSN: 1664-2392 (Aug. 2018).

100. Larsen, T. M., Toubro, S. & Astrup, A. PPARgamma agonists in the treatment of type II diabetes: is increased fatness commensurate with long-term efficacy? *International Journal of Obesity* **27,** 147–161. ISSN: 0307-0565 (2 Feb. 2003).

101. Kaul, S., Bolger, A. F., Herrington, D., Giugliano, R. P. & Eckel, R. H. Thiazolidinedione drugs and cardiovascular risks. *Circulation* **121,** 1868–1877. ISSN: 0009-7322 (16 Apr. 2010).

102. Hill, A. A. *et al.* Activation of NF-$\kappa\beta$ drives the enhanced survival of adipose tissue macrophages in an obesogenic environment. *Molecular Metabolism* **4,** 665–677. ISSN: 22128778 (10 Oct. 2015).

103. Kanda, H. MCP-1 contributes to macrophage infiltration into adipose tissue, insulin resistance, and hepatic steatosis in obesity. *Journal of Clinical Investigation* **116,** 1494–1505. ISSN: 0021-9738 (6 June 2006).

104. Guerre-Millo, M. Adipose tissue hormones. *Journal of Endocrinological Investigation* **25,** 855–861. ISSN: 0391-4097 (10 Nov. 2002).

105. Weisberg, S. P. *et al.* Obesity is associated with macrophage accumulation in adipose tissue. *Journal of Clinical Investigation* **112,** 1796–1808. ISSN: 0021-9738 (12 Dec. 2003).

106. Xu, H. *et al.* Chronic inflammation in fat plays a crucial role in the development of obesity-related insulin resistance. *Journal of Clinical Investigation* **112,** 1821–1830. ISSN: 0021-9738 (12 Dec. 2003).

107. Cox, N. & Geissmann, F. Macrophage ontogeny in the control of adipose tissue biology. *Current Opinion in Immunology* **62,** 1–8. ISSN: 09527915 (Feb. 2020).

108. Cox, N. *et al.* Diet-regulated production of PDGFcc by macrophages controls energy storage. *Science* **373.** ISSN: 0036-8075 (6550 July 2021).

109. Lumeng, C. N., Bodzin, J. L. & Saltiel, A. R. Obesity induces a phenotypic switch in adipose tissue macrophage polarization. *Journal of Clinical Investigation* **117,** 175–184. ISSN: 0021-9738 (1 Jan. 2007).

110. Ito, A. *et al.* Role of CC chemokine receptor 2 in bone marrow cells in the recruitment of macrophages into obese adipose tissue. *Journal of Biological Chemistry* **283,** 35715–35723. ISSN: 00219258 (51 Dec. 2008).

111. Kim, J. *et al.* Silencing CCR2 in macrophages alleviates adipose tissue inflammation and the associated metabolic syndrome in dietary obese mice. *Molecular Therapy - Nucleic Acids* **5,** e280. ISSN: 21622531 (2016).

112. Orr, J. S. *et al.* Obesity alters adipose tissue macrophage iron content and tissue iron distribution. *Diabetes* **63,** 421–432. ISSN: 0012-1797 (2 Feb. 2014).

113. Hubler, M. J., Erikson, K. M., Kennedy, A. J. & Hasty, A. H. MFe^{hi} adipose tissue macrophages compensate for tissue iron perturbations in mice. *American Journal of Physiology-Cell Physiology* **315,** C319–C329. ISSN: 0363-6143 (3 Sept. 2018).

114. Li, C. *et al.* Single-cell transcriptomics–based MacSpectrum reveals macrophage activation signatures in diseases. *JCI Insight* **4.** ISSN: 2379-3708 (10 May 2019).

115. Kratz, M. *et al.* Metabolic dysfunction drives a mechanistically distinct proinflammatory phenotype in adipose tissue macrophages. *Cell Metabolism* **20,** 614–625. ISSN: 15504131 (4 Oct. 2014).

116. Jaitin, D. A. *et al.* Lipid-associated macrophages control metabolic homeostasis in a Trem2-dependent manner. *Cell* **178,** 686–698.e14. ISSN: 00928674 (3 July 2019).

117. Macdougall, C. E. & Longhi, M. P. Adipose tissue dendritic cells in steady-state. *Immunology,* imm.13034. ISSN: 0019-2805 (Dec. 2018).

118. Rajan, S. S. & Longhi, M. P. Dendritic cells and adipose tissue. *Immunology* **149,** 353–361. ISSN: 00192805 (4 Dec. 2016).

119. Chen, Y. *et al.* Adipose tissue dendritic cells enhances inflammation by prompting the generation of Th17 cells. *PLoS ONE* **9,** e92450. ISSN: 1932-6203 (3 Mar. 2014).

120. Weid, P.-Y. V. D. & Rainey, K. J. Review article: lymphatic system and associated adipose tissue in the development of inflammatory bowel disease. *Alimentary Pharmacology& Therapeutics* **32,** 697–711. ISSN: 02692813 (6 Sept. 2010).

121. Stutte, S. *et al.* High-fat diet rapidly modifies trafficking, phenotype, and function of plasmacytoid dendritic cells in adipose tissue. *The Journal of Immunology* **208,** 1445–1455. ISSN: 0022-1767 (6 Mar. 2022).

122. Bolus, W. R., Kennedy, A. J. & Hasty, A. H. Obesity-induced reduction of adipose eosinophils is reversed with low-calorie dietary intervention. *Physiological Reports* **6,** e13919. ISSN: 2051817X (22 Nov. 2018).

123. Bolus, W. R. *et al.* Elevating adipose eosinophils in obese mice to physiologically normal levels does not rescue metabolic impairments. *Molecular Metabolism* **8,** 86–95. ISSN: 22128778 (Feb. 2018).

124. Esnault, S. *et al.* Identification of genes expressed by human airway eosinophils after an in vivo allergen challenge. *PLoS ONE* **8,** e67560. ISSN: 1932-6203 (7 July 2013).

125. Poglio, S. *et al.* Adipose tissue as a dedicated reservoir of functional mast cell progenitors. *Stem Cells* **28,** 2065–2072. ISSN: 1066-5099 (11 Nov. 2010).

126. Finlin, B. S. *et al.* Adipose tissue mast cells promote human adipose beiging in response to cold. *Scientific Reports* **9,** 8658. ISSN: 2045-2322 (1 Dec. 2019).

127. Elgazar-Carmon, V., Rudich, A., Hadad, N. & Levy, R. Neutrophils transiently infiltrate intra-abdominal fat early in the course of high-fat feeding. *Journal of Lipid Research* **49,** 1894–1903. ISSN: 00222275 (9 Sept. 2008).

128. Watanabe, Y. *et al.* Bidirectional crosstalk between neutrophils and adipocytes promotes adipose tissue inflammation. *The FASEB Journal* **33,** 11821–11835. ISSN: 0892-6638 (11 Nov. 2019).

129. Eberl, G., Colonna, M., Santo, J. P. D. & McKenzie, A. N. J. Innate lymphoid cells: a new paradigm in immunology. *Science* **348.** ISSN: 0036-8075 (6237 May 2015).

130. Bénézech, C. & Jackson-Jones, L. H. ILC2 orchestration of local immune function in adipose tissue. *Frontiers in Immunology* **10.** ISSN: 1664-3224 (Feb. 2019).

131. O'Sullivan, T. E. *et al.* Adipose-resident group 1 innate lymphoid cells promote obesity-associated insulin resistance. *Immunity* **45,** 428–441. ISSN: 10747613 (2 Aug. 2016).

132. Hildreth, A. D. *et al.* Single-cell sequencing of human white adipose tissue identifies new cell states in health and obesity. *Nature Immunology* **22,** 639–653. ISSN: 1529-2908 (5 May 2021).

133. Lee, B.-C. *et al.* Adipose natural killer cells regulate adipose tissue macrophages to promote insulin resistance in obesity. *Cell Metabolism* **23,** 685–698. ISSN: 15504131 (4 Apr. 2016).

134. Zhang, Y. & Huang, B. *The development and diversity of ILCs, NK cells and their relevance in health and diseases* 225–244 (2017).

135. O'Shea, D. & Hogan, A. E. Dysregulation of natural killer cells in obesity. *Cancers* **11,** 573. ISSN: 2072-6694 (4 Apr. 2019).

136. Hoehn, K. B., Fowler, A., Lunter, G. & Pybus, O. G. The diversity and molecular evolution of B-cell reptors during infection. *Molecular Biology and Evolution* **33,** 1147–1157. ISSN: 0737-4038 (5 May 2016).

137. Spits, H. Development of $\alpha\beta$ T cells in the human thymus. *Nature Reviews Immunology* **2,** 760–772. ISSN: 1474-1733 (10 Oct. 2002).

138. Liu, W., Tolar, P., Song, W. & Kim, T. J. Editorial: BCR signaling and B cell activation. *Frontiers in Immunology* **11.** ISSN: 1664-3224 (Jan. 2020).

139. Kaufmann, S. H. Gamma/delta and other unconventional T lymphocytes: what do they see and what do they do? *Proceedings of the National Academy of Sciences* **93,** 2272–2279. ISSN: 0027-8424 (6 Mar. 1996).

140. Xiong, Y. & Bosselut, R. CD4–CD8 differentiation in the thymus: connecting circuits and building memories. *Current Opinion in Immunology* **24,** 139–145. ISSN: 09527915 (2 Apr. 2012).

141. Vignali, D. A. A., Collison, L. W. & Workman, C. J. How regulatory T cells work. *Nature Reviews Immunology* **8,** 523–532. ISSN: 1474-1733 (7 July 2008).

142. Ziegler, S. F. & Buckner, J. H. FOXP3 and the regulation of Treg/Th17 differentiation. *Microbes and Infection* **11,** 594–598. ISSN: 12864579 (5 Apr. 2009).

143. Cipolletta, D. *et al.* PPAR-γ is a major driver of the accumulation and phenotype of adipose tissue Treg cells. *Nature* **486,** 549–553. ISSN: 0028-0836 (7404 June 2012).

144. Zeng, Q. *et al.* A unique population: adipose-resident regulatory T cells. *Frontiers in Immunology* **9.** ISSN: 1664-3224 (Sept. 2018).

145. Kolodin, D. *et al.* Antigen- and cytokine-driven accumulation of regulatory T cells in visceral adipose tissue of lean mice. *Cell Metabolism* **21,** 543–557. ISSN: 15504131 (4 Apr. 2015).

146. Li, C. *et al.* TCR transgenic mice reveal stepwise, multi-site acquisition of the distinctive fat-Treg phenotype. *Cell* **174,** 285–299.e12. ISSN: 00928674 (2 July 2018).

147. Deiuliis, J. *et al.* Visceral adipose inflammation in obesity is associated with critical alterations in Tregulatory cell numbers. *PLoS ONE* **6,** e16376. ISSN: 1932-6203 (1 Jan. 2011).

148. Zhao, X.-Y. *et al.* The obesity-induced adipokine sST2 exacerbates adipose T_{reg} and ILC2 depletion and promotes insulin resistance. *Science Advances* **6.** ISSN: 2375-2548 (20 May 2020).

149. Stark, J. M., Tibbitt, C. A. & Coquet, J. M. The metabolic requirements of Th2 celldifferentiation. *Frontiers in Immunology* **10.** ISSN: 1664-3224 (Sept. 2019).

150. McLaughlin, T. *et al.* T-cell profile in adipose tissue is associated With insulinresistance and systemic inflammation in humans. *Arteriosclerosis, Thrombosis, and Vascular Biology* **34,** 2637–2643. ISSN: 1079-5642 (12 Dec. 2014).

151. Zhao, Y. *et al.* CD4+ T cells in obesity and obesity-associated diseases. *Cellular Immunology* **332,** 1–6. ISSN: 00088749 (Oct. 2018).

152. Szabo, S. J. *et al.* Distinct effects of T-bet in T_H 1 Lineage Commitment and IFN-γ production in CD4 and CD8 T cells. *Science* **295,** 338–342. ISSN: 0036-8075 (5553 Jan. 2002).

153. Khan, I. M. *et al.* Attenuated adipose tissue and skeletal muscle inflammation in obese mice with combined CD4+ and CD8+ T cell deficiency. *Atherosclerosis* **233,** 419–428. ISSN: 00219150 (2 Apr. 2014).

154. Nishimura, S. *et al.* CD8+ effector T cells contribute to macrophage recruitment and adipose tissue inflammation in obesity. *Nature Medicine* **15,** 914–920. ISSN: 1078-8956 (8 Aug. 2009).

155. Zhang, N. & Bevan, M. J. CD8+ T cells: foot soldiers of the immune system. *Immunity* **35,** 161–168. ISSN: 10747613 (2 Aug. 2011).

156. Kohlgruber, A. C. *et al.* $\gamma\delta$ T cells producing interleukin-17A regulate adipose regulatory T cell homeostasis and thermogenesis. *Nature Immunology* **19,** 464–474. ISSN: 1529-2908 (5 May 2018).

157. Macho-Fernandez, E. & Brigl, M. The extended family of CD1d-restricted NKT cells: sifting through a mixed bag of TCRs, antigens, and functions. *Frontiers in Immunology* **6.** ISSN: 1664-3224 (July 2015).

158. Wu, L. *et al.* Activation of invariant natural killer T cells by lipid excess promotes tissue inflammation, insulin resistance, and hepatic steatosis in obese mice. *Proceedings of the National Academy of Sciences* **109.** ISSN: 0027-8424 (19 May 2012).

159. Lynch, L. *et al.* Adipose tissue invariant NKT cells protect against diet-induced obesity and metabolic disorder through regulatory cytokine production. *Immunity* **37,** 574–587. ISSN: 10747613 (3 Sept. 2012).

160. Subramanian, S. *et al.* Deficiency of invariant natural killer T cells does not protect against obesity but exacerbates atherosclerosis in Ldlr/ mice. *International Journal of Molecular Sciences* **19,** 510. ISSN: 1422-0067 (2 Feb. 2018).

161. Huh, J. Y. *et al.* A novel function of adipocytes in lipid antigen presentation to iNKT cells. *Molecular and Cellular Biology* **33,** 328–339. ISSN: 0270-7306 (2 Jan. 2013).

162. Huh, J. Y. *et al.* Deletion of CD1d in adipocytes aggravates adipose tissue inflammation and insulin resistance in obesity. *Diabetes* **66,** 835–847. ISSN: 0012-1797 (4 Apr. 2017).

163. Huh, J. Y., Park, Y. J. & Kim, J. B. Adipocyte CD1d determines adipose inflammation and insulin resistance in obesity. *Adipocyte,* 1–8. ISSN: 2162-3945 (Mar. 2018).

164. Xiao, R. *et al.* Adipocyte CD1d gene transfer induces T cell expansion and adipocyte inflammation in CD1d knockout mice. *The Journal of Immunology,* ji2100313. ISSN: 0022-1767 (Apr. 2022).

165. Satoh, M. *et al.* Adipose invariant NKT cells interact with CD1d-expressing macrophages to regulate obesity-related inflammation. *Immunology* **165,** 414–427. ISSN: 0019-2805 (4 Apr. 2022).

166. Pond, C. M. Paracrine interactions of mammalian adipose tissue. *Journal of Experimental Zoology Part A: Comparative Experimental Biology* **295A,** 99–110. ISSN: 15488969 (1 Dec. 2002).

167. Pond, C. M. *Interactions of adipose and lymphoid tissues* 133–150 (Humana Press, 2007).

168. Villarroya, F., Cereijo, R., Gavaldà-Navarro, A., Villarroya, J. & Giralt, M. Inflammation of brown/beige adipose tissues in obesity and metabolic disease. *Journal of Internal Medicine* **284,** 492–504. ISSN: 09546820 (5 Nov. 2018).

169. Tsao, C.-H., Shiau, M.-Y., Chuang, P.-H., Chang, Y.-H. & Hwang, J. Interleukin-4 regulates lipid metabolism by inhibiting adipogenesis and promoting lipolysis. *Journal of Lipid Research* **55,** 385–397. ISSN: 00222275 (3 Mar. 2014).

170. Shiau, M.-Y. *et al.* Mechanism of interleukin-4 reducing lipid deposit by regulating hormone-sensitive lipase. *Scientific Reports* **9,** 11974. ISSN: 2045-2322 (1 Dec. 2019).

171. Loke, P. *et al.* IL-4 dependent alternatively-activated macrophages have a distinctive in vivo gene expression phenotype. *BMC Immunology* **3,** 7. ISSN: 14712172 (1 2002).

172. Rajbhandari, P. *et al.* IL-10 signaling remodels adipose chromatin architecture to limit thermogenesis and energy expenditure. *Cell* **172,** 218–233.e17. ISSN: 00928674 (1-2 Jan. 2018).

173. Rajbhandari, P. *et al.* Single cell analysis reveals immune cell–adipocyte crosstalk regulating the transcription of thermogenic adipocytes. *eLife* **8.** ISSN: 2050-084X (Oct. 2019).

174. Beppu, L. Y. *et al.* Tregs facilitate obesity and insulin resistance via a Blimp-1/IL-10 axis. *JCI Insight* **6.** ISSN: 2379-3708 (3 Feb. 2021).

175. Wu, D. *et al.* Eosinophils sustain adipose alternatively activated macrophages associated with glucose homeostasis. *Science* **332,** 243–247. ISSN: 0036-8075 (6026 Apr. 2011).

176. Duffen, J. *et al.* Modulation of the IL-33/IL-13 axis in obesity by IL-13Rα2. *The Journal of Immunology* **200,** 1347–1359. ISSN: 0022-1767 (4 Feb. 2018).

177. Surmi, B. & Hasty, A. Macrophage infiltration into adipose tissue: initiation, propagation and remodeling. *Future Lipidology* **3,** 545–556. ISSN: 1746-0875 (5 Jan. 2008).

178. Caër, C. *et al.* Immune cell-derived cytokines contribute to obesity-related inflammation, fibrogenesis and metabolic deregulation in human adipose tissue. *Scientific Reports* **7,** 3000. ISSN: 2045-2322 (1 Dec. 2017).

179. Makki, K., Froguel, P. & Wolowczuk, I. Adipose tissue in obesity-related inflammation and insulin resistance: cells, cytokines, and chemokines. *ISRN Inflammation* **2013,** 1–12. ISSN: 2090-8695 (Dec. 2013).

180. McKernan, K., Varghese, M., Patel, R. & Singer, K. Role of TLR4 in the induction of inflammatory changes in adipocytes and macrophages. *Adipocyte* **9,** 212–222. ISSN: 2162-3945 (1 Jan. 2020).

181. Holland, W. L. *et al.* Lipid-induced insulin resistance mediated by the proinflammatory receptor TLR4 requires saturated fatty acid–induced ceramide biosynthesis in mice. *Journal of Clinical Investigation* **121,** 1858–1870. ISSN: 0021-9738 (5 May 2011).

182. Kurts, C., Heath, W. R., Carbone, F. R., Kosaka, H. & Miller, J. F. A. P. *Cross-presentation of self antigens to CD8+ T cells: The balance between tolerance and autoimmunity* 172–190 (Sept. 2007).

183. Roep, B. O. & Peakman, M. Antigen targets of type 1 diabetes autoimmunity. *Cold Spring Harbor Perspectives in Medicine* **2,** a007781–a007781. ISSN: 2157-1422 (4 Apr. 2012).

184. Nakamura, T., Shirouzu, T., Nakata, K., Yoshimura, N. & Ushigome, H. The role of major histocompatibility complex in organ transplantation: donor specific anti-major histocompatibility complex antibodies analysis goes to the next stage. *International Journal of Molecular Sciences* **20,** 4544. ISSN: 1422-0067 (18 Sept. 2019).

185. Yewdell, J., Schubert, U. & Bennink, J. At the crossroads of cell biology and immunology: DRiPs and other sources of peptide ligands for MHC class I molecules. *Journal of Cell Science* **114,** 845–851. ISSN: 1477-9137 (5 Mar. 2001).

186. Ramachandra, L., Simmons, D. & Harding, C. V. MHC molecules and microbial antigen processing in phagosomes. *Current Opinion in Immunology* **21,** 98–104. ISSN: 09527915 (1 Feb. 2009).

187. Croft, N. P. *et al.* Most viral peptides displayed by class I MHC on infected cells are immunogenic. *Proceedings of the National Academy of Sciences* **116,** 3112–3117. ISSN: 0027-8424 (8 Feb. 2019).

188. Carson, G. R., Kuestner, R. E., Ahmed, A., Pettey, C. L. & Concino, M. F. Six chains of the human T cell antigen receptor.CD3 complex are necessary and sufficient for processing the receptor heterodimer to the cell surface. *The Journal of biological chemistry* **266,** 7883–7. ISSN: 0021-9258 (12 Apr. 1991).

189. Call, M. E., Pyrdol, J., Wiedmann, M. & Wucherpfennig, K. W. The organizing principle in the formation of the T cell receptor-CD3 complex. *Cell* **111,** 967–979. ISSN: 00928674 (7 Dec. 2002).

190. Mørch, A. M., Bálint, Š., Santos, A. M., Davis, S. J. & Dustin, M. L. Coreceptors and TCR signaling – the strong and the weak of it. *Frontiers in Cell and Developmental Biology* **8.** ISSN: 2296-634X (Oct. 2020).

191. Duttagupta, P. A., Boesteanu, A. C. & Katsikis, P. D. Costimulation signals for memory CD8+ T cells during viral infections. *Critical Reviews™ in Immunology* **29,** 469–486. ISSN: 2162-6472 (6 2009).

192. Xia, F. *et al.* TCR and CD28 concomitant stimulation elicits a distinctive calcium response in naive T cells. *Frontiers in Immunology* **9.** ISSN: 1664-3224 (Dec. 2018).

193. Suresh, M. *et al.* Role of CD28-B7 interactions in generation and maintenance of CD8 Tcell memory. *The Journal of Immunology* **167,** 5565–5573. ISSN: 0022-1767 (10 Nov. 2001).

194. Boesteanu, A. C. & Katsikis, P. D. Memory T cells need CD28 costimulation to remember. *Seminars in Immunology* **21,** 69–77. ISSN: 10445323 (2 Apr. 2009).

195. Hendriks, J. *et al.* CD27 is required for generation and long-term maintenance of T cell immunity. *Nature Immunology* **1,** 433–440. ISSN: 1529-2908 (5 Nov. 2000).

196. Munitic, I., Kuka, M., Allam, A., Scoville, J. P. & Ashwell, J. D. CD70 deficiency impairs effector CD8 T cell generation and viral clearance but is dispensable for the recall response to lymphocytic choriomeningitis virus. *The Journal of Immunology* **190,** 1169–1179. ISSN: 0022-1767 (3 Feb. 2013).

197. Vital, E. M. & Emery, P. Abatacept in the treatment of rheumatoid arthritis. *Therapeutics and Clinical Risk Management* **2,** 365–375. ISSN: 1176-6336 (4 Dec. 2006).

198. Rudd, C. E., Taylor, A. & Schneider, H. CD28 and CTLA-4 coreceptor expression and signal transduction. *Immunological Reviews* **229,** 12–26. ISSN: 01052896 (1 May 2009).

199. Martinez, G. J. *et al.* The transcription factor NFAT promotes exhaustion of activated CD8 + T cells. *Immunity* **42,** 265–278. ISSN: 10747613 (2 Feb. 2015).

200. Conley, J. M., Gallagher, M. P. & Berg, L. J. T cells and gene regulation: the switching on and turning up of genes after T cell receptor stimulation in CD8 T cells. *Frontiers in Immunology* **7.** ISSN: 1664-3224 (Feb. 2016).

201. Kelly, J. *et al.* A role for Stat5 in $CD8^+$ T cell homeostasis. *The Journal of Immunology* **170,** 210–217. ISSN: 0022-1767 (1 Jan. 2003).

202. Teague, R. M., Tempero, R. M., Thomas, S., Murali-Krishna, K. & Nelson, B. H. Proliferation and differentiation of $CD8^+$ T Cells in the absence of IL-2/15 receptor β-chain expression or STAT5 activation. *The Journal of Immunology* **173,** 3131–3139. ISSN: 0022-1767 (5 Sept. 2004).

203. Snijders, A. High-level IL-12 production by human dendritic cells requires two signals. *International Immunology* **10,** 1593–1598. ISSN: 14602377 (11 Nov. 1998).

204. Chang, J. T., Segal, B. M. & Shevach, E. M. Role of costimulation in the induction of the IL-12/IL-12 receptor pathway and the development of autoimmunity. *The Journal of Immunology* **164,** 100–106. ISSN: 0022-1767 (1 Jan. 2000).

205. Maini, M. K., Casorati, G., Dellabona, P., Wack, A. & Beverley, P. C. T-cell clonality in immune responses. *Immunology Today* **20,** 262–266. ISSN: 01675699 (6 June 1999).

206. Swadling, L. & Maini, M. K. T cells in COVID-19 — united in diversity. *Nature Immunology* **21,** 1307–1308. ISSN: 1529-2908 (11 Nov. 2020).

207. Akondy, R. S. *et al.* Origin and differentiation of human memory CD8 T cells after vaccination. *Nature* **552,** 362–367. ISSN: 0028-0836 (7685 Dec. 2017).

208. Kaech, S. M., Wherry, E. J. & Ahmed, R. Effector and memory T-cell differentiation: implications for vaccine development. *Nature Reviews Immunology* **2,** 251–262. ISSN: 1474-1733 (4 Apr. 2002).

209. Farber, D. L., Yudanin, N. A. & Restifo, N. P. Human memory T cells: generation, compartmentalization and homeostasis. *Nature Reviews Immunology* **14,** 24–35. ISSN: 1474-1733 (1 Jan. 2014).

210. Schumann, J., Stanko, K., Schliesser, U., Appelt, C. & Sawitzki, B. Differences in CD44 surface expression levels and function discriminates IL-17 and IFN-γ producing helper T cells. *PLOS ONE* **10,** e0132479. ISSN: 1932-6203 (7 July 2015).

211. Chen, A., Engel, P. & Tedder, T. F. Structural requirements regulate endoproteolytic release of the L-selectin (CD62L) adhesion receptor from the cell surface of leukocytes. *Journal of Experimental Medicine* **182,** 519–530. ISSN: 0022-1007 (2 Aug. 1995).

212. Sckisel, G. D. *et al.* Differential phenotypes of memory CD4 and CD8 T cells in the spleen and peripheral tissues following immunostimulatory therapy. *Journal for ImmunoTherapy of Cancer* **5,** 33. ISSN: 2051-1426 (1 Dec. 2017).

213. Qi, Q. *et al.* Diversity and clonal selection in the human T-cell repertoire. *Proceedings of the National Academy of Sciences* **111,** 13139–13144. ISSN: 0027-8424 (36 Sept. 2014).

214. Palmer, S., Albergante, L., Blackburn, C. C. & Newman, T. J. Thymic involution and rising disease incidence with age. *Proceedings of the National Academy of Sciences* **115,** 1883–1888. ISSN: 0027-8424 (8 Feb. 2018).

215. Fülöp, T., Larbi, A. & Witkowski, J. M. Human Inflammaging. *Gerontology* **65,** 495–504. ISSN: 0304-324X (5 2019).

216. Mogilenko, D. A. *et al.* Comprehensive profiling of an aging immune system reveals clonal GZMK+ CD8+ T cells as conserved hallmark of inflammaging. *Immunity* **54,** 99–115.e12. ISSN: 10747613 (1 Jan. 2021).

217. Bouwman, A. C., van Daalen, K. R., Crnko, S., ten Broeke, T. & Bovenschen, N. Intracellular and extracellular roles of granzyme K. *Frontiers in Immunology* **12.** ISSN: 1664-3224 (May 2021).

218. Goldberg, E. L. & Dixit, V. D. Drivers of age-related inflammation and strategies for healthspan extension. *Immunological Reviews* **265,** 63–74. ISSN: 01052896 (1 May 2015).

219. Mau, T. & Yung, R. Adipose tissue inflammation in aging. *Experimental Gerontology* **105,** 27–31. ISSN: 05315565 (May 2018).

220. Jubel, J. M., Barbati, Z. R., Burger, C., Wirtz, D. C. & Schildberg, F. A. The role of PD-1 in acute and chronic infection. *Frontiers in Immunology* **11.** ISSN: 1664-3224 (Mar. 2020).

221. Lázár-Molnár, E. *et al.* Programmed death-1 (PD-1)–deficient mice are extraordinarily sensitive to tuberculosis. *Proceedings of the National Academy of Sciences* **107,** 13402–13407. ISSN: 0027-8424 (30 July 2010).

222. Wang, J. *et al.* PD-1 deficiency results in the development of fatal myocarditis in MRL mice. *International Immunology* **22,** 443–452. ISSN: 1460-2377 (6 June 2010).

223. Blank, C. U. *et al.* Defining 'T cell exhaustion'. *Nature Reviews Immunology* **19,** 665–674. ISSN: 1474-1733 (11 Nov. 2019).

224. Porsche, C. E., Delproposto, J. B., Geletka, L., O'Rourke, R. & Lumeng, C. N. Obesity results in adipose tissue T cell exhaustion. *JCI Insight* **6.** ISSN: 2379-3708 (8 Apr. 2021).

225. Wang, Z. *et al.* Paradoxical effects of obesity on T cell function during tumor progression and PD-1 checkpoint blockade. *Nature Medicine* **25,** 141–151. ISSN: 1078-8956 (1 Jan. 2019).

226. Couturier, J. *et al.* Human adipose tissue as a reservoir for memory CD4+ T cells and HIV. *AIDS* **29,** 667–674. ISSN: 0269-9370 (6 Mar. 2015).

227. May, M. T. *et al.* Impact on life expectancy of HIV-1 positive individuals of CD4+ cell count and viral load response to antiretroviral therapy. *AIDS* **28,** 1193–1202. ISSN: 0269-9370 (8 May 2014).

228. Pao, V., Lee, G. A. & Grunfeld, C. HIV therapy, metabolic syndrome, and cardiovascular risk. *Current Atherosclerosis Reports* **10,** 61–70. ISSN: 1523-3804 (1 Jan. 2008).

229. Wanjalla, C. N. *et al.* Adipose tissue in persons With HIV is enriched for CD4+ T effector memory and T effector memory RA+ cells, which show higher CD69 expression and CD57, CX3CR1, GPR56 Co-expression With increasing glucose intolerance. *Frontiers in Immunology* **10.** ISSN: 1664-3224 (Mar. 2019).

230. Wanjalla, C. N. *et al.* Single-cell analysis shows that adipose tissue of persons with both HIV and diabetes is enriched for clonal, cytotoxic, and CMV-specific CD4+ T cells. *Cell Reports Medicine* **2,** 100205. ISSN: 26663791 (2 Feb. 2021).

231. Chen, S., Zhou, Y., Chen, Y. & Gu, J. fastp: an ultra-fast all-in-one FASTQ preprocessor. *Bioinformatics* **34,** i884–i890. ISSN: 1367-4803 (17 Sept. 2018).

232. Patro, R., Duggal, G., Love, M. I., Irizarry, R. A. & Kingsford, C. Salmon provides fast and bias-aware quantification of transcript expression. *Nature Methods* **14,** 417–419. ISSN: 1548-7091 (4 Apr. 2017).

233. Robinson, M. D., McCarthy, D. J. & Smyth, G. K. edgeR: a bioconductor package for differential expression analysis of digital gene expression data. *Bioinformatics* **26,** 139–140. ISSN: 1367-4803 (1 Jan. 2010).

234. Love, M. I., Huber, W. & Anders, S. Moderated estimation of fold change and dispersion for RNA-seq data with DESeq2. *Genome Biology* **15,** 550. ISSN: 1474-760X (12 Dec. 2014).

235. Manno, G. L. *et al.* RNA velocity of single cells. *Nature* **560,** 494–498. ISSN: 0028-0836 (7719 Aug. 2018).

236. Young, M. D. & Behjati, S. SoupX removes ambient RNA contamination from droplet-based single-cell RNA sequencing data. *GigaScience* **9.** ISSN: 2047-217X (12 Dec. 2020).

237. Hao, Y. *et al.* Integrated analysis of multimodal single-cell data. *Cell* **184,** 3573–3587.e29. ISSN: 00928674 (13 June 2021).

238. Bergen, V., Lange, M., Peidli, S., Wolf, F. A. & Theis, F. J. Generalizing RNA velocity to transient cell states through dynamical modeling. *Nature Biotechnology* **38,** 1408–1414. ISSN: 1087-0156 (12 Dec. 2020).

239. McGinnis, C. S., Murrow, L. M. & Gartner, Z. J. DoubletFinder: doublet detection in single-cell RNA sequencing data using artificial nearest neighbors. *Cell Systems* **8,** 329–337.e4. ISSN: 24054712 (4 Apr. 2019).

240. Aran, D. *et al.* Reference-based analysis of lung single-cell sequencing reveals a transitional profibrotic macrophage. *Nature Immunology* **20,** 163–172. ISSN: 1529-2908 (2 Feb. 2019).

241. Dann, E., Henderson, N. C., Teichmann, S. A., Morgan, M. D. & Marioni, J. C. Differential abundance testing on single-cell data using k-nearest neighbor graphs. *Nature Biotechnology* **40,** 245–253. ISSN: 1087-0156 (2 Feb. 2022).

242. Heather, J. M. *et al.* Stitchr: stitching coding TCR nucleotide sequences from V/J/CDR3 information. *Nucleic Acids Research.* ISSN: 0305-1048 (Mar. 2022).

243. Brissova, M. *et al.* Pancreatic islet production of vascular endothelial growth factor-A Is essential for islet vascularization, revascularization, and function. *Diabetes* **55,** 2974–2985. ISSN: 0012-1797 (11 Nov. 2006).

244. Hruby, A. & Hu, F. B. The epidemiology of obesity: a big picture. *PharmacoEconomics* **33,** 673–689. ISSN: 1170-7690 (7 July 2015).

245. Organization, W. H. *Obesity And Overweight* 2021.

246. Ferrante, A. W. Macrophages, fat, and the emergence of immunometabolism. *Journal of Clinical Investigation* **123,** 4992–4993. ISSN: 0021-9738 (12 Dec. 2013).

247. Russo, L. & Lumeng, C. N. Properties and functions of adipose tissue macrophages in obesity. *Immunology* **155,** 407–417. ISSN: 00192805 (4 Dec. 2018).

248. Zatterale, F. *et al.* Chronic adipose tissue inflammation linking obesity to insulin resistance and type 2 diabetes. *Frontiers in Physiology* **10.** ISSN: 1664-042X (Jan. 2020).

249. Khan, S., Chan, Y. T., Revelo, X. S. & Winer, D. A. The immune landscape of visceral adipose tissue during obesity and aging. *Frontiers in Endocrinology* **11.** ISSN: 1664-2392 (May 2020).

250. Anderson, E. K., Gutierrez, D. A., Kennedy, A. & Hasty, A. H. Weight cycling increases T-cell accumulation in adipose tissue and impairs systemic glucose tolerance. *Diabetes* **62,** 3180–3188. ISSN: 0012-1797 (9 Sept. 2013).

251. Zou, J. *et al.* CD4+ T cells memorize obesity and promote weight regain. *Cellular & Molecular Immunology* **15,** 630–639. ISSN: 1672-7681 (6 June 2018).

252. Weinstock, A. *et al.* Single-cell RNA sequencing of visceral adipose tissue leukocytes reveals that caloric restriction following obesity promotes the accumulation of a distinct macrophage population with features of phagocytic cells. *Immunometabolism.* ISSN: 26330407 (2019).

253. Stoeckius, M. *et al.* Simultaneous epitope and transcriptome measurement in single cells. *Nature Methods* **14,** 865–868. ISSN: 1548-7091 (9 Sept. 2017).

254. Stoeckius, M. *et al.* Cell Hashing with barcoded antibodies enables multiplexing and doublet detection for single cell genomics. *Genome Biology* **19,** 224. ISSN: 1474-760X (1 Dec. 2018).

255. DeFronzo, R. A., Gunnarsson, R., Björkman, O., Olsson, M. & Wahren, J. Effects of insulin on peripheral and splanchnic glucose metabolism in noninsulin-dependent (type II) diabetes mellitus. *Journal of Clinical Investigation* **76,** 149–155. ISSN: 0021-9738 (1 July 1985).

256. Kelley, D. *et al.* Skeletal muscle glycolysis, oxidation, and storage of an oral glucose load. *Journal of Clinical Investigation* **81,** 1563–1571. ISSN: 0021-9738 (5 May 1988).

257. Weinstock, A., Silva, H. M., Moore, K. J., Schmidt, A. M. & Fisher, E. A. Leukocyte heterogeneity in adipose tissue, including in obesity. *Circulation Research* **126,** 1590–1612. ISSN: 0009-7330 (11 May 2020).

258. Kane, H. & Lynch, L. Innate immune control of adipose tissue homeostasis. *Trends in Immunology* **40,** 857–872. ISSN: 14714906 (9 Sept. 2019).

259. Groom, J. R. & Luster, A. D. CXCR3 in T cell function. *Experimental Cell Research* **317,** 620–631. ISSN: 00144827 (5 Mar. 2011).

260. Martin, M. D. & Badovinac, V. P. Defining memory CD8 T cell. *Frontiers in Immunology* **9.** ISSN: 1664-3224 (Nov. 2018).

261. Tang-Huau, T.-L. *et al.* Human in vivo-generated monocyte-derived dendritic cells and macrophages cross-present antigens through a vacuolar pathway. *Nature Communications* **9,** 2570. ISSN: 2041-1723 (1 Dec. 2018).

262. Carlyle, J. R. *et al.* Evolution of the Ly49 and Nkrp1 recognition systems. *Seminars in Immunology* **20,** 321–330. ISSN: 10445323 (6 Dec. 2008).

263. Van der Leun, A. M., Thommen, D. S. & Schumacher, T. N. CD8+ T cell states in human cancer: insights from single-cell analysis. *Nature Reviews Cancer* **20,** 218–232. ISSN: 1474-175X (4 Apr. 2020).

264. Sade-Feldman, M. *et al.* Defining T cell states associated with response to checkpoint immunotherapy in melanoma. *Cell* **176,** 404. ISSN: 00928674 (1-2 Jan. 2019).

265. Andreatta, M. *et al.* Interpretation of T cell states from single-cell transcriptomics data using reference atlases. *Nature Communications* **12,** 2965. ISSN: 2041-1723 (1 Dec. 2021).

266. Yang, J., Zhang, L., Yu, C., Yang, X.-F. & Wang, H. Monocyte and macrophage differentiation: circulation inflammatory monocyte as biomarker for inflammatory diseases. *Biomarker Research* **2,** 1. ISSN: 2050-7771 (1 Dec. 2014).

267. Kawamura, S. & Ohteki, T. Monopoiesis in humans and mice. *International Immunology*. ISSN: 0953-8178 (Sept. 2018).

268. Yu, J. *et al.* The CD9, CD81, and CD151 EC2 domains bind to the classical RGD-binding site of integrin vβ3. *Biochemical Journal* **474,** 589–596. ISSN: 0264-6021 (4 Feb. 2017).

269. Hamers, A. A. *et al.* Human monocyte heterogeneity as revealed by high-dimensional mass cytometry. *Arteriosclerosis, Thrombosis, and Vascular Biology* **39,** 25–36. ISSN: 1079-5642 (1 Jan. 2019).

270. Attanasio, J. & Wherry, E. J. Costimulatory and coinhibitory receptor pathways in infectious disease. *Immunity* **44,** 1052–1068. ISSN: 10747613 (5 May 2016).

271. Sun, T., Nguyen, A. & Gommerman, J. L. Dendritic cell subsets in intestinal immunity and inflammation. *The Journal of Immunology* **204,** 1075–1083. ISSN: 0022-1767 (5 Mar. 2020).

272. Bosteels, C. *et al.* Inflammatory type 2 cDCs acquire features of cDC1s and macrophages to orchestrate immunity to respiratory virus infection. *Immunity* **52,** 1039–1056.e9. ISSN: 10747613 (6 June 2020).

273. Riol-Blanco, L. *et al.* The chemokine receptor CCR7 activates in dendritic cells two signaling modules that independently regulate chemotaxis and migratory speed. *The Journal of Immunology* **174,** 4070–4080. ISSN: 0022-1767 (7 Apr. 2005).

274. Orecchioni, M., Ghosheh, Y., Pramod, A. B. & Ley, K. Macrophage polarization: different gene signatures in M1(LPS+) vs. classically and M2(LPS–) vs. alternatively activated macrophages. *Frontiers in Immunology* **10.** ISSN: 1664-3224 (May 2019).

275. Stonier, S. W., Ma, L. J., Castillo, E. F. & Schluns, K. S. Dendritic cells drive memory CD8 T-cell homeostasis via IL-15 transpresentation. *Blood* **112,** 4546–4554. ISSN: 0006-4971 (12 Dec. 2008).

276. Harasymowicz, N. S. *et al.* Single-cell RNA sequencing reveals the induction of novel myeloid and myeloid-associated cell populations in visceral fat with long-term obesity. *The FASEB Journal* **35.** ISSN: 0892-6638 (3 Mar. 2021).

277. Roberts, A. W. *et al.* Tissue-Rresident macrophages are locally programmed for silent clearance of apoptotic cells. *Immunity* **47,** 913–927.e6. ISSN: 10747613 (5 Nov. 2017).

278. Ouyang, J. F., Kamaraj, U. S., Cao, E. Y. & Rackham, O. J. L. ShinyCell: simple and sharable visualization of single-cell gene expression data. *Bioinformatics* **37,** 3374–3376. ISSN: 1367-4803 (19 Oct. 2021).

279. Zamarron, B. F. *et al.* Macrophage proliferation sustains adipose tissue inflammation in formerly obese mice. *Diabetes* **66,** 392–406. ISSN: 0012-1797 (2 Feb. 2017).

280. Vatarescu, M. *et al.* Adipose tissue supports normalization of macrophage and liver lipid handling in obesity reversal. *Journal of Endocrinology* **233,** 293–305. ISSN: 0022-0795 (3 June 2017).

281. Kosteli, A. *et al.* Weight loss and lipolysis promote a dynamic immune response in murine adipose tissue. *Journal of Clinical Investigation* **120,** 3466–3479. ISSN: 0021-9738 (10 Oct. 2010).

282. De Oliveira, M. F. A., Talvani, A. & Rocha-Vieira, E. IL-33 in obesity: where do we go from here? *Inflammation Research* **68,** 185–194. ISSN: 1023-3830 (3 Mar. 2019).

283. Li, Y. *et al.* Insulin signaling establishes a developmental trajectory of adipose regulatory T cells. *Nature Immunology* **22,** 1175–1185. ISSN: 1529-2908 (9 Sept. 2021).

284. Shirakawa, K. *et al.* Obesity accelerates T cell senescence in murine visceral adipose tissue. *Journal of Clinical Investigation* **126,** 4626–4639. ISSN: 0021-9738 (12 Nov. 2016).

285. Shirakawa, K. *et al.* Negative legacy of obesity. *PLOS ONE* **12,** e0186303. ISSN: 1932-6203 (10 Oct. 2017).

286. McDonnell, W. J. *et al.* High CD8 T-cell receptor clonality and altered CDR3 properties are associated with elevated isolevuglandins in adipose tissue during diet-induced obesity. *Diabetes* **67,** 2361–2376. ISSN: 0012-1797 (11 Nov. 2018).

287. Maier, B. *et al.* A conserved dendritic-cell regulatory program limits antitumour immunity. *Nature* **580,** 257–262. ISSN: 0028-0836 (7802 Apr. 2020).

288. Félix, I. *et al.* Single-Cell proteomics reveals the defined heterogeneity of resident macrophages in white adipose tissue. *Frontiers in Immunology* **12.** ISSN: 1664-3224 (July 2021).

289. Xu, X. *et al.* Obesity activates a program of lysosomal-dependent lipid metabolism in adipose tissue macrophages independently of classic activation. *Cell Metabolism* **18,** 816–830. ISSN: 15504131 (6 Dec. 2013).

290. Coats, B. R. *et al.* Metabolically activated adipose tissue macrophages perform detrimental and beneficial functions during diet-induced obesity. *Cell Reports* **20,** 3149–3161. ISSN: 22111247 (13 Sept. 2017).

291. Molgora, M. *et al.* TREM2 modulation remodels the tumor myeloid landscape enhancing Anti-PD-1 immunotherapy. *Cell* **182,** 886–900.e17. ISSN: 00928674 (4 Aug. 2020).

292. Champion, T. C. *et al.* Monocyte subsets have distinct patterns of tetraspanin expression and different capacities to form multinucleate giant cells. *Frontiers in Immunology* **9.** ISSN: 1664-3224 (June 2018).

293. Braune, J. *et al.* Multinucleated giant cells in adipose tissue are specialized in adipocyte degradation. *Diabetes* **70,** 538–548. ISSN: 0012-1797 (2 Feb. 2021).

294. Cinti, S. *et al.* Adipocyte death defines macrophage localization and function in adipose tissue of obese mice and humans. *Journal of Lipid Research* **46,** 2347–2355. ISSN: 00222275 (11 Nov. 2005).

295. Adam, K., Iuga, A., Tocheva, A. S. & Mor, A. A novel mouse model for checkpoint inhibitor-induced adverse events. *PLOS ONE* **16,** e0246168. ISSN: 1932-6203 (2 Feb. 2021).

296. Mueller, S. N. & Mackay, L. K. Tissue-resident memory T cells: local specialists in immune defence. *Nature Reviews Immunology* **16,** 79–89. ISSN: 1474-1733 (2 Feb. 2016).

297. Beura, L. K. *et al.* T Cells in nonlymphoid tissues give rise to lymph-node-resident memory T cells. *Immunity* **48,** 327–338.e5. ISSN: 10747613 (2 Feb. 2018).

298. Johnson, J. D. On the causal relationships between hyperinsulinaemia, insulin resistance, obesity and dysglycaemia in type 2 diabetes. *Diabetologia* **64,** 2138–2146. ISSN: 1432-0428 (10 2021).

299. Page, M. M. & Johnson, J. D. Mild suppression of hyperinsulinemia to treat obesity and insulin resistance. *Trends in Endocrinology & Metabolism* **29,** 389–399. ISSN: 10432760 (6 June 2018).

300. Mehran, A. E. *et al.* Hyperinsulinemia drives diet-induced obesity independently of brain insulin production. *Cell Metabolism* **16,** 723–737. ISSN: 15504131 (6 Dec. 2012).

301. DeFronzo, R. A. From the triumvirate to the ominous octet: a new paradigm for the treatment of type 2 diabetes mellitus. *Diabetes* **58,** 773–795. ISSN: 0012-1797 (4 Apr. 2009).

302. Corkey, B. E. Banting Lecture 2011. *Diabetes* **61,** 4–13. ISSN: 0012-1797 (1 Jan. 2012).

303. Templeman, N. M., Skovsø, S., Page, M. M., Lim, G. E. & Johnson, J. D. A causal role for hyperinsulinemia in obesity. *Journal of Endocrinology* **232,** R173–R183. ISSN: 0022-0795 (3 Mar. 2017).

304. Prentki, M. Islet cell failure in type 2 diabetes. *Journal of Clinical Investigation* **116,** 1802–1812. ISSN: 0021-9738 (7 July 2006).

305. Cottam, M. A., Caslin, H. L., Winn, N. C. & Hasty, A. H. Multiomics reveals persistence of obesity-associated immune cell phenotypes in adipose tissue during weight loss and subsequent weight regain in mice. *Nature Communications* (2022).

306. Fabbrini, E. *et al.* Intrahepatic fat, not visceral fat, is linked with metabolic complications of obesity. *Proceedings of the National Academy of Sciences* **106,** 15430–15435. ISSN: 0027-8424 (36 Sept. 2009).

307. Ciaula, A. D. *et al.* Nonalcoholic fatty liver disease (NAFLD) - mitochondria as players and targets of therapies? *International Journal of Molecular Sciences* **22,** 5375. ISSN: 1422-0067 (10 May 2021).

308. Paschen, M. *et al.* Diet-induced β-cell insulin resistance results in reversible loss of functional β-cell mass. *The FASEB Journal* **33,** 204–218. ISSN: 0892-6638 (1 Jan. 2019).

309. Villareal, D. T., Banks, M. R., Patterson, B. W., Polonsky, K. S. & Klein, S. Weight loss therapy improves pancreatic endocrine function in obese older adults. *Obesity* **16,** 1349–1354. ISSN: 19307381 (6 June 2008).

310. Rothberg, A. E. *et al.* Weight loss improves β-cell function in people with severe obesity and impaired fasting glucose: a window of opportunity. *The Journal of Clinical Endocrinology & Metabolism* **105,** e1621–e1630. ISSN: 0021-972X (4 Apr. 2020).

311. Solomon, T. P. *et al.* Improved pancreatic β-cell function in type 2 diabetic patients after lifestyle-induced weight loss is related to glucose-dependent insulinotropic polypeptide. *Diabetes Care* **33,** 1561–1566. ISSN: 0149-5992 (7 July 2010).

312. Guldstrand, M., Ahrén, B. & Adamson, U. Improved β-cell function after standardized weight reduction in severely obese subjects. *American Journal of Physiology-Endocrinology and Metabolism* **284,** E557–E565. ISSN: 0193-1849 (3 Mar. 2003).

313. Rosenfalck, A. M. *et al.* Minor long-term changes in weight have beneficial effects on insulin sensitivity and β-cell function in obese subjects. *Diabetes, Obesity and Metabolism* **4,** 19–28. ISSN: 14628902 (1 Jan. 2002).

314. Goldstein, D. J. Beneficial health effects of modest weight loss. *International journal of obesity and related metabolic disorders : journal of the International Association for the Study of Obesity* **16,** 397–415 (6 June 1992).

315. Do Amaral, M. E. C. *et al.* Caloric restriction recovers impaired β-cell-β-cell gap junction coupling, calcium oscillation coordination, and insulin secretion in prediabetic mice. *American Journal of Physiology-Endocrinology and Metabolism* **319,** E709–E720. ISSN: 0193-1849 (4 Oct. 2020).

316. Ferrannini, E. *et al.* Beta-cell function in obesity. *Diabetes* **53,** S26–S33. ISSN: 0012-1797 (suppl_3 Dec. 2004).

317. Speakman, J. R. If body fatness is under physiological regulation, then how come we have an obesity epidemic? *Physiology* **29,** 88–98. ISSN: 1548-9213 (2 Mar. 2014).

318. Yong, J., Johnson, J. D., Arvan, P., Han, J. & Kaufman, R. J. Therapeutic opportunities for pancreatic β-cell ER stress in diabetes mellitus. *Nature Reviews Endocrinology* **17,** 455–467. ISSN: 1759-5029 (8 Aug. 2021).

319. Guo, S. *et al.* Inactivation of specific β cell transcription factors in type 2 diabetes. *Journal of Clinical Investigation* **123,** 3305–3316. ISSN: 0021-9738 (8 Aug. 2013).

320. Taylor, B. L., Benthuysen, J. & Sander, M. Postnatal β-cell proliferation and mass expansion is dependent on the transcription factor Nkx6.1. *Diabetes* **64,** 897–903. ISSN: 0012-1797 (3 Mar. 2015).

321. Matsuoka, T.-a. *et al.* Preserving Mafa expression in diabetic islet β-cells improves glycemic control in Vivo. *Journal of Biological Chemistry* **290,** 7647–7657. ISSN: 00219258 (12 Mar. 2015).

322. Johnson, J. D. *et al.* Increased islet apoptosis in Pdx1+/– mice. *Journal of Clinical Investigation* **111,** 1147–1160. ISSN: 0021-9738 (8 Apr. 2003).

323. Spaeth, J. M. *et al.* Defining a novel role for the Pdx1 transcription factor in islet β-cell maturation and proliferation during weaning. *Diabetes* **66,** 2830–2839. ISSN: 0012-1797 (11 Nov. 2017).

324. Robertson, R. P., Harmon, J., Tran, P. O., Tanaka, Y. & Takahashi, H. Glucose toxicity in β-cells: type 2 diabetes, good radicals gone bad, and the glutathione connection. *Diabetes* **52,** 581–587. ISSN: 0012-1797 (3 Mar. 2003).

325. Tiedge, M., Lortz, S., Drinkgern, J. & Lenzen, S. Relation between antioxidant enzyme gene expression and antioxidative defense status of insulin-producing cells. *Diabetes* **46,** 1733–1742. ISSN: 0012-1797 (11 Nov. 1997).

326. Lenzen, S., Drinkgern, J. & Tiedge, M. Low antioxidant enzyme gene expression in pancreatic islets compared with various other mouse tissues. *Free Radical Biology and Medicine* **20,** 463–466. ISSN: 08915849 (3 Jan. 1996).

327. Sjöström, L. *et al.* Randomised placebo-controlled trial of orlistat for weight loss and prevention of weight regain in obese patients. *The Lancet* **352,** 167–172. ISSN: 01406736 (9123 July 1998).

328. Brown, E., Wilding, J. P., Barber, T. M., Alam, U. & Cuthbertson, D. J. Weight loss variability with SGLT2 inhibitors and GLP-1 receptor agonists in type 2 diabetes mellitus and obesity: mechanistic possibilities. *Obesity Reviews* **20,** 816–828. ISSN: 1467-7881 (6 June 2019).

329. Drucker, D. J. Mechanisms of action and therapeutic application of glucagon-like peptide-1. *Cell Metabolism* **27,** 740–756. ISSN: 15504131 (4 Apr. 2018).

330. Akbari, P. *et al.* Sequencing of 640,000 exomes identifies *GPR75* variants associated with protection from obesity. *Science* **373.** ISSN: 0036-8075 (6550 July 2021).

331. Fothergill, E. *et al.* Persistent metabolic adaptation 6 years after "The Biggest Loser" competition. *Obesity* **24,** 1612–1619. ISSN: 19307381 (8 Aug. 2016).

332. Zeeni, N., Dagher-Hamalian, C., Dimassi, H. & Faour, W. H. Cafeteria diet-fed mice is a pertinent model of obesity-induced organ damage: a potential role of inflammation. *Inflammation Research* **64,** 501–512. ISSN: 1023-3830 (7 July 2015).

333. Prendeville, H. & Lynch, L. Diet, lipids, and antitumor immunity. *Cellular & Molecular Immunology* **19,** 432–444. ISSN: 1672-7681 (3 Mar. 2022).

334. Lodge, M. *et al.* Fructose metabolism and regulation of extracellular matrix protein gene expression in activated macrophages. *Current Developments in Nutrition* **4,** 1527–1527. ISSN: 2475-2991 (Supplement$_2$ June 2020).

335. Ernsberger, P., Koletsky, R. J., Baskin, J. S. & Collins, L. A. Consequences of weight cycling in obese spontaneously hypertensive rats. *American Journal of Physiology-Regulatory, Integrative and Comparative Physiology* **270,** R864–R872. ISSN: 0363-6119 (4 Apr. 1996).

336. Schofield, S. E. *et al.* Metabolic dysfunction following weight cycling in male mice. *International Journal of Obesity* **41,** 402–411. ISSN: 0307-0565 (3 Mar. 2017).

337. Simonds, S. E., Pryor, J. T. & Cowley, M. A. Repeated weight cycling in obese mice causes increased appetite and glucose intolerance. *Physiology & Behavior* **194,** 184–190. ISSN: 00319384 (Oct. 2018).

338. Ruiz-Ojeda, Méndez-Gutiérrez, Aguilera & Plaza-Díaz. Extracellular matrix remodeling of adipose tissue in obesity and metabolic diseases. *International Journal of Molecular Sciences* **20,** 4888. ISSN: 1422-0067 (19 Oct. 2019).

339. Lee, J.-T. *et al.* Macrophage metalloelastase (MMP12) regulates adipose tissue expansion, insulin sensitivity, and expression of inducible nitric oxide synthase. *Endocrinology* **155,** 3409–3420. ISSN: 0013-7227 (9 Sept. 2014).

340. Klement, J. D. *et al.* An osteopontin/CD44 immune checkpoint controls CD8+ T cell activation and tumor immune evasion. *Journal of Clinical Investigation* **128,** 5549–5560. ISSN: 0021-9738 (12 Nov. 2018).

341. Weng, X., Maxwell-Warburton, S., Hasib, A., Ma, L. & Kang, L. The membrane receptor CD44: novel insights into metabolism. *Trends in Endocrinology & Metabolism* **33,** 318–332. ISSN: 10432760 (5 May 2022).

342. Ng, C. W., Tam, I. Y. S., Sam, S. W., Yu, Y. & Lau, H. Y. A. Immobilized osteopontin enhances adhesion but suppresses cytokine release of anti-IgE activated human mast cells. *Frontiers in Immunology* **9.** ISSN: 1664-3224 (May 2018).

343. Diao, H. *et al.* Osteopontin regulates development and function of invariant natural killer T cells. *Proceedings of the National Academy of Sciences* **105,** 15884–15889. ISSN: 0027-8424 (41 Oct. 2008).

344. Oh, Y. S., Bae, G. D., Baek, D. J., Park, E.-Y. & Jun, H.-S. Fatty acid-induced lipotoxicity in pancreatic beta-cells during development of type 2 diabetes. *Frontiers in Endocrinology* **9.** ISSN: 1664-2392 (July 2018).

345. Böni-Schnetzler, M. *et al.* IL-1beta promotes the age-associated decline of beta cell function. *iScience* **24,** 103250. ISSN: 25890042 (11 Nov. 2021).

346. Tonkin, D. R. & Haskins, K. Regulatory T cells enter the pancreas during suppression of type 1 diabetes and inhibit effector T cells and macrophages in a TGF-β-dependent manner. *European Journal of Immunology* **39,** 1313–1322. ISSN: 00142980 (5 May 2009).

347. Carvalho-Pinto, C. *et al.* Leukocyte attraction through the CCR5 receptor controls progress from insulitis to diabetes in non-obese diabetic mice. *European Journal of Immunology* **34,** 548–557. ISSN: 0014-2980 (2 Feb. 2004).

348. Burke, S. J. *et al.* Regulation of the CCL2 gene in pancreatic β-cells by IL-1β and glucocorticoids: role of MKP-1. *PLoS ONE* **7,** e46986. ISSN: 1932-6203 (10 Oct. 2012).

349. Rajendran, S. *et al.* IL-6 is present in beta and alpha cells in human pancreatic islets: Expression is reduced in subjects with type 1 diabetes. *Clinical Immunology* **211,** 108320. ISSN: 15216616 (Feb. 2020).

350. Laffitte, B. A. *et al.* LXRs control lipid-inducible expression of the apolipoprotein E gene in macrophages and adipocytes. *Proceedings of the National Academy of Sciences* **98,** 507–512. ISSN: 0027-8424 (2 Jan. 2001).

351. Reschen, M. E. *et al.* Lipid-induced epigenomic changes in human macrophages identify a coronary artery disease-associated variant that regulates PPAP2β expression through altered C/EBP-beta binding. *PLOS Genetics* **11,** e1005061. ISSN: 1553-7404 (4 Apr. 2015).

352. Nawaz, A. *et al.* CD206+ M2-like macrophages regulate systemic glucose metabolism by inhibiting proliferation of adipocyte progenitors. *Nature Communications* **8,** 286. ISSN: 2041-1723 (1 Dec. 2017).

353. Jin, S. *et al.* Inference and analysis of cell-cell communication using CellChat. *Nature Communications* **12,** 1088. ISSN: 2041-1723 (1 Dec. 2021).

354. Efremova, M., Vento-Tormo, M., Teichmann, S. A. & Vento-Tormo, R. CellPhoneDB: inferring cell–cell communication from combined expression of multi-subunit ligand–receptor complexes. *Nature Protocols* **15,** 1484–1506. ISSN: 1754-2189 (4 Apr. 2020).

355. Emont, M. P. *et al.* A single-cell atlas of human and mouse white adipose tissue. *Nature* **603,** 926–933. ISSN: 0028-0836 (7903 Mar. 2022).

356. Ho, A. W. S. *et al.* Lung CD103$^+$ dendritic cells efficiently transport influenza virus to the lymph node and load viral antigen onto MHC class I for presentation to CD8 T cells. *The Journal of Immunology* **187,** 6011–6021. ISSN: 0022-1767 (11 Dec. 2011).

357. Rebeles, J. *et al.* Obesity-induced changes in T-cell metabolism are associated with impaired memory T-cell response to influenza and are not reversed with weight loss. *The Journal of Infectious Diseases* **219,** 1652–1661. ISSN: 0022-1899 (10 Apr. 2019).

358. Joeckel, L. T., Allison, C. C., Pellegrini, M., Bird, C. H. & Bird, P. I. Granzyme K-deficient mice show no evidence of impaired antiviral immunity. *Immunology & Cell Biology* **95,** 676–683. ISSN: 0818-9641 (8 Sept. 2017).